MAY - AUG. 2008
Volume XIV Number II
ISSN 0859 144X

THE ASEAN JOURNAL OF RADIOLOGY

Published by The Radiological Society and
The Royal College of Radiologists of Thailand,
Bangkok, Thailand

MAY - AUG. 2008
Volume XIV Number II

ISSN 0859 144X

THE ASEAN JOURNAL OF RADIOLOGY

Published by The Radiological Society and The Royal College of Radiologists of Thailand, Bangkok, Thailand

Chief Editor

Professor Kawee Tungsubutra
Kaweevej Hospital, 318 Tarksin Road, Dhonburi, Bangkok 10600, Thailand.

Asean Journal of Radiology.
Instructions for Authors.

1. The Asean Journal of Radiology publishes the papers on Radiological Sciences, such as research work, review articles, case reports, innovations in Medical Sciences related to all branches of Radiology, and letters to the editor. The aforementioned materials can be written in English only.

2. The authors have to submit 2 copies of the manuscript and a diskette: **to Prof. Dr. Kawee Tungsubutra.** 318 Kaweevej Hospital, Tarksin Road, Dhonburi, Bangkok 10600, Thailand.

3. The original copy to be submitted must be typed in a double space on one side of the page of 8.1/2" x 11.1/2" paper.

4. The format of the article must include :
   a. Title page and address of the author (s)
   b. Abstract
   c. Introduction (Background)
   d. Material and Method
   e. Results and discussion (Tables and Illustrations)
   f. Acknowledgement (if any)
   g. References (Follow the Vancouver style developed by ICMJE)

5. We will provide 5 copies of reprints for the author (s) who submit (s) an article for publication in the Asean Journal.

6. The illustrations and tables must be clearly prepared with legends in English as they are the art works to be reproduced.

7. The authors are reponsible for the contents of the article as to its facts and findings.

8. Ethics.

Paper reporting studies which might be interpreted as human experimentation (e.g. controlled trials) should conform to the standards of the Declaration of Helsinki (see British Medical Journal 1964: 2: 177) and should indicate that, approval that such studies may proceed, has been granted by the local or hospital Ethics Committee.

When reporting experiments on animals indicate whether the institution's or the National Research Council's guide for, or any national law on, the care and use of laboratory animals was followed.

THE ASEAN JOURNAL OF RADIOLOGY

Volume XIV Number II MAY - AUG. 2008

CONTENTS

THE ASEAN JOURNAL OF RADIOLOGY

Volume XIV Number II MAY - AUG. 2008

CONTENTS

THE EFFECT OF THE IMPLEMENTATION OF THE QUALITY CONTROL PROGRAM OF THE COMPUTED RADIOGRAPHY SYSTEM

Petcharleeya SUWANPRADIT, M.Sc.,[1] Anchali KRISANACHINDA, Ph.D.,[2] Sukalaya LERDLUM, MD., M.Sc.,[2] Kiat ARJHANSIRI, MD.,[2] Weeranuch KITSUKJIT, M.Sc.[2]

ABSTRACT

Objectives: To study the relationship between the patient radiation doses, the image quality and the repeated and rejected rates both before and after the implementation of the quality control (QC) program to the computed radiography (CR) system at the Outpatient Division, Department of Radiology of King Chulalongkorn Memorial Hospital, Thai Red Cross Society.

Materials: Two systems of single-phase x-ray machine (Hitachi model DR-155HM), and another system of the CR system (Fuji model FCR 5000) with standard type of imaging plates, QC accessories, CR workstation with high resolution display system were compared.

Methods: Experimental prospective study, before and after QC program to the CR system were designed; 1,384 examinations of the adult patients, eight projections of CR images, skull PA, lateral cephalometry, cervical spine AP, chest PA, abdomen AP, lumbo-sacral spine AP and lateral and pelvis AP were performed under patient consent form and calculated the entrance skin dose (ESD). The radiographic patient dose was defined as the comparison of the rejected and retaken rates for the before and after QC of equipment. CR image quality evaluation had been done by two of the equivalent experienced radiologists.

Results: There were the significantly differences ($P < 0.05$) for the decreasing of the rejected and retaken rate and the decreasing of average of ESD after the implementation of the QC program of the CR system.

Conclusion: After the implementation of quality control program for the computed radiography system, the reduction of the rejected and retaken rate was 55 percent and the reduction of the entrance skin dose was 18 percent in PA chest and 16 percent in the lumbo-sacral spines while maintaining optimum image quality. The QC program of the CR system shows the useful parameters benefited for the optimization of the patient doses and the image quality.

Key words: Quality control program, computed radiography.

[1] Department of Radiology, King Chulalongkorn Memorial Hospital, Thai Red Cross Society, Rama IV Road, Patumwan, Bangkok, Thailand. Tel. +662-2564414, Fax +662-2564417; E-mail: petch_chula@yahoo.com

[2] Department of Radiology, Chulalongkorn University, Rama IV Road, Patumwan, Bangkok, Thailand. Tel. +662-2564418, Fax +662-2564417.

INTRODUCTION

With two passing decades since the computed radiography (CR) worldwide introduction, it has become a mainstay technology for acquiring ordinary radiographic projections in digital form that produces images equivalent or better than conventional screen -film (S-F) systems. The success of CR leads to the misconception that quality assurance (QA) and quality control (QC) processes are no longer necessary. As a matter of fact, QA and QC processes for CR are no less important than they are for conventional radiography, and must be modified to take into consideration the unique characteristics of CR technology.[1] A good QC program utilizes tests that are sensitive and can be utilized frequent enough to detect degradation in equipment performance before diagnostic information is lost, with a special focus on potential dose reduction.[2] The radiation dose reduction and the diagnostic information are the output of quality control tests to assess the efficiency of computed radiographic system.[3] QA represents a comprehensive, ongoing program to evaluate all aspects of medical imaging.

ESD = Entrance Skin Dose

The ultimate goal of a QA program is to optimize image quality and patient safety. QC typically refers to the performance of periodic monitoring of imaging performance. Some authors[4] showed that the reduced retaken rate due to exposure factors by using CR led to a reduction in the overall retaken rate. Despite 50 percent dosage reduction, films were of better or equal quality when compared to conventional radiography. Several authors[5-8] suggested that the dose reduction can be achieved by means of a reduction in the number of examinations that must be repeated owing to incorrect exposure factors. In addition, it is often suggested that the computed radiography could be used with lower radiation doses than the conventional systems and thus reduce the patient doses.[9] Though the artifacts on radiographic images are distracting and may compromise accurate diagnosis, users' understanding the potential sources of CR artifacts will aid in identifying and resolving problems quickly and help to prevent future occurrences.[10] The first CR system (Fuji FCR 5000) was installed in the year 2000 in the department of radiology, King Chulalongkorn Memorial Hospital, Thai Red Cross Society, with standard resolution phosphor imaging plates (ST-V_N), Fuji Photo Film Co., Ltd..In clinical practice, several problems have been found such as Moiré patterns, too dark, too bright, too noisy images, superimposed appearances, post-processing parameter mismatch, rejected and retaken rate over 9 percents for 6 examinations (84 cases from total 934 cases in 6 months), incorrect imaging plate handle, lack of QC protocol for routine job, etc. For the long term, it is expected that the rejected and retaken rate should be reduced to 5 percent or less, the unnecessary patient radiation doses could be reduced, with the costs reduction. The goal of CR acceptance testing is to establish the CR reader and phosphor screen baseline performance. Quality control testing then detects changes in the CR system that could affect radiographic image quality. In this study, two main parameters are identified as influencing diagnostic reference levels (DRL)[11,12] and entrance skin dose (ESD) for determining which had been affected to the reduction of whether there was any statistically significant difference between before and after QC implementation of the rejected and retaken rates (and thus, reduction of radiation doses to the patient), and thus improve the image quality.

MATERIALS AND METHODS

This work has been designed as a prospective experimental study comparing the patient doses and image qualities between before (controls group) and after (experimental group) implementation of QC of the CR system (Table 1-2), and performed on the routine clinical examinations that the ethical approval by the Ethics Committee of Faculty of Medicine, Chulalongkorn University had been determined the patient information and informed consent had to be processed. All data was collected under the criteria developed by the senior technologist (Table 3). The entrance skin dose (ESD) was calculated and the comparable images quality evaluated by two radiologists of the same experience.

Patient data was collected at the general x-ray room (Room number 4 and 5), section of outpatient Department of Radiology, (Por Por Ror Building 4th floor), King Chulalongkorn Memorial Hospital, Bangkok, Thailand. Two systems of single-phase x-ray machine (Hitachi DR-155HM, Hitachi, Japan, 1989) with bucky table, non -automatic exposure control (non-AEC) were used. Another system of the CR system was a Fuji computed radiography (Fuji, FCR 5000, Fuji Photo Film Co. Ltd., Tokyo, Japan, 2000). Imaging phosphors were Europium doped barium fluoro -bromide. Imaging plate size for skull PA from paranasal sinuses series, lateral cephalometry, and cervical spine AP was 24 x 30 cm, and 35 x 43 cm for chest PA, abdomen AP, lumbo-sacral spine AP, lumbo-sacral spine lateral and pelvis AP. Soft copies were obtained by Totoku high resolution monochrome LCD display model ME 201L using Fuji CR Workstation model HI-C 655. Hard copies were obtained from Fuji computed radiography film type 780-H (25.7 x 36.4 cm) and type LI-LM (35 x 43 cm), Fuji wet laser imager model FL-IM D containing a helium neon laser (633 nm) with developer (RD-20) and Fixer (RF-15).

Sample random technique

The selected randomly of the target patients had been done by the preliminary survey of 8 given radiographic projections and 4 age groups (16-30, 31-45, 46-60 and 61-75 years old) for 33 working days. Select 692 sample cases of "Before QC program" (control group) and meet the criteria; collect, complete and analyze the patient data for the period of 1.5 months. Calibrate the x-ray using AAPM protocol[13] in table 1 and the CR systems using AAPM protocol Task Group No.10[14] and KCARE CR QA Protocol Draft 4.0 by Kings College Hospital[15] in table 2 for 1 month. Select 692 sample cases of "After QC program" (experimental group) and meet the criteria; collect, complete and analyze the patient data for the period of 1.5 months. Calculate ESD for each examination and compare the radiation dose and image quality of the control group to the experimental group.

Data Analysis

The retaken data, the patient dose and image quality score were analyzed by using the SPSS version 11.5 for Windows software package to test for statistical significance before and after implementation of the QC program. The analysis was performed first according to the actual modality that was used for each examination. This was of interest because, if the patient underwent imaging with the different x-ray machine; the quantity of the entrance surface air kerma (ESAK, mGy/mAs), the back scatter factor and the entrance skin dose (mGy) would be different.

RESULTS

The results can be concluded into 2 groups, the first was the equipment performance (table 4 and table 5) and the second was the assessment of image quality and radiation dose before and after QC implementation in term of the percentage rejected and retaken radiographs (table 6) including the exposure factors (table 7), the mean entrance skin dose and the image quality comparing (table 8 to table 10).

The Computed Radiography System Quality control

Both of the x-ray machine and the computed radiography performances were in the acceptable range. The QC results were shown in table 4 - 5.

Table 1. The items of x-ray machine QC and list of test tools which were used.

QC items (AAPM Protocol)	**Test tools**
1. General mechanical conditions	1. Ionization chamber (Victoreen 4000M+)
2. All indicator lamps and "beam ON indicator"	2. Pure Aluminum plates (0.1, 0.5 and 1.0 mm in thickness)
3. Dead man switch	3. Beam alignment test tool
4. Source image distance (SID)indicator	4. Collimator test tool
5. Mechanical motion test	5. Sensitometer
6. Field size indication	6. Densitometer
7. Light versus radiation congruence	7. Tape measure
8. Cross-hair centering	
9. Automatic collimation or Positive beam limit (PBL)	
10. Photo timer reproducibility and density compensation	
11. Exposure reproducibility	
12. Linearity of exposure with mR/mAs	
13. Timer accuracy	
14. Beam quality (HVL)	
15. kVp accuracy	
16. Entrance skin exposure (ESE)	

Table 2. The items of CR machine QC and list of test tools which were used

QC items (AAPM Task Group 10 Protocol and	**Test tools**
1. Monitor & laser printer	1. TO20 threshold contrast test object or equivalent
2. Dark Noise	2. Small lead or Copper block (~5 x 5 cm)
3. Erasure cycle efficiency	3. 1.5 mm Copper filtration (>10 x 10 cm)
4. Sensitivity Index calibration	4. Farmer Ionization chamber 0.6 cc.
5. Sensitivity Index consistency	5. Huttner test object or equivalent
6. Uniformity	6. M1 geometry test object or lead ruler
7. Scaling errors	7. Contact mesh
8. Blurring	8. Steel ruler
9. Limiting Spatial Resolution	9. Adhesive tape
10. Threshold Contrast Detail Detectability (TCDD)	10. Tape measure
11. Laser beam function	
12. Moiré Patterns	
In all tests, the QC CR imaging plate number A 09234079 was selected for all procedures.	

Table 3. Details of patient characteristic were colleted for each examination.

Variable	Description	Method
Data group	Before or after QC group	Obtained from collected data period
Patient identification	Hospital number, age, sex and date of examination	Notes from patient identification
Exposure conditions:		
Examination type	1.skull PA 2.lateral cephalometry 3.cervical spine AP 4.chest PA 5.abdomen AP 6.lumbo-sacral spine AP 7.lumbo-sacral spine lateral 8. pelvis AP	Examination and position during exposure
Wt, Ht	body weight (kg) and height (cm)	Measured by technologist
BMI	Body mass index for each patient	Calculate by formula; $BMI = \frac{Weight(kg)}{Height\ (m)^2}$
Thickness	Patient body part of thickness (cm) in the central field for each examination	Measured by technologist
kVp	kilovoltage peak across x-ray tube	Record from control panel
mAs	milliampere second product	Record from control panel
SID	Source-image receptor distance (cm)	Measured by technologist
SSD	Source -skin distance (cm)	*SSD = SID – (Patient thickness + table to image receptor distance)*
Room ID	No. 4 or No. 5	X-ray machine (Hitachi model DR-155HM)
S-value	Sensitivity value of each image	Record from CR reader panel
ESD (mGy)	Entrance Skin Dose in milliGray unit	Calculated by formula; $ESD= mAs\ x ESD_M\ x\ (SSD/100)^2$
Image Quality	Image quality grading for chest PA, abdomen AP, L-S spine AP and lateral view	Grading by senior radiologists using criteria from European guideline forms by 0, 0.5 and 1 scale; *0 - Not fulfill, 0.5 - Partial fulfill 1 – Fulfill, P - Pathology/Excluded*
Repeat image	Yes or No	Mark by qualified technologist
Causes of reject or retake image	1. position 2. motion 3. technical error 4. selected menu 5. high "S" value 6. low "S" value 7. artifacts	Mark by qualified technologist

Note. Some data are missing in subsequence tables of the results for one of the three reasons: not recorded, unavailable, mismatch.

Table 4. Main report of x-ray machine performance room number 4 and 5 had been done.

LOCATION:	PPR 4F King Chulalongkorn Memorial Hospital			
DATE:	9/10/2004		15/10/2004	
ROOM NUMBER:	**4**		**5**	
MANUFACTURE:	Hitachi, Japan; April 1989			
MODEL NUMBER	DR-155HM (Tube unit; U-6GE-55T)		DR-155HM (Tube unit; U-6GE-55T)	
SERIAL NUMBER	KC12808904		KC 17714403	
General mechanical conditions		**P**		**P**
All indication lamps and "Beam on indicator"		**P**		**P**
Dead man switch	-	**N/A**	-	**N/A**
Source image distance indicator	0.5% SID	**P**	1.0% SID	**P**
Mechanical motion test		**P**		**P**
Field size indication	A-C =1.19%, perpend. = 0.19%	**P**	A-C = 0.5%, Perpend. = 1.0%	**P**
Light VS Radiation congruence	A-C =0.31%, perpend. = 0.63%	**P**	A-C =1.0%, Perpend. = 1.19%	**P**
Cross hair centering	0.31%	**P**	1.31%)	**P**
Automatic collimation (PBL)	-	**N/A**	-	**N/A**
Photo timer reproducibility and density compensation	-	**N/A**	-	**N/A**
Exposure reproducibility	CV = 0.016	**P**	CV = 0.010	**P**
Linearity of exposure with mR/mAs	0.030	**P**	0.036	**P**
Timer accuracy	5.00%	**P**	5.00%	**P**
Beam quality (HVL)	3.02 mmAl at 80 kVp	**P**	2.83 mmAl at 80 kVp	**P**
kVp accuracy	4.00 – 8.92%	**P**	1.80 – 4.82%	**P**
Entrance skin exposure (ESE)		**P**		**P**

Table 5. Main report of CR system performance had been done.

CR system Calibration Test	Tolerance -The Established Criteria	Result
1. Monitor & laser printer set-up	The 5% on 0% and 95% on 100% details were clearly visible. The horizontal and vertical resolutions differ by lesser than 20%.	P
2. Dark Noise	Many artifacts were found on the images of 4 years IP used but were not on the new one.	P
3. Erasure cycle efficiency	Absence of a ghost image of the lead block from the first exposure in the re-exposed image.	P
4. Sensitivity Index calibration	The indicated exposure should agree with the measured exposure within 20%.	P
5. Sensitivity Index consistency	The variation in the calculated indicated exposures should not differ by greater than 20% between plates.	P
6. Uniformity	The images do not have obvious artifacts. The maximum variations in pixel values were within a range of 10% of each other.	P
7. Scaling errors	The measured distances x and y should agree within 3% of the actual distances. All calculated aspect ratios were within 1.00 ± 0.03.	P
8. Blurring	No blurring was present.	P
9. Limiting Spatial Resolution	For the 45° angled test object the resolved line pairs per mm should be *>1.2/2p* where p is the pixel dimension in mm. In the scan and subscan directions the limiting resolution should be >0.85/2p.	P
10. Threshold Contrast Detail Detectability (TCDD)	The results of this test are used to set a baseline for future QA tests. Results could be compared to those from other similar systems if available.	P
11. Laser beam function	Ruler edges were straight and continuous without any under- or overshoot of the scan lines in light to dark transitions.	P
12. Moiré Patterns	Moiré patterns had been visible with the routine stationary grid using.	F

P = Pass **N/P = Not performed**

F = Fail **NOTE = Recommendation suggested**

N/A = Not applicable

Patient Data

The 1,384 examinations were met the criteria and included in the study. Two groups of study were well matched for number, age, sex, the body weight and the body height.

The rejected-retaken data

The difference of rejected-retaken rate before, 22 from 692 examinations and after, 10 from 692 examinations, is statistically significant (Pearson Chi-square Test, P < 0.05) as shown in table 6.

Table 6. Shown the percentage of the rejected and retaken by different causes.

Types of reject and retake examination	Before group		After group		Total		*P- value*
	Retake number	%	Retake number	%	Retake number	%	
Positioning error	8	1.16	6	0.87	14	1.01	**0.591**
Motion	2	0.29	0	0.00	2	0.14	**0.157**
Technical error	2	0.29	1	0.14	3	0.22	**0.350**
Selected menu	0	0.00	0	0.00	0	0.00	-
High "S" value	7	1.01	0	0.00	7	0.51	**0.008**
Low "S" value	0	0.00	0	0.00	0	0.00	-
Artifacts	3	0.43	3	0.43	6	0.43	**1.000**
Total	22	3.18	10	1.45	32	2.31	**0.032**
Pearson Chi-square Test (χ^2) for association							

Exposure Conditions

The comparison of body part thickness (cm) and BMI that effected to the patient entrance skin doses of both groups were not different. The exposure factors (kVp and mAs) had been compared as shown in table 7.

Table 7. Shown the exposure factor data were compared between before and after QC program of examinations.

Types of exam.	Before QC group				After QC group			
	kVp		mAs		kVp		mAs	
	Mean	SD (min-max)	Mean	SD (min-max)	Mean	SD (min-max)	Mean	SD (min-max)
Skull PA	69.77	2.20 (65-75)	42.38	4.54 (40-51)	70.77	1.88 (70-75)	34.62	5.50 (32-50)
Ceph. lat	77.00	1.73 (75-78)	21.67	5.77 (15-25)	75.33	2.31 (74-78)	8.00	2.00 (6-10)
C sp. AP	69.00	5.06 (58-79)	16.90	6.86 (8-40)	67.67	4.14 (66-85)	16.52	19.20 (7-100)
Chest PA	73.65	3.51 (66-85)	13.13	2.71 (6-20)	71.22	2.71 (63-80)	11.11	2.25 (5-16)
Abd. AP	76.43	1.97 (75-82)	59.49	12.20 (50-100)	75.45	1.99 (70-80)	55.82	10.50 (40-100)
L-S AP	76.91	2.89 (70-82)	61.73	15.21 (40-104)	75.42	1.66 (70-80)	53.00	12.25 (40-100)
L-S lat	82.70	2.77 (77-89)	112.40	19.12 (80-165)	85.65	3.18 (80-93)	104.38	19.01 (64-158)
Pelvis AP	74.81	4.79 (70-85)	45.88	7.54 (32-64)	72.47	2.90 (67-75)	45.80	5.02 (40-52)

Patient doses and image quality

Most of the entrance skin dose (ESD) between two groups of the study were higher in the before QC group (compared median) as shown in table 8 and the bar graph figure 1.

Table 8. Shown the entrance skin dose (mGy) data were compared between before and after QC program of 8 examinations.

Types of exam.	ESD, mGy (IAEA)	ESD (mGy) Before QC group			ESD (mGy) After QC group			P ***
		Mean	Median	SD (min-max)	Mean	Median	SD (min-max)	
PNS PA	5	1.90	2.00	0.21 (1.62 – 2.27)	1.46	1.29	0.38 (1.23-2.44)	0.001
Ceph. Lat.	0.25	0.29	0.34	0.10 (0.18 - 0.35)	0.15	0.17	0.03 (0.11-0.17)	-
C sp. AP	0.25	0.18	0.17	0.09 (0.08 - 0.53)	0.12	0.11	0.03 (0.06-0.20)	0.000
Chest PA	0.4	0.17	0.18	0.04 (0.06 - 0.37)	0.14	0.12	0.09 (0.06-1.84)	0.000
Abd. AP	10	4.39	4.02	1.42 (2.67 - 8.91)	3.82	3.48	1.23 (2.02-8.81)	0.010
L-S AP	10	4.37	3.9	1.66 (1.86-10.41)	3.49	3.21	1.26 (2.08-7.91)	0.001
L-S lat.	30	11.09	10.39	3.59 (5.47-24.39)	11.15	10.39	3.68 (5.02-22.64)	0.485
Pelvis AP	10	3.12	2.4	1.37 (1.86 - 6.44)	2.90	3.06	0.84 (1.8 - 4.14)	0.326

*** *Mann-Whitney Test* (1-tailed)

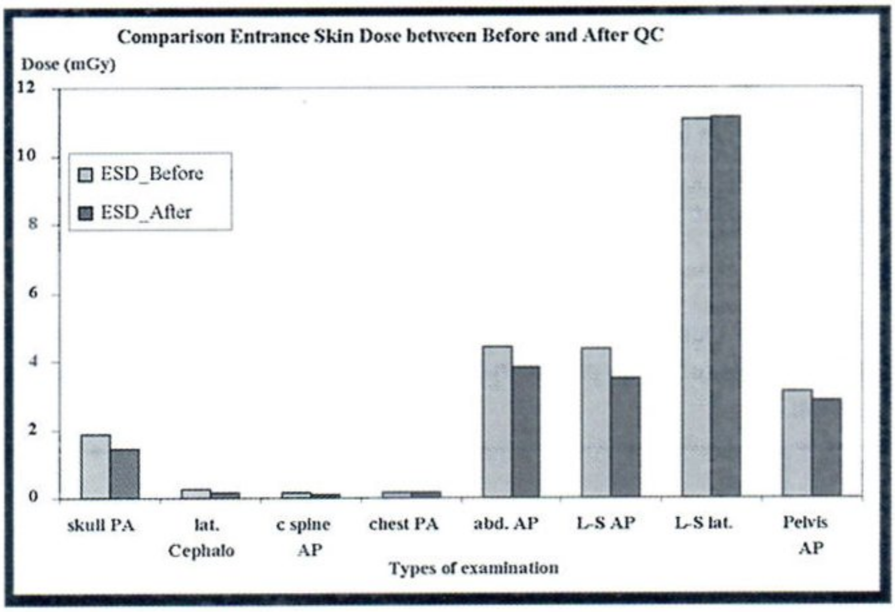

Fig.1 Bar graphs of the average entrance skin dose (mGy) were compared between before and after QC group.

Table 9. Shown the image quality data which was compared between before and after QC program of 4 examinations.

Types of exam.	Total scores	Before QC group			After QC group			
		Mean	Median	SD (min-max)	Mean	Median	SD (min-max)	*P-value*
Chest PA	**12**	9.81	10.00	1.19 (7.25 -11.75)	9.74	10.00	1.21 (7.00 - 11.50)	**0.976**
Abd. AP	**14**	11.84	12.25	1.46 (8.50 - 13.50)	11.34	11.75	1.35 (9.00 - 13.75)	**0.197**
L-S AP	**8**	5.75	6.125	1.64 (3.00 - 7.75)	5.34	5.125	1.73 (3.00 – 7.50)	**0.710**
L-S lat.	7	4.93	5.125	0.87 (3.50 - 6.25)	5.00	5.25	0.97 (3.50 - 6.50)	**0.790**
Mann-Whitney *Test* (2-tailed)								

Statistical significant of the 4 main examinations (chest PA, abdomen AP, lumbo-sacral spine AP and lateral view) were compared, the mean of image quality between two groups was shown in table 9.

Matching the major parameters of the 4 main examinations that effect to the null and alternative hypotheses which chest PA, abdomen AP and lumbo-sacral spine AP are accepted null hypotheses except lumbo-sacral spine lateral is rejected null hypotheses is shown in table 10.

Table 10 Shown the relationship between the body part thickness (cm) and BMI to the entrance skin dose (mGy) and the image quality of 4 main examinations in both groups were matched by using P value presentation.

Type of examinations	*P- value*			
	Thickness (cm)	**BMI (kg/m^2)**	**ESD (mGy)**	**Image Quality**
Chest PA	0.093	0.822	0.000	0.976
Abd. AP	0.064	0.367	0.010	0.197
L-S AP	0.065	0.243	0.001	0.710
L-S lat.	0.087	0.751	0.485	0.790

Result Comparison

A statistically significant decrease in the entrance skin dose and repeated exposures were obtained using Mann-Whitney analysis, $P < 0.05$. The recommended exposure chart was followed in the routine work. More than 95 percent of examinations for both groups did not need to be repeated, but there was less than 2 percent (10 of 692 examinations) of repeated after the quality control program applied.

Median ESD of the group data collected after implementation of QC was significant lower than the Dose Reference Level (DRL) by IAEA and NPRB.

Median ESDs of the group after implementation of QC are statistically significant lower than for the data before QC except L-S spine lateral, pelvis AP view (not significant) and cephalometry lateral view (data not consistent due to use of different technique).

ESD of room number 4 (35.9 μGy/mAs) is lower than room number 5 (41.2 μGy/mAs) at 80 kVp, large focus, at 100 cm FSD for the same exposure factors and the same condition.

There was no significant difference between the two groups ($P > 0.05$) in the image quality by the meaning of the effort to reduce the ESD.

DISCUSSION AND CONCLUSION

Two groups of patients in this study were well matched. 10 of 692 examinations were retaken when the quality control of the computed radiography system was initiated and the reject and retake rate was reduced to 1.45 percent from 3.18 percent (differentiate reduction 54.55 percent, $P < 0.05$). The entrance skin doses is reduced to 17.65 percent in chest PA view (mean, 0.17 mGy for before QC group and 0.14 mGy for after QC group) and 16.22 % for lumbo-sacral spine AP (mean, 4.37 mGy for before QC group and 3.49 mGy for after QC group) while maintaining optimum image quality. The exposure chart is implemented and applied for every examination in case of manual setting of the x-ray system. The performance of the x-ray system shows lower ESD from the system of room number 4 than the system of room number 5 for the same exposure factors and the same condition. The quality control program is used to inspect the system performance to keep it in optimal condition.

The quality control program is effective to assess the quality of the machine and predict the image quality. In order to practice the QC procedures, the phantom, the testing device, and operators are most important.

Both of the x-ray machine performances were the manual exposure factor setting that still in the acceptable range. Room number 4 x-ray machine had given the lower the entrance surface air kerma (ESAK) which correlated to the ESD than room number 5.

The computed radiography system performance was also quite good condition. The only one item that must be improved is the Moiré pattern testing because the recommended grid ratio for the bucky grid or the stationary grid should be 12:1 with lead strips at least 103 lines per inches.

RECOMMENDATION

In order to establish the first computed radiography system, the test device must be provided for the quality control program. X-ray machines with automatic exposure control (AEC) are strongly recommended to optimize radiation dose to the patient. For the manual setting x-ray machine, the detailed exposure factor chart must be strictly used in order to keep the ALARA (As Low As Reasonably Achievable) rule. Continuous training is scheduled for the quality improvement for the new technology in order to improve and increase the competence of the radiological technologists working with the digital modalities.

This study is part of Coordinated Research Project (CRP) of International Atomic Energy Agency (IAEA) title "Variation of post processing parameters for the improvement of the Computed Radiography image quality and the patient dose reduction" for the year 2002 - 2005. The authors acknowledge the contribution from the section of Patient Protection Department of Human Health, IAEA to make this study firstly established in Thailand.

REFERENCES

1. Willis CE. 10 Fallacies about CR. Journal of Imaging Technology Management December 2002: 1-6.
2. Reiner B, Siegel E. Putting the quality back into QA without the headaches. insights & images 2003: 5-8.
3. Williams J.R, Catling MK. Short communication, An Investigation of x-ray equipment factors influencing patient dose in radiography. BJR 1998; 71: 1192-8.
4. Polunin N, Lim TA, Tan, KP. Reduction in retake rate and radiation dosage through computed radiography. Annual Academy of Medicine, November 1998; 27(6): 805-7.
5. Artz DS. Computed radiography for radiological technologists. Semin Roentgenol 1997; 32: 12-24.

6. Weatherburn GC, Bryan S, West M. A comparison of image reject rates when using film, hard copy computed radiography and soft copy imaged on picture archiving and communication systems (PACS) workstations. BJR 1999; 72: 653-60.
7. Murphet MD, Quale JL, Martin NL, Bramble JM, Cook LT, Dwyer SJ. Computed radiography in musculoskeletal imaging. AJR Am J Roentgenol 1992;158:19-27.
8. Bowman JE. The future is now: digital radiography. Bytes Imaging's Future 1998; 30: 12-5.
9. Weatherburn GC, Bryan S, Davies JG. Comparison of doses for bedside examinations of the chest with conventional screen-film and computed radiography: results of a randomized controlled trial. Radiology 2000; 217: 707-12.
10. Cesar LJ, Schueler BA, Zink FE, Daly TR, Taubel JP, Jorgenson LL. Artifacts found in computed radiography. BJR 2001; 74: 195-202.
11. Committee 3 of the International Commission on Radiological Protection (ICRP). Diagnostic reference levels in medical imaging: Review and additional advice, 2001.
12. Clark RH, Dunster HJ, Guskova AK, et al. Annual of the ICRP publication 60. 2nd ed. Oxford: Pergamon Press, 1991.
13. Pasad. Report of Radiographic System Performance. ENH 2000:1-6.
14. Seibert JA, Bogucki TM, Ciona T, et al. Acceptance testing and quality control of photo stimulable phosphor imaging systems report of Task Group 10 American Association of Physicists in Medicine. AAPM Task Group 10 version 3.1, October 1997:1-56.
15. Protocol for the QA of Computed Radiography System Commissioning and Annual QA Tests, KCARE CR QA Protocol Draft 4.0. Kings College Hospital, March 2003: 1-14.

EVALUATION OF DOSIMETRIC EFFECT OF RESPIRATORY GATING ON LUNG IMRT DELIVERY

Taweap SANGHANGTHUM, M.Sc.,[1] Sivalee SURIYAPEE, M.Eng.,[2] Sornjarod OONSIRI, M.Sc.,[1] Chotika JUMPANGERN, M.Sc.,[1] Isra ISRANGKUL-NA-AYUTHAYA, M.Sc.,[1] Puntiwa INSANG, M.Sc.[1]

ABSTRACT

Purpose: For treatment of 3 dimensional conformal or intensity modulated radiation therapy (IMRT) of lung cancer, it is essential that respiratory gating is used to reduce the margins of clinical target volume (CTV). In this study, we evaluate the accuracy of dose in gated-IMRT when dynamic multileaf collimator (DMLC) mode was selected.

Materials and Methods: The Real-time Positioning Management (RPM) respiratory gating was installed on General Electric computed tomography (CT) simulator to view the movement of tumor and the other one gating on Varian Clinac 23 EX linear accelerator to deliver the dose at selected phases of breathing. The beam intensities of IMRT are varied by using DMLC which this mode of MLC may be introduced the dose errors from leaf lag and this error may be exacerbated when the gating is used. The 1 cm leaves gap and wedge shape patterns were created by using MLC shaper software to verify the accuracy of dose in gating method. These patterns were compared between gated and nongated delivery at 300 monitor unit/min dose rate and 1.25 cm/s leaves speed. For gated delivery, the mechanical motion device which Varian supplied was placed nearby the solid water phantom to simulate the breathing motion. Kodak X-Omat Verification (XV) film was employed to measure dose distributions of these patterns, while enhance dose range (Kodak EDR2) film and 0.13 cm3 ionization chamber with DOSE1 dosemeter were used for a lung IMRT pre-treatment verification. OmniProTM I'mRT software was the tool to analyze the film, 3% dose difference at low dose gradient region and 3 mm distance of isodose difference at high dose gradient region (3/3) were set in the clinical criteria for quantitative evaluation of dose distributions.

Result: The Kodak X-Omat V films of a 1 cm wide leaf gap sliding across a 10 cm wide field of undergated and nongated showed the uniform dose distribution across the field. The comparison of central axis profile was almost congruent and there are a few area that 3/3 is higher than unity. For 14x14 cm^2 wedge field, no gamma value higher than unity appeared, while the isodose comparison also well result. In case of lung IMRT QA, the ratio of point dose from chamber between gated and nongated was 1.0033 which is so minute discrepancy. EDR2 film confirmed the impression result because it showed small area that $\gamma_{3/3}$ larger than unity and isodose lines of both gated and nongated were nearly congruent too.

CTV = Clinical Target Volume
DMLC = Dynamic Multileaf Collimator
RPM = Real-time Positioning Management
IMRT = Intensity Modulated Radiation Therapy

[1] Department of Radiology; King Chulalongkorn Memorial Hospital, Bangkok, Thailand
[2] Department of Radiology; Faculty of Medicine, Chulalongkorn University, Bangkok, Thailand

Conclusions: For moderate dose rate of 300 MU/min, the dosimetric difference between with and without gated DMLC deliveries was so small. So, the repeat beam-on and beam-off from Real-time positioning management (RPM) gating have insignificant impact on the dosimetry of DMLC-IMRT.

INTRODUCTION

Intensity modulated radiotherapy (IMRT) is a state-of-the-art cancer treatment method that delivers high doses of radiation to cancer cells while sparing the surrounding healthy tissue. The dynamic multileaf collimator (DMLC) is one of the IMRT delivery mode in which the leaves continuously move and shape the beam intensity while the radiation is turned on.

Intrafraction motion is one type of organ motion that is so influential in the treatment technique of IMRT and image guide radiotherapy (IGRT). This type of motion can be caused by three main systems that are the respiratory, skeletal muscular, cardiac and gastrointestinal system but the most significant is the first one because the respiratory motion is one potential source of error in radiotherapy.[1] During normal respiration, internal anatomy motion can be significant in some instances up to several centimeters[2] especially in lung tumor. Bernes et al.[3] found the average motion of tumor in the lower lung lobe to be significantly greater than other lobes (18.5 mm vs 7.5 mm average superior/inferior direction).

Respiratory gating is a new technique in radiation therapy (4D radiotherapy; time is the 4^{th} dimension in radiotherapy) where the radiation is selectively at a moving target as a patient breath. The goal of this technique is to reduce the motion by synchronizing the dose delivery from a treatment accelerator with patient breathing so the clinical target volume (CTV) to planning target volume (PTV) margins for treatment planning should be reduced too. Controlling the motion of tumor may improve the precision of the dose delivery, thereby sparing more normal tissue complication probability. Paul JK et al[4] founded that dosimetric reductions for the cord, heart, and lungs were found for 4D planning compared with 3D planning. The principle of respiratory gating technique is to deliver radiation in a small window of each gating cycle at the phases where tumor moves so less. Alternative methods to reduce respiration induced motion include deep inspiration breath hold (DIBH),[5] active breathing control (ABC) with airflow valves,[6] and the use of abdominal pressure.[7] Xia et al[8] studied the communication lag between treatment console and MLC workstation in IMRT technique. They founded that DMLC increases the dose variations at high dose rate and low monitor unit.

The operation of linear accelerators in conjunction with DMLCs has been extensively studied. Jun Duan et al[9] studied about the effect of leaf lag, a delay in the communications between the DMLC and the accelerator, on the accuracy of dose delivered in gated IMRT at various respiratory rate, dose rate, and leaf speed. The results showed that low dose rates, slow leaf speeds and low frequencies of beam interruptions reduce the effect of delay-and-catch-up cycle. The purpose of this study was to investigate the dosimetric effect of DMLC on gated and nongated delivery at 300 MU/min which is the dose rate used to treat all the patients.

MATERIALS and METHODS

A Varian Clinac 23 EX linear accelerator (Varian Medical Systems, Palo Alto, CA) with 120 leaves was employed in this study. The width of leaves is 5 mm at the central 20 cm and 1 cm at the 10 cm outer of each side for the maximum field size of 40x40 cm^2. This machine can use the MLC in both segmented multileaf collimator (SMLC) mode and dynamic multileaf collimator (DMLC) mode but the latter one was chosen for IMRT treatment in our institute and in this study also. The delay between the accelerator and DMLC was reported to be 50 to 80 ms.[10] The limitation of our leaf speed is set at 2.5 cm/

s and the leaf position tolerance at isocenter is set at 0.05 cm following the recommendation of Varian Company.

The Real-Time Position Management (RPM) Respiratory Gating System (Varian Medical Systems, Palo Alto, CA) consists of (a) a wall-mounted infrared illuminator and charge-coupled device camera; (b) a reflective external marker placed on the patient's chest or abdomen; (c) a PC workstation to process the patient breathing signals; and (d) a trigger to the linear accelerator or CT simulator as shown in figure 1.

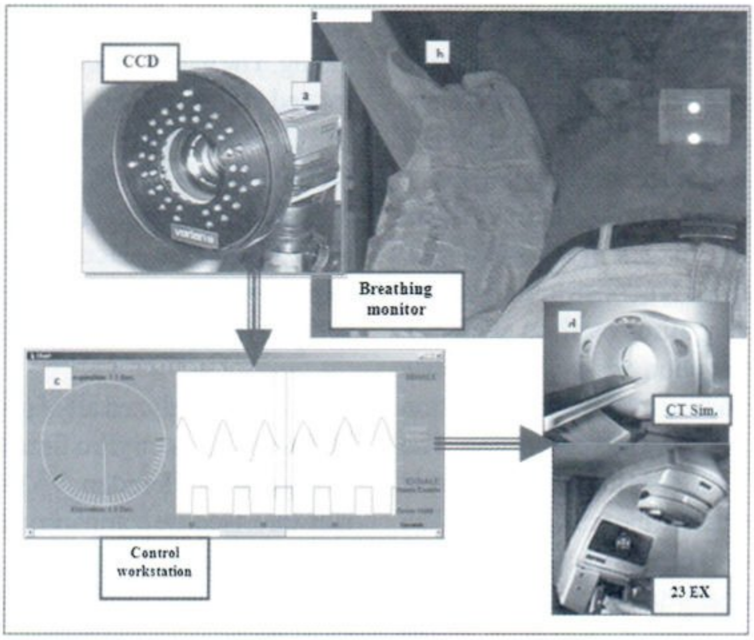

Fig. 1 A pictorial schematic of the functioning of the Varian RPM system.

To evaluate the accuracy of dose of the respiratory gating system, we divided our experimental into to 3 parts.

First, the DMLC pattern was made by the 1 cm wide leaf gap sliding across a 10 cm wide field. This DMLC file was generated by MLC shaper software that supplied from Varian. Fifty-six monitor unit (MU) was exposed at 300 MU/min, this dose rate corresponds to 1.25 cm/s DMLC leaf speeds.

Second, the pattern was made by the 14 cm wide wedge field shaped by opening leaf gap in DMLC mode. Forty MU was delivered to our detector in order to get the leaf speed at 1.25 cm/s also. Kodak X-Omat V (XV), Eastman Kodak Company, Rochester, NY, was used as a film dosimetry to measure the dose distributions in planar plane for both 1 cm wide leaf gap and wedge field shaped. Dose delivered to the rectangular solid water phantom at 5 cm depth with source-to-axis -distance technique between gated and nongated were compared. For gated delivery, however, we do not have a moving phantom to simulate the patient breathing. So, we applied a mechanical motion device with the infrared reflective marker box which Varian supplied as part of its' RPM system to use in this experimental. This device was placed near the stationary solid water phantom and moves sinusoidally in cranio-caudal direction.

Finally, we used the IMRT plan of lung cancer patient to verify the accuracy of dose distribution for gating method. A patient in this study is a 61-year-old male with the diagnosis of stage I T2N2M1 non-small lung cancer thigh metastasis. At the time of simulation, patient was immobilized in the supine position on a Vac-Loc (Med Tech Inc., Orange City, IA) with his arm raised over his head. The video camera tracks respiratory motion by monitoring the markers that were attached halfway between the xiphoid tip and the umbilicus of patient. The corners of the block were then drawn by permanent ink on the skin to ensure reproducible positioning of the block during the remainder of the simulation during all treatments. A GE LightSpeed RT CT simulator (GE Medical Systems, Milwaukee, WI) was used to scan in cine mode with retrospective gating. The gating system sends the patient breathing signal to Advantage 4D software in order to synchronize this signal with CT images. Advantage 4D software showed the movement of tumor volume on CT images in all directions. Figure 2 shows the scan and reconstruction of this patient in retrospective gating method with CT simulator machine. The duration of x-ray in ON mode is equal to the average breathing cycle plus the duration of data acquisition for an image reconstruction. The duration of x-ray in OFF mode is the period for table translation from one position to the next position. The gating system provides two modes of operation, base either on the phase of breathing cycle or on the trace amplitude. Phase-based gating was chosen and we divided the images to 10 phases (peak inhale = 0% phase, peak exhale = 50% phase). Maximum intensity projection (MIP) images were created from Advantage 4D software then these MIP images were exported to Eclipse planning software to be used for IMRT planning. At the linear accelerator machine, the gating system sends the gating signal to the machine to trigger beam hold-off when the target volume moves beyond the preset limits. The treatment phases were selected by the radiation oncologist. For this case, the 30%-80% phases were selected because the end-expiration is more reproducible than inspiration. Pre-treatment IMRT verification plans were performed by using extended dose range 2 (EDR) film and ion chamber in solid water phantom both with and without gating. The gantry, collimator, and couch angles were rotated to zero degree. A 0.13 cm^3 ionization chamber (IC 13, Scanditronix Wellhofer, Schwarzenbruck, Germany) was placed at 10 cm depth for point dose measurement using with DOSE1 dosemeter while a EDR2 film was placed at isocenter point of 5 cm depth for planar dose measurement as shown the setup in figure 3.

We analyzed all of our films by using a Vidar VXR-16 DosimetryPro film digitizer (Vidar Systems Corporations, Herndon, VA) and OmniProTM I'mRT software. Isodose comparison for the dose distributions between gated and nongated was evaluated. Moreover, gamma (γ) was used for quantitative comparison. Gamma is an index proposed by Low et al.[11] for quantitative evaluation of dose distributions. γ3/3 (3% dose difference at low dose gradient region and 3 mm distance of isodose difference at high dose gradient region) was set in the clinical criteria. The area that γ value was higher than unity means that the dose different between gated and nongated is out of the criteria.

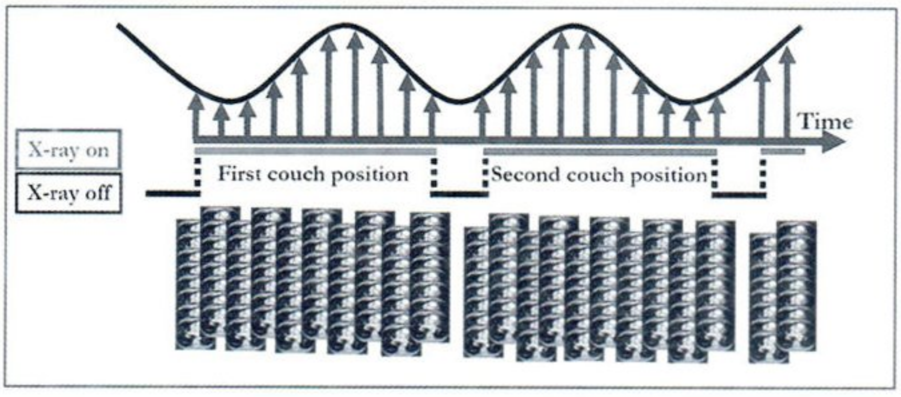

Fig.2 The scanning and image reconstruction of 4D CT in retrospective method.

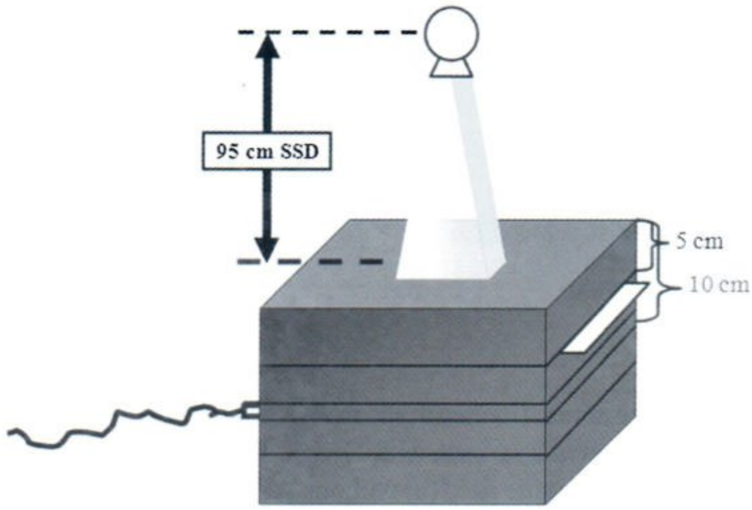

Fig.3 The phantom setup for pre-treatment IMRT verification.

RESULTS AND DICUSSION

The dose error by respiratory gating depends on several factors such as the respiratory rate, dose rate, or leaf speed but in this experiment we studied at only dose rate of 300 MU/min. For the DMLC mode, when the beam is turn on, the leaves are not move immediately but their remains stationary and then moving accelerate to their leaves speed. While the beam off trigger by gating, the leaves do not stop instantly but they also moving forward decelerate to stop. When the beam is on again, the leaves starting from the position where they are overdue.

The dose distributions in this experiment are shown in figure 4. Its comprise of a) 1 cm gap sliding across a 10 cm wide, b) 14x14 cm^2 opening wedge, and c) lung IMRT plan.

Fig.4 a,b,c Fluence maps from treatment planning of a) 1 cm wide DMLC leaf gap sliding across a 10 cm wide field, b) 14 cm wide opening wedge field, and c) lung IMRT field.

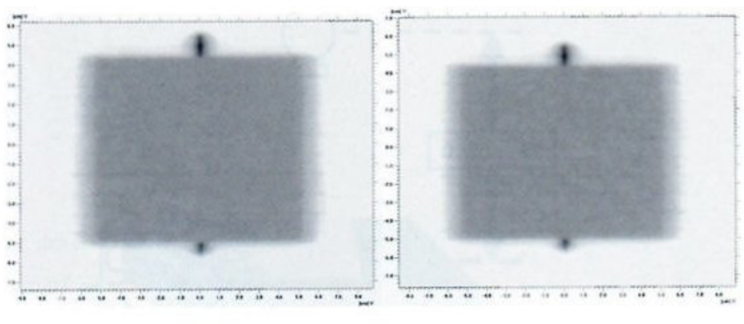

a b

Fig.5 The actual fluence maps from Kodak X-Omat V films delivered by a 1 cm wide DMLC leaf gap sliding across a 10 cm wide field (a) without and (b) with gating of 30 -80% phases.

Figure 5 shows the actual fluence maps of a 1 cm wide DMLC leaf gap sliding across a 10 cm wide field on Kodak X-Omat V films by (a) nongated and (b) gated deliveries at a dose rate of 300 MU/min and a leaf speed of 1.25 cm/s after 40 MU exposed. Both films show the uniform dose distribution across the field. Dose profiles along the midline across these two plans are shown in figure 6. The red line represents of without gate delivery while green one means gate delivery. The doses without gated were normalized to central axis. The profiles are nearly congruent while the γ3/3 shows so less gamma value higher than unity.

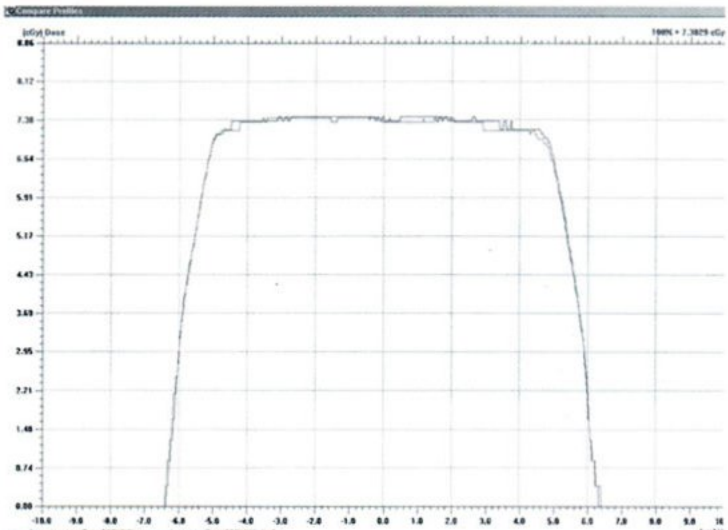

Fig.6 Dose profile comparison between gated and nongated at the center of field across the beams in Fig. 5.

The results of 14x14 cm^2 single wedge shapes between gated and nongated delivery are shown in figure 7. Left upper quadrant is the fluence from XV film of 14x14 cm^2 wedge fields for nongated delivery, left lower quadrant is under gated delivery, right upper quadrant shows isodose comparison between these fluences, and the last quadrant shows the gamma value with the limit of 3% dose difference and 3 mm distance. It will appear as a dot if gamma value is not in a limit (the value greater than1). Fifty-six MU was delivered at 300 MU/min which this dose rate is correspond to 1.25 cm/s DMLC leaf speeds. A 15 cycles/min respiratory rate and 1.0 sec gating window that center at the end of expiration were used in gated delivery. Isodose distributions of gated beam are overlain on those with nongated beam to check the dose differences. The dose discrepancy between them is very small as shown in isodose comparison and no γ3/3 values higher than unity.

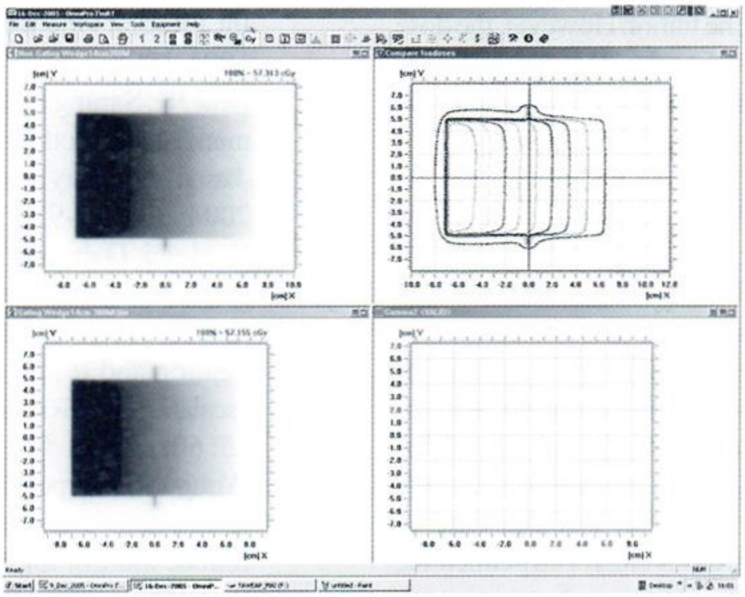

Fig.7 OmniProTM I'mRT software for film analysis and comparisons.

The lung IMRT field presented in figure 8 demonstrates the difference between IMRT dose distributions delivered at 300 MU/min to a solid water phantom on gated and non gated. Isodose distributions delivered on gated and nongated were overlain for comparison. Solid lines represent isodose lines for nongated delivery and dashed ones for gated delivery. These data were measured by using the EDR film for planar dose verification and the ion chamber for point dose verification. For planar dose measurement, the γ3/3 showed very minute value higher than unity that is congruent of these isodose lines. For point dose measurement, the dose from chamber of gated and nongated are 171.87 and 171.31 cGy, respectively, while from planning is 175.8 cGy.

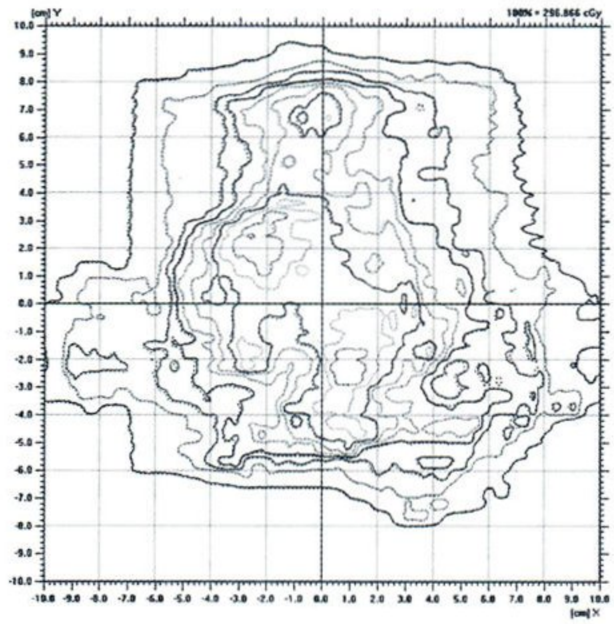

Fig.8 Isodose overlaying of a lung IMRT field delivered to a solid water phantom between under respiratory gating (solid lines) and no respiration gating (dashed lines).

For lung tumor patient, the respiration during radiation treatment may be induced tumor movement. Adequate margins must be established around the CTV to account for tumor motion but the normal surrounding tissues are increasing irradiated. The use of the RPM gating system significantly reduced the size of the margins by turning the beam on and off based on the motion of the tumor. However, the dose errors may be occurred when the DMLC is used and these errors may be exacerbated when the gating is used due to delay-and-catch up phenomenon.

CONCLUSION

The fluence of 1 cm leaf gap across 10 cm on film should be shown the pattern of cold strips in every step that the beam is on. Figure 5 And figure 6, however, show the smoothing fluence across the film and congruence of beam profiles, it can be noted that error of dose at 300 MU/min dose rate at 1.25 cm/s leave speed is insignificantly. For the case of wedge-shaped, this pattern is clearer explained the delay-and-catch-up phenomenon because each position has the difference dose. Anyway, in this study, the data shows satisfied result as presented in figure 7. Therefore, the dose distribution in gated delivery agrees with a reference dose distribution in nongated delivery within the clinical criteria. The results are confirmed again by clinical IMRT results as shown in planar and point dose measurements. Lung IMRT fields are generated by sweeping leaf gaps across the field, requiring both banks to move. The ratio of dose from ionization chamber between gated to nongated deliveries is 1.0033 that is very small dose discrepancies due to lags of the leaves.

In summary, the dose rate of 300 MU/min that we used seems to be a good compromise so that the leaf lag has no effect to the isodose distribution.

REFERENCES

1. Paul JK, Gig M, et al. Managing Respiratory Motion in Radiation Therapy, Report of AAPM Task Group 76; 2004: 1-16.
2. Kubo HD and Hill BC. Respiration gated radiotherapy treatment: A technical study. Phy Med Biol 1996; 41: 83-91.
3. Barnes EA, Murray BR, Robinson DM, et al. Underwood LJ, Hanson J and Roa WH, Dosimetric evaluation of lung tumor immobilization using breath hold at deep inspiration. Int J Radiat Oncol Biol Phys 2001; 50(4): 1091-1098.
4. Paul JK, Sarang J, Radhe M, et al. Four-dimensional radiotherapy planning for DMLC -based respiratory motion tracking. Med. Phys. 2004; 32: 942-951.
5. Hanley J, Debois MM, Mah D, et al. Deep inspiration breath hold technique for lung tumors: The potential value of target immobilization and reduced lung density in dose escalation. Int J Radiat Oncol Biol Phys 1999; 45: 603-611.
6. Wong JW, Sharpe MB, Jaffray DA, et al. The use of active breathing control (ABC) to reduce margin for breathing motion. Int J Radiat Oncol Biol Phys 1999; 44: 911-919.
7. Li XA, Stepaniak C, and Gore E. Technical and dosimetric aspects of respiratory gating using a pressure-sensor motion monitoring system. Med Phys 2006; 33: 145-154.
8. Xia P, Chuang CF, and Verhey LJ. Communication and sampling rate limitations in IMRT delivery with a dynamic multileaf collimator system. Med Phys 2002; 29: 412-423.
9. Duan J, Shen S, Fiveash JB, et al. Dosimetric effect of respiration-gated beam on IMRT delivery. Med Phys 2003; 30: 2241-2252.
10. Litzenberg DW, Mooran JM, and Fraass BA. Incorporation of realistic delivery limitations into dynamic MLC treatment delivery. Med Phys 2002; 29: 810-820.
11. Low DA, Harms WB, Mutic S, and Puedy JA. A technique for the quantitative evaluation of dose distributions. Med Phys 1998; 25, 656-661.

PREOPERATIVE CT SCAN TO PREDICT ORBITAL INVASION BY PARANASAL SINUS CANCER

Pipat CHIEWVIT,[1] PHAWIN KESKOOL,[2] Kanograt PORNPANICH,[3] Kullathorn THEPHAMONGKHOL[1]

INTRODUCTION

Paranasal sinus (PNS) cancers are relatively uncommon. They present late in their course of disease nature, often with extensive disease. The standard treatment of PNS cancer is surgical resection. Extension to the orbit has an impact on patient prognosis and the surgical approach of these tumors. If orbital invasion is suspected, the surgeon and the patient are confronted with the difficult decision of orbital exenteration. Orbital exenterention is required for complete tumor resection but can be emotionally traumatic for patients and bring major change in their life. The difficult decision regarding the eye cannot be made on the basis of ophthalmic symptoms alone. Most surgeons (otolaryngologist) at our institute uses computerized tomography (CT scan) for preoperative evaluation for cancer extension including orbital invasion. Basically, if CT imaging found the mass from sinuses continuity and/or breaking bony orbit, the diagnosis of orbital invasion was not difficult. In cases in which the clinical examination and imaging are unclear, preoperative patient counseling regarding the eye is complex. A more accurate assessment of orbital invasion preoperatively would benefit both the surgeon and the patient. In addition, accurate preoperative assessment is mandatory for surgical planning. Most surgeons use the relationship between the tumor and the periorbital areas to determine whether orbital exenteration is necessary or not. Tumor invasion through the periorbital areas may warrant exenteration, whereas intact periorbital areas typically warrants preservation. When tumor abuts the periorbital areas however, assessing periorbital invasion may be difficult.

OBJECTIVE

The purpose of this study was to determine whether preoperative CT scan could offer an accurate assessment of cancer extension to the orbit. Involvement of the orbital fat manifested as soft tissue stranding in the fat is the current imaging criterion suggestive of neoplastic invasion. However, the accuracy of this criteria to predict invasion into the orbit is poorly studied. In this study we establish various criterias for predicting orbital invasion, then evaluate the accuracy of the CT scan criterias in predicting cancer invasion to the orbit.

MATERIALS AND METHODS

A retrospective study was performed involving all patients who were diagnosed paranasal sinus cancer at Siriraj hospital, by ICD 10 coding C31, from January 1995 to December 2004. Patients were undergone major operations with curative intent such as maxillectomy, ethmoidectomy or wide excision. By these criterias, there were 34 patients (23 male and 11 female) included in this study.

Of those patients, preoperative CT scans of the paranasal sinuses and operative records were re-

[1] Department of Radiology,
[2] Otolaryngology and
[3] Ophthalomology, Faculty of Medicine Siriraj Hospital, Mahidol University, Bangkok 10700, Thailand.

quested to diagnose periorbital invasion. Patients were excluded from the study if preoperative CT scan and operative record were not available or operative record was not adequate for assessing periorbital involvement. By these exclusion criterias, patients during the year 1995 to 2001 were excluded because of unavailable CT scan.

Finally, there were 9 patients (6 male, 3 female) with 10 operations between 2002 to 2004 were included in this study. Note that a male patient was performed 2 operations in 2 different episodes.

Nine CT criterias for early diagnosed tumor invasion to orbit were used to assess each patient. Two criterias were the tumor's relationship to the periorbital areas i.e. tumor adjacent to the periorbital[1] and periorbita displacement.[2] One was for extraconal fat invasion, characterized by soft tissue stranding or infiltration within the extraconal fat contiguous with the primary tumor.[3] Four criterias were corresponded to extraocular muscle (EOM) i.e. EOM displacement,[4] EOM enhancement as compared with other normal EOM,[5] EOM enlargement[6] and EOM abnormal density.[7] The two other criterias were nodular tumor interface with orbit[8] and lytic bone.[9]

One consultant neuroradiologist interpreted CT scan following the mentioned 9 items as either positive or negative without intraoperative informations.

Gold standard of positive periorbital involvement is it's involvement seen intraoperatively Data analyses were done by describtive method because of small population.

EOM = Extra Ocular muscle

RESULTS

During January1995 to December 2001, there were 4 positive surgically confirmed cases of orbital invasion by paranasal sinus cancers without preoperative CT scan available because our hospital, during that time, did not collect any film of patient with no follow up more than 5 years or they are lost because of other reasons. So only 10 operations of 9 patients during 2002 to 2004 were included in this study. Note that one patient were done 2 operations at two different times.

Table 1 Patients of paranasal sinus cancer who were undergone operation between 1995-2004.

year	n	male	female	Periorbital invasion
1995	3	2	1	1
1996	4	2	2	1
1997	10	7	3	1
1998	-	-	-	-
1999	3	3	0	1
2000	3	1	2	0
2001	1	1	0	0
2002	5	3	2	1
2003	4	3	1	0
2004	1	1	0	0
total	**34**	**23**	**11**	**5**

Of the included 10 operations, there was only one patient (patient no.3) who had intraoperatively proven orbital invasion by paranasal sinus cancer. This case had frontal sinus carcinoma with intraoperatively comfirmed tumor invasion through the periorbital to the right orbit. This case is the only one that orbital exenteration was done.

Table 2 The results of CT scan interpretation criterias for orbital invasion by paranasal sinus cancer in 10 patients during 2002-2004.

Patient No.	No. 1	No 2	No. 3	No. 4	No. 5	No. 6	No. 7	No. 8	No. 9	No. 10
1.Tumor adjacent to the periorbital	Y	Y	Y	Y	Y	Y	Y	Y	Y	Y
2.Periorbital displaced	Y	Y	Y	Y	Y	Y	Y	Y	N	Y
3.Extraconal fat involvement	Y	Y	Y	Y	N	Y	N	Y	N	N
4.EOM displaced	N	Y	Y	Y	N	Y	N	N	N	N
5.EOM abnormally enhanced	N	Y	Y	Y	N	N	N	Y	N	N
6.EOM enlarged	N	N	Y	Y	N	N	N	N	N	N
7.EOM abnormal density	N	Y	Y	Y	N	N	N	N	N	N
8.Nodular tumor interface with orbit	Y	Y	Y	Y	N	Y	N	Y	N	Y
9.Lytic bone	Y	Y	Y	Y	Y	Y	Y	Y	N	Y

Y = yes or positive, N = no or negative EOM = Extra Ocular Muscle

Pathological reports of cancer cell types could be found in 32 of 34 cases during the entire length of study between 1995 to 2004. No pathological or surgical report was found in two cases. Squamous cell carcinoma is the most frequent cancer cell type, demonstrated in 20 of 32 cases.

Adenoidcystic carcinoma and undifferentiated carcinoma were the second most common in this study, both were shown by 4 from 20 cases. Only one case for each was found, i.e. neuroendocrine tumor, malignant fibrous histiocytoma, squamous hyperplasia and adenocarcinoma.

The paranasal sinuses, most frequently involved by cancer in this study, of the 34 cases, 32 cases were maxillary sinuses and the other two, each one for ethmoid and frontal sinuses. If considering only pathological available cases, thirty are of maxillary sinuses and each one for ethmoid and frontal sinus.

Among 32 maxillary sinus cancer, the most common cell type is squamous cell carcinoma found in 19 cases, adenoidcystic carcinoma in 4 cases, undifferentiated carcinoma in 3 cases and each one for neuroendocrine tumor, malignant fibrous histiocytoma, squamous hyperplasia and adenocarcinoma.

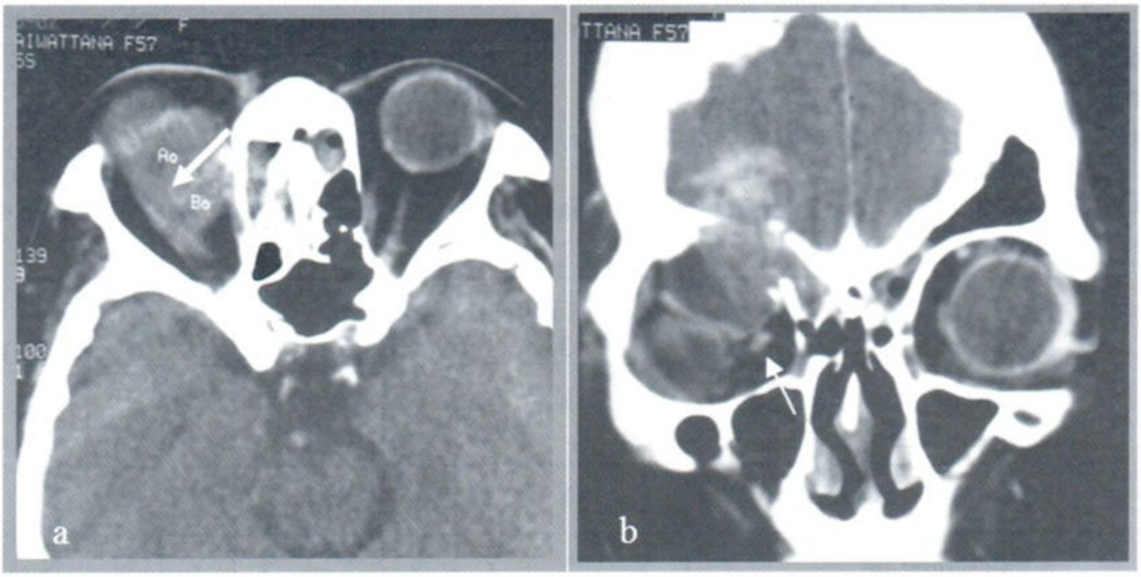

Fig.1 Patient no.3 who had right frontal sinus squamous cell carcinoma with intraoperatively confirmed periorbital invasion. Axial scan (a) shows medial rectus displacement (thick arrow). Coronal scan (b) shows bony destruction at the roof and superomedial right orbit, medial rectus enlargement (thin arrow) and inferolaterally displaced eye ball.

Patient no.3 was the only one who had operatively confirmed periorbital rupture indicating orbital invasion. This case was positive in every criterias especially extraocular muscle enlargement (see figure 1).

Extraocular muscle enlargement is the criteria that is least interpreted positive. Only 2 cases (patient no.3 and 4) were positive by this criteria.

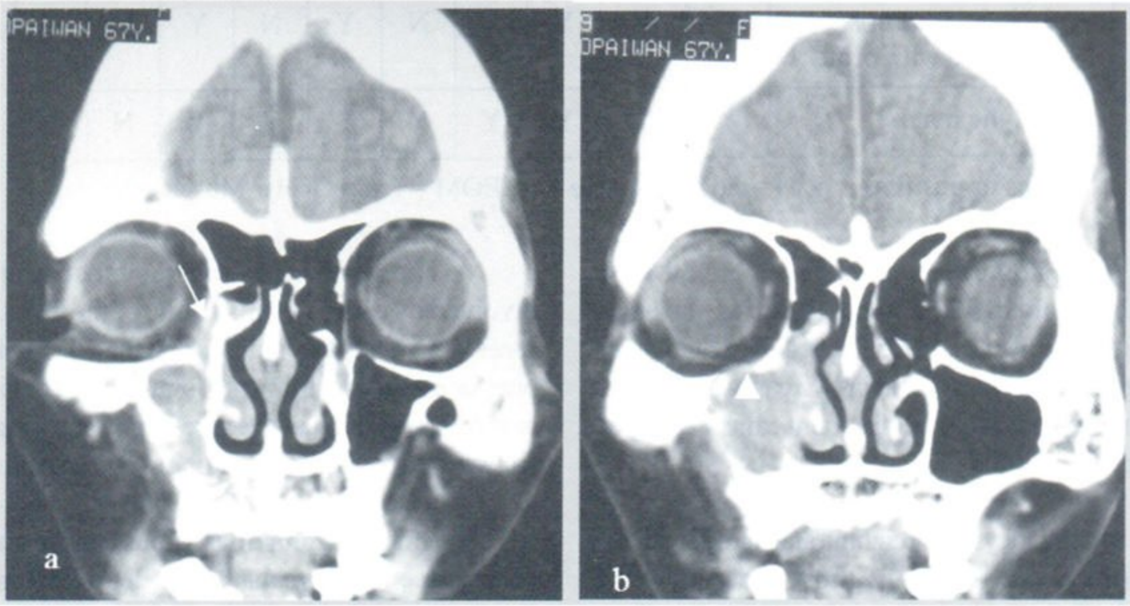

Fig.2 Patient no.1 who had right maxillary sinus squamous cell carcinoma with intraoperatively confirmed intact periorbital. Coronal scan (a) shows periorbital displacement (arrow). Picture b shows bony dehiscence (arrow head). This patient was lack of EOM criterias.

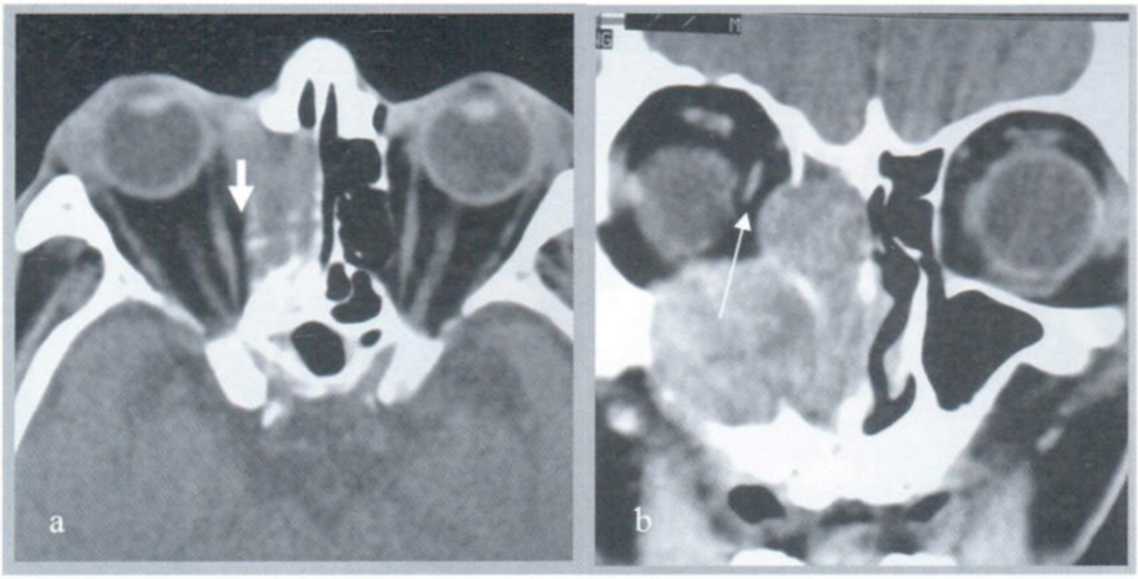

Fig.3 Patient no.2 who had squamous cell carcinoma of the right maxillary sinus with positive in all criterias except extraocular muscle enlargement. Axial scan (a) shows periorbital bow laterally and extraconal fat involvement (thick arrow) but lack of extraconal muscle enlargement. Coronal scan (b) shows lytic bony orbit inferiorly and medially and extraocular muscle displacement (thin arrow). This patient showed intact periorbital intraoperatively.

Fig.4 Patient no.4 who had right maxillary sinus squamous cell carcinoma. This patient's scan were interpreted positive in all criterias but intraoperation showed intact periorbital.

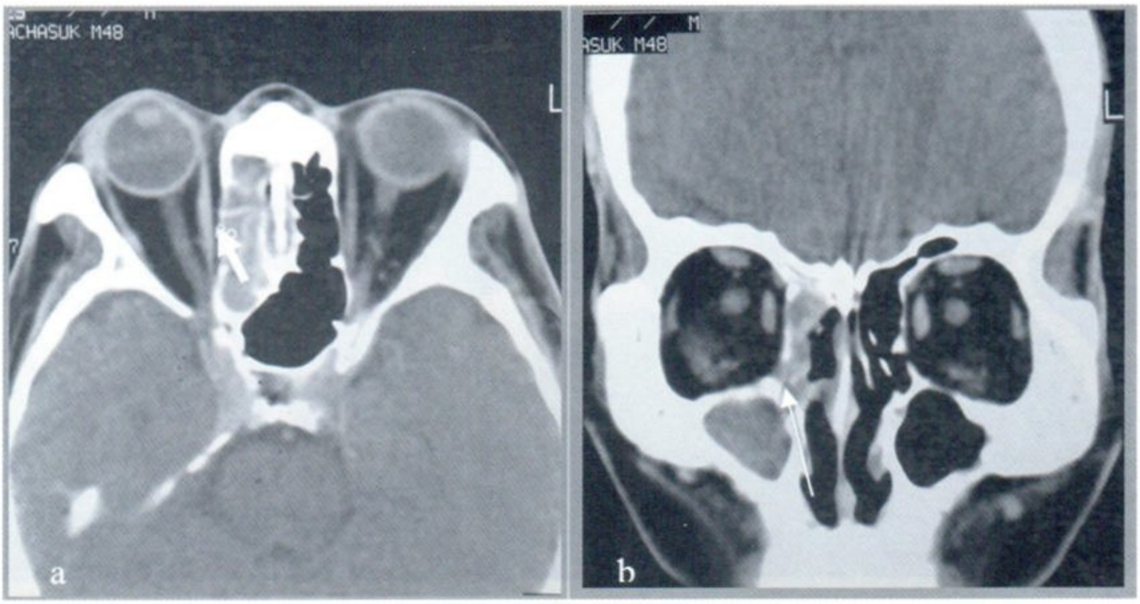

Fig.5 Patient no.5 who had right maxillary squamous cell carcinoma with intact periorbital seen intraoperatively. Axial scan (a) shows tumor adjacent to the periorbital and periorbital displacement (thick arrow). Coronal scan (b) shows tumor mass in right maxillary sinus and bony dehiscence (thin arrow).

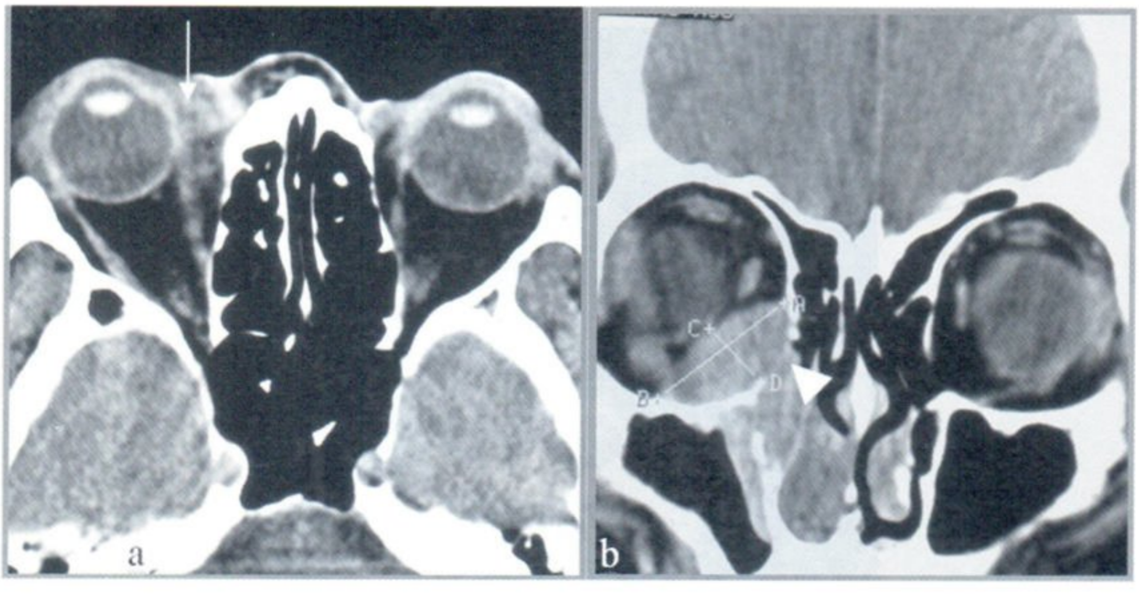

Fig.6 Patient no.6 who had right maxillary undifferentiated carcinoma. Axial scan showed tumor mass adjacent to periorbita (arrow). Coronal scan (b) shows bony orbit inferomedially dehiscence, periorbita bowed laterally and extraconal muscle displacement (arrow head). This patient showed intact periorbital intraoperatively.

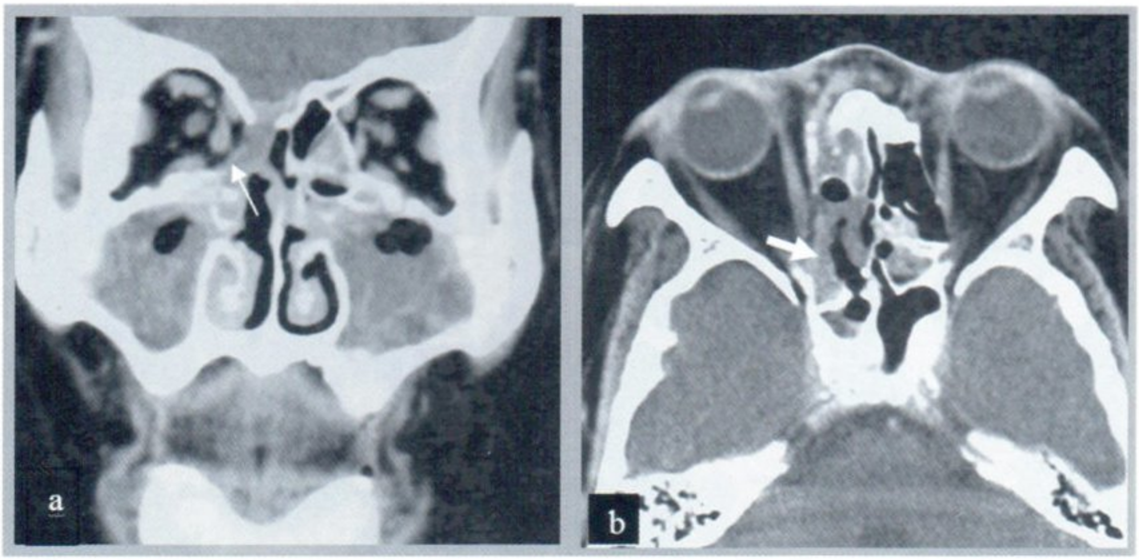

Fig.7 Patient no.7 who had right ethmoid and frontal squamous cell carcinoma. Coronal scan (a) shows periorbita displacement and bony dehiscence (thin arrow). Axial scan (b) shows tumor mass in right ethmoid sinus with bony dehiscence (thick arrow). This patient was lack of EOM displacement, enhancement, enlargement or abnormal density.

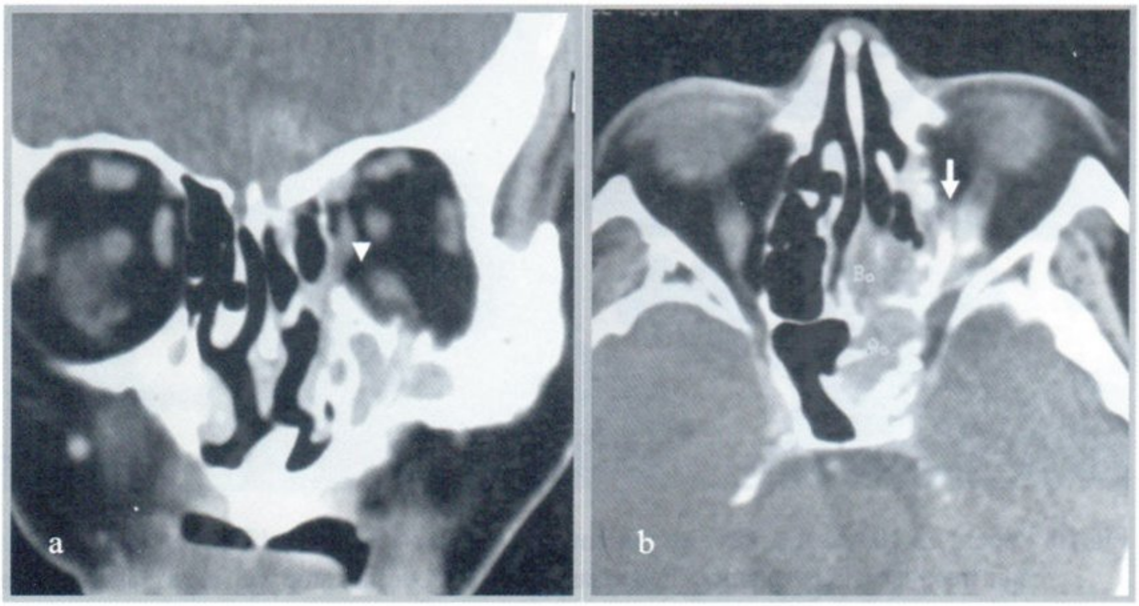

Fig.8 Patient no.8 who had left ethmoid squamous cell carcinoma with intact periorbita shown intraoperatively. Coronal scan (a) shows left medial rectus muscle displacement (arrow head). Axial scan (b) shows bony dehiscence and extraconal fat involvement (arrow).

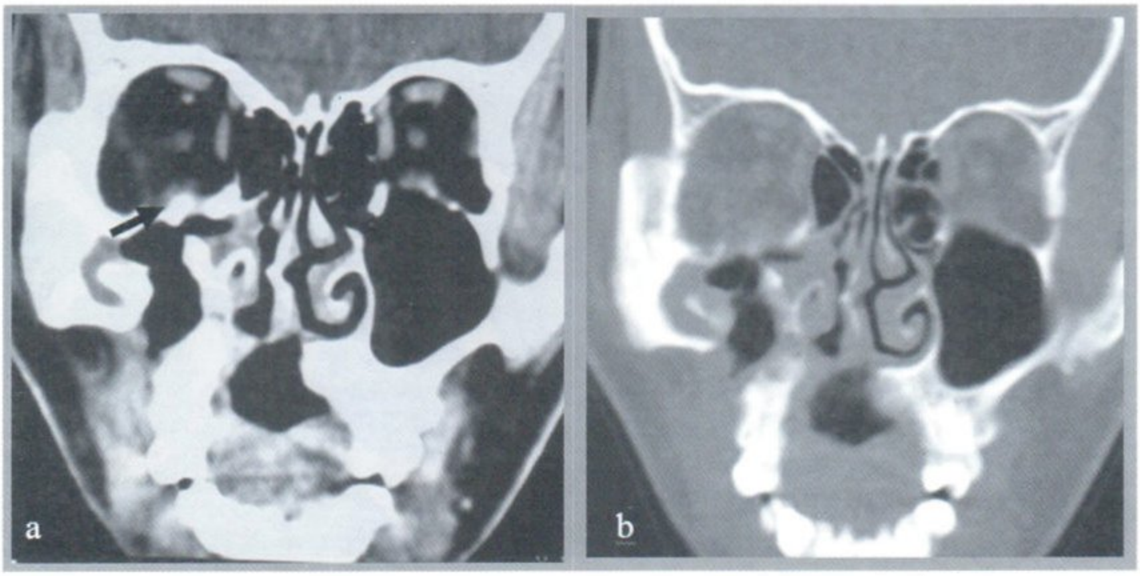

Fig.9 Patient no.9 who had squamous hyperplasia of right maxillary sinus with intact periorbital seen intraoperatively. There was only tumor adjacent to periorbita (arrow) shown in picture a. The remaining 8 criterias were interpreted negative.

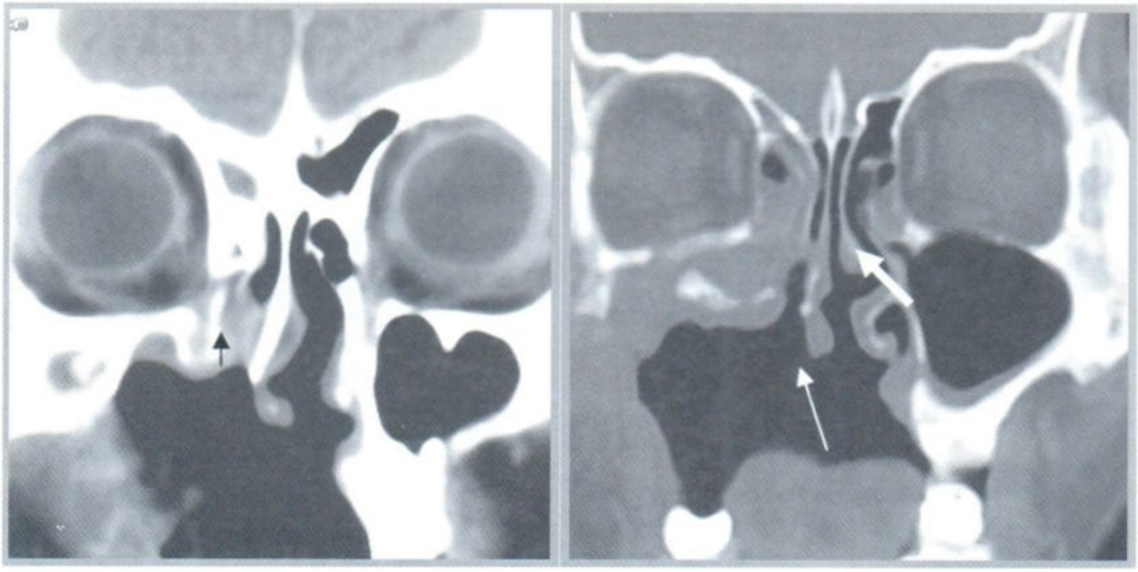

Fig.10 Patient no.10 was the previous patient no.9 who was performed Denker operation for right maxillary sinus squamous hyperplasia. This episode, he came with recurrent squamous cell carcinoma. Both picture a and b shows bony defecs from previous operation. There were periorbital displacement (thin arrow) shown in picture a. and bony dehiscence (thick arrow) shown in picture b.

DISCUSSION

Paranasal sinus tumors, especially cancers, are relatively rare and tend to have an indolent course. Therefore, they are usually diagnosed at advanced stages. In most patients diagnosed with sinonasal carcinoma, the cause is unclear. Several types of nasal cavity and paranasal sinus cancer are relatively more common in individuals engaged in certained occupations or exposed in certain chemical compounds. Adenocarcinoma of the nasal cavity and ehthmoid sinus, for instance, occurs more often in carpenters and sawmill workers who are exposed to wood dust, and squamous cell carcinoma of the nasal cavity develops more often in nickel workers. Maxillary sinus carcinoma was associated with thorium oxide (thorotrast recipient), a radioactive thorium-containing contrast material used for radiographic study of the maxillary sinuses.[6,7,8] Occupational exposure in the production of chromium, mustard gas, isopropyl alcohol, or radium also increase the risk of sinonasal carcinoma.

Maxillary sinus cancer is the most extensive and the highest prevalence among paranasal sinus cancer. The incidence ratio between male and female is about 2:1. When early in the disease or small, it is usually misdiagnosed as chronic sinusitis, nasal polyp, lacrimal duct obstruction or cranial arteritis.

The presenting symptoms, at M.D. Anderson Cancer Center between 1969-1985 among 73 patients, are face swelling/ pain/ paresthesia of cheek,[26] nasal symptom e.g.epistaxis and nasal discharge,[20] oral symptom e.g.ill-fitting denture and palatal mass[19] and eye symptom e.g.proptosis and diplopia.[5,9]

The diagnoses were done by history taking and physical examination. The history taking must be comprised of risk factor for cancer, too. Physical examination must include nasal and oral cavities, palpation of the cheek, evaluation of eye movement and function, cranial nerve examination. Imagings are begun with plain film of the paranasal sinus. This film provides haziness of paranasal sinus and bony destruction. CT or MRI are always accompanied for further visualization of extension and operative treatment planning. At our institution, MRI is rarely done because CT scan usually gives adequate information of bony destruction and extension of pathology for operative treatment planning.

Orbital invasion has very importance in the course of disease. Nowadays according to the surgical view point, orbital invasion is characterized by tumor invading through periorbita into orbital content. Orbital exenteration is usually done, if there is orbital invasion, for complete treatment or curative intent.

Orbit is a cone-shape space comprised of 7 bones i.e. the frontal, greater and lesser wings of the sphenoid, the zygoma, the maxilla, the lacrimal and the ethmoid. The condensed periosteum of these bones makes up "periorbital" which is continuous with dura mater at the optic foramen and superior orbital fissure. Because of it's strength and durability, it is considered an effective barrier to tumor extension to the orbit.

The periorbita itself is very thin to be visualized by CT or MRI. Because of it's strength, durability and elasticity, it may be still intact even cancer protrude deep into the orbit. When we see tumor extends into orbit alone, it may or may not cause periorbital rupture. There is still no definite CT scan criteria to predict cancer invading through periorbita. Currently we use the CT finding as orbital fat stranding to predict orbital invasion. Due to these problems, we tried to establish other reliable criterias for more accurate prediction.

The study by Eisen et.al.[5] revealed that CT scan had more accuracy in predicting orbital invasion than MRI because of the ability to assess fat and bone better. They found that the criteria "adjacent to periorbital " was the most sensitive (90%) and the criteria "extraocular muscle enlargement" was the most specific (94%). They also found that the "extraconal fat involvement", the widely used criteria, strongly predicting orbital invasion but lack of extraconal fat involvement cannot rule out invasion.

The information by Byron J.Bailey[5] reveals that MRI had much more accuracy than CT acan in predicting orbital invasion by paranasal sinus cancer. The reason was that CT scan could not distinguish tumor adjacent to periorbital from real invasion. Operative reassurement must be done in every case.

In our study we had the limitations due to retrospective study, too small study population and furthermore there is only one case which was intraoperatively proven as positive for periorbital invasion. Among the set up criterias, we compare the different findings found in positive case (case no.3) to negative cases, we notified that this case is the only one in 2 cases that had "extraocular muscle enlargement" and also only this case that all 9 criterias are positive. The "extraocular muscle enlargement" criteria of CT scan interpretion may be a good predictor for orbital invasion by paranal sinus cancer. This was hypothesized that the tumor has directly invaded passing through the bony orbital wall and also the extraconal fat until involving the conal muscles. Therefore, it is implied that the periorbital must already had been invaded. By concerning the sign of "extraocular muscle enlargement" which is not the pathognomonic sign for this specific disease, we strongly recommended using only the muscles that has proximity to the tumor and to use in adjunction with the other criterias.

However, the other case (case no.4) that shared this positive sign but intraoperatively an intact periorbital was found, this may be due to the tumor density is isodense to the extraocular muscle and may be overestimated size have been involved. By concerning of this issue, we suggest that MRI orbit with fat suppression with gadolinium contrast agent could be the next or the most proper investigation in the analysis of extraocular muscle invasion.

The conclusion of the sinus involvement and cell type of cancer were not surprising. The maxillary sinus is the most frequently involved sinus, 32 from 34 cases. The squamous cell carcinoma is the most common cell type, seen in 19 from 32 pathological proven cases, followed by adenoidcystic carcinoma, 4 of 32 and undifferentiated carcinomas were demonstrated in 3 of 32 cases. These cell type findings are similar to widely known information such as from Byron J. Bailey's information.

CONCLUSION

CT scan may aid in screening, staging and counseling patients about surgical planning and prognosis of paranasal sinus cancer. Even though, CT scan is not sufficiently accurate to substitute intraoperative assessment of periorbital invasion, CT orbital scan, using the sign of "extraocular muscle invasion or enlargement", may be a good predictor for periorbital invasion by paranasal cancer. In case of CT scan has an equivocal in the evaluation of extraocular muscle invasion or enlargement, we recommend that MRI with fat suppression technique would be the next investigation.

REFERENCES

1. Byron J. Bailey; Neoplasm of the Nose and Paranasal Sinuses. *Head and Neck Surgery.* Philadelphia; 1993: 1091-1117
2. Peter M. Som and Hugh D. Curtin; tumor and tumor-like conditions, sinonasal cavity. *Head and Neck Imaging.* Mosby; 2003: 261-373
3. Jame D.Cox and K.Kian Ang; The nasal fossa and Paranasal Sinuses. *Radiation Oncology.* Mosby; 2003: 160-176
4. Jatin P. Shah; Nasal cavity and paranasal sinuses. Head and Neck Surgery. Mosby wolfe; 1996: 49-83
5. Marc D Eisen, David M. Yousem; Preoperative imaging to predict orbital invasion by tumor; Head & Neck August 2000; 456-462
6. Torjussen W, Solberg LA, Hgetviet AC. Histopathological changes of nasal mucosa in nickel workers: a pilot study. Cancer 1979; 44: 963-974.
7. Acheson ED, Hadfield EH, Macbeth RG. Carcinoma of the nasal cavity and accessory sinuses in woodworkers. Lancet 1967; 1: 311-312.
8. Acheson ED, Cowdell RH, Hadfield E, et al. Nasal cancer in wood workers in the furniture industry. Br Med J 1968; 2: 587-596.
9. Jiang GL, Ang KK, Peters LJ, et al. Maxillary sinus carcinomas: natural history and results of postoperative radiotherapy. Radiother Oncol 1991; 21: 193-200.

THE APPLICATION OF CHANNELIZED HOTELLING OBSERVER IN LESION DETECTION IN HEPATIC SPECT IMAGES

Tawatchai EKJEEN, MSc,[1] Chiraporn TOCHAROENCHAI, PhD,[1] Pawana PUSUWAN, MD[2]

OBJECTIVE: The purposes of the study were to apply the channelized hotelling observer (CHO) to study factors affecting lesion detectability in hepatic single photon emission computed tomography (SPECT) images.

MATERIALS AND METHODS: The 4-dimensional NURBS-based Cardiac-Torso (4D NCAT) phantom was used with organ uptake ratios related to the biodistribution of ^{99m}Tc-hydrazinonicotinyl-Tyr^{3}-octreotide (^{99m}Tc-HYNIC-TOC) at 4 hrs after injection. The Monte Carlo simulation, simulation system for emission tomography (SIMSET) code, was used to generate projection data of 128x128 matrix size and 120 views over 360 degrees. To study factors affecting lesion detectability, 3 different sizes of 8-mm, 10-mm and 15-mm with a lesion contrast ratio of 2:1 were created with count density of ~5 M counts. To study the detectability of 8-mm lesion size, the lesion contrast ratios of 2:1 and 5:1 were investigated and 2 different count densities of ~5 M and ~10 M counts at lesion contrast ratio of 2:1 were also studied. Ninety projection data of lesion-present and lesion-absent for each test condition were generated for CHO application. To reconstruct images, ordered subset expectation maximization (OSEM) algorithm with 2 iterations and 4 subsets were used with Butterworth filter at cutoff frequency of 0.25 cycle/pixel and order of 10. The area under curve (AUC) was used as lesion detectability index.

RESULTS: The results showed that at lesion contrast ratio of 2:1 with ~5 M counts, the AUCs of 8-mm, 10-mm and 15-mm lesion sizes were 0.6119, 0.7176 and 0.9795, respectively, and the AUC of 8-mm lesion with lesion contrast ratio of 5:1 was 0.9308. At count densities of ~5 M and ~10 M counts, the AUCs were 0.6119 and 0.7160, respectively.

CONCLUSION: In conclusion, the detectability was increased with lesion size and lesion contrast ratio. However, this study showed that the detectability was slightly increased when increasing the count density. It may be due to the limitation of the performance characteristics of the imaging system. Moreover, this study demonstrated that CHO is a good research tool for lesion detectability.

Keywords: Channelized Hotelling Observer, Lesion detection, Monte Carlo simulation, NCAT phantom

1 Department of Radiological Technology, Faculty of Medical Technology, Mahidol University
2 Division of Nuclear Medicine, Department of Radiology, Siriraj Hospital

Recently, a Tc-99m-labeled somatostatin analog based on Tyr[3]-octreotide (TOC) and hydrazinonicotinic acid (HYNIC) has been developed. This radiopharmaceutical has a similar biodistribution to In-111-diethylenediaminepentaacetic acid-D-Phe[1] -octreotide (^{111}In-DTPA-octreotide), rapid tumor uptake, on-site availability and low costs.[1,2] For lesion detection using ^{99m}Tc-HYNIC-TOC, Gabriel et al[1] found the 3 small metastases in the right liver lobe and 2 small metastases in the left liver lobe, all of which were in the range of 1.0 cm. Moreover, a solitary pulmonary metastasis of a papillary carcinoma of the thyroid gland was found and a lesion size of this metastasis was 1.3x1.4 cm. Bangard et al[3] found a medullary thyroid carcinoma with a diameter of 7 mm located in the posterior basal lobe of the left lung. Dydejczyk et al[4] found a smallest lesion size of 4 mm in the patient of rectal tumor. Several studies mentioned that detection of liver metastasis by somatostatin analogues was very important. Because the liver represents the most commonly site of metastases in neuroendocrine tumors and the survival rate of patient with liver involvement was decreased when compared with nonmetastases liver disease.[5,6] Thus the liver was an organ of interest for the lesion detectability in ^{99m}Tc-HYNIC-TOC single photon emission computed tomography (SPECT) images.

A preliminary study of ^{99m}Tc-HYNIC-TOC SPECT imaging has recently been performed at Division of Nuclear medicine, Department of Radiology, Faculty of Medicine, Siriraj Hospital. The lesions in the liver less than 15 mm in diameter were difficult to detect. Human observer study has been widely used for medical image quality assessment. Due to many drawbacks of human observer study, the channelized hotelling observer (CHO), a linear observer, was of interest. Several studies[7,8] found that CHO provided good predictions with the results of human observer study. The aim of this study was to study factors affecting on lesion detectability such as lesion size, lesion contrast ratio and count density in hepatic SPECT.

MATERIALS AND METHODS

Phantom Design

The 4-dimensional NURBs-based Cardio-Torso (NCAT) phantom was used to provide a realistic model of the activity distribution of ^{99m}Tc-HYNIC-TOC at 4 hrs after injection. The organ uptake ratios in NCAT phantom were obtained from five patients at Division of Nuclear medicine, Department of Radiology, Siriraj Hospital. To study of the effect of lesion size on lesion detectability, three different sizes of 8-mm, 10-mm and 15-mm were generated with lesion contrast ratio of 2:1. This lesion contrast ratio was obtained from patients who underwent ^{99m}Tc-HYNIC-TOC SPECT imaging at Division of Nuclear Medicine, Siriraj Hospital. Moreover, factors affecting lesion detectability of a small lesion of 8-mm was interested. The effects of lesion contrast ratio and count density on lesion detectability were studied. For the effect of lesion contrast ratio on lesion detectability, two different lesion contrast ratios of 2:1 and 5:1 (from Meisetschlager et al[9] were selected. To study the effect of count density on lesion detectability of the 8-mm lesion size with lesion contrast ratio of 2:1, two count densities of ~5 M counts (~10 mCi) and ~10 M counts (~20 mCi) were used. The count density of ~5 M counts was obtained from the count density of the patients who was injected of ~10 mCi and assuming that the count density of ~10 M counts would obtain from the injection of ~20 mCi ^{99m}Tc -HYNIC-TOC. For each study, three different locations of lesion in the liver were set as shown in Figure 1. In summary, there were 4 sets of phantom for lesion-present and 1 phantom for lesion-absent used in this study (Figure 1).

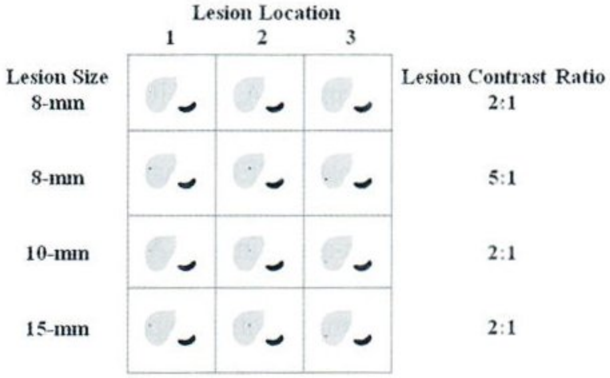

Fig.1 Four sets of phantom with different lesion sizes and different lesion contrast ratios; 8-mm with lesion contrast ratio of 2:1 (first row), 8-mm with lesion contrast ratio of 5:1 (second row). The 10-mm (third row) and 15-mm (fourth row) of lesion contrast ratio of 2:1.

Projection Data Generation and Image Reconstruction

To generate projection data, the Monte Carlo simulation, simulation system for emission tomography (SIMSET) code was used.[10] The clinical protocol used for ^{99m}Tc-HYNIC-TOC SPECT imaging at Division of Nuclear Medicine, Siriraj Hospital was used in the simulation as followed. SPECT system with 3/8 inch of thallium-activated sodium iodide NaI(Tl) crystal was modeled and equipped with low-energy high resolution collimator. Energy window width was set at 20% of 140 keV. The projection data were generated using 128x128 matrix size with bin size of 3.45 mm at 25 cm radius of rotation and 120 views over 360 degrees. For the study of the effects of lesion size and lesion contrast ratio on lesion detectability, the projection data were generated at count density of ~5 M counts. For the effect of count density on lesion detectability, the projection data were generated at two different count densities of ~5 M counts and ~10 M counts. To be used in CHO study, an equal number of lesion-present and lesion-absent projection data were used. To obtain 90 lesion-present images (30 images for training and 60 images for testing) for each test condition, 30 projection data with different noise realizations were generated for each phantom (3 different locations of the lesion). To obtain 90 lesion-absent images, 90 projection data with different noise realizations were created. Each projection data was reconstructed using iterative ordered subset expectation maximization (OSEM) algorithm with 4 subsets and 2 iterations (a clinical protocol). To smooth the image noise, Butterworth filter with order of 10 at cutoff frequency of 0.25 cycle/pixel was used. The reconstructed images with matrix size of 128x128 for the effects of lesion size, lesion contrast ratio and count density on lesion detectability studies are shown in Figure 2-4, respectively. To run CHO study, the image slice which was at the center of the lesion was selected and extracted into 32x32 matrix size which the lesion was in the field of view with random locations.

Application of Channelized Hotelling Observer

Traditionally, a task-based evaluation for a defect detection task has required human observer study. However, this observer is time consuming. To recruit physicians to perform observer study is also difficult. From the drawbacks of human observer, the channelized hotelling observer was used.

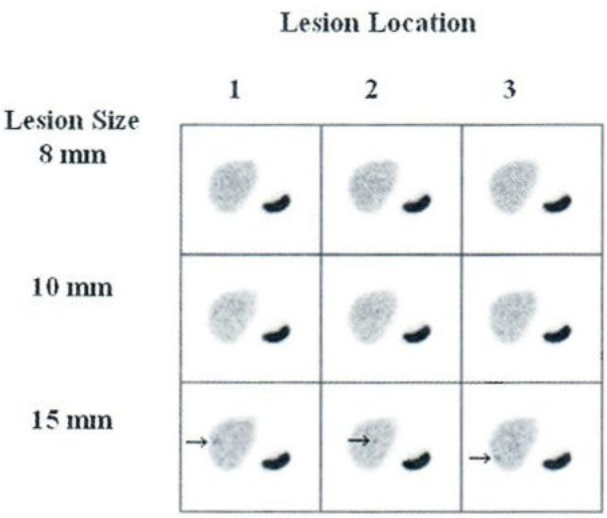

Fig.2 Reconstructed images of 3 sets of phantom with different lesion sizes; 8-mm (top row), 10-mm (middle row) and 15-mm (bottom row) of lesion contrast ratio of 2:1, at count density of ~5 M counts.

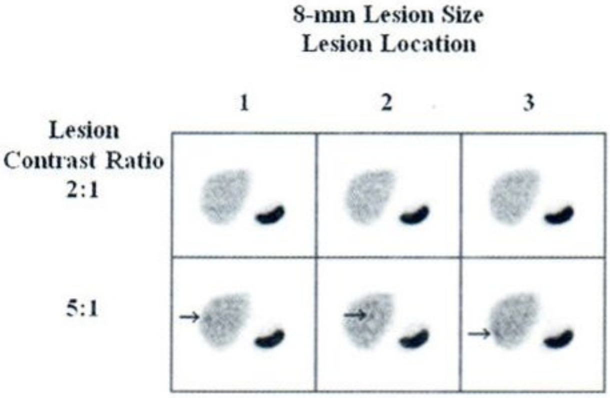

Fig.3 Reconstructed images of 2 sets of phantom of 8-mm lesion size with 2 different lesion contrast ratios; 2:1 (top row) and 5:1 (bottom row), at count density of ~5 M counts.

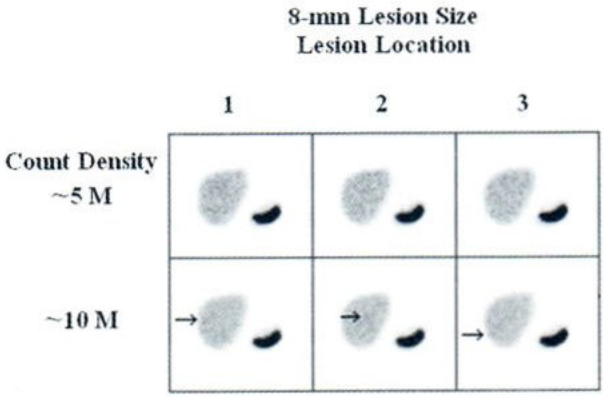

Fig.4 Reconstructed images of 2 sets of phantom of 8-mm lesion size of lesion contrast ratio of 2:1 with 2 different count densities; ~5 M counts (top row) and ~10 M counts (bottom row).

The CHO software program used in this study was contributed from Professor Eric C. Frey, Johns Hopkins University, USA. In CHO study, there were two classes of image including lesion-present and lesion-absent of hepatic SPECT images, resulting in two classes of feature vector corresponding to lesion-present and lesion-absent images. A four-element feature vector of each image was created by taking the dot product of the image with the spatial domain template for each channel. The spatial domain template for each channel was obtained from the frequency domain channel by taking the inverse Fourier Transform following a phase shift to move the center of the template to lesion.[11] Thus there were four frequency domain channels, resulting in four spatial domain channels for three lesion locations as shown in Figure 5.

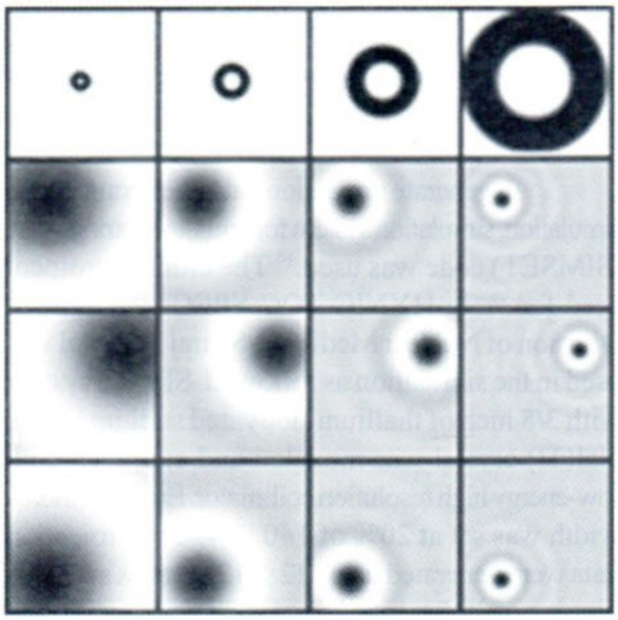

Fig.5 Images with 32x32 matrix size of four frequency-domain channels (first row) and shifted spatial domain templates (second to fourth rows) for three lesion locations.

In this study, the CHO was trained using 30 feature vectors of each class to learn the differences between the two classes of images. After training CHO, the mean vectors and covariance were generated and used later in testing CHO. Once the CHO was trained, it was tested by applying to a different, independent ensemble of feature vectors of each class. Then the CHO was tested using 60 feature vectors of each class. In testing CHO, the mean vectors and covariance were used to formulate a new vector called CHO template vector. After a CHO template vector was then applied to each testing input feature vector by taking the dot product and the scalar value known as the test statistic results.

Receiver Operating Characteristic(ROC) Analysis

The resulting test statistic is analogous to the rating which obtains from a human observer. Thus, the resulting rating data for each test condition were then analyzed using LABROC4 program.[12] This program sorts ranking values and converts to pairs of true positive fraction (TPF) and false positive fraction (FPF) and corresponding area under the curve (AUC) was also given. Finally, the pairs of TPF and FPF used to form the ROC curve and the AUC was used as a lesion detectability index.

RESULTS

The AUC in lesion detection for factors affecting on lesion detectability in hepatic SPECT images such as lesion size, lesion contrast ratio and count density were reported in Table 1. For the effect of lesion size on lesion detectability with lesion contrast-ratio of 2:1, the AUCs of 8-mm, 10-mm and 15-mm lesions were 0.6119, 0.7176 and 0.9795, respectively. The ROC curves of three different lesion sizes were shown in Figure 6. All three curves did not cross each other. It implied that detectability of 15-mm lesion size was better than the other two lesion sizes at all possible confidence thresholds. To study the effect of lesion contrast ratio on the detectability of 8-mm lesion at count density of ~5 M counts, the AUCs of lesion contrast ratio of 2:1 and 5:1 were 0.6119 and 0.9308, respectively. As shown in Figure 7, the ROC curve of lesion contrast ratio of 5:1 was higher than lesion contrast ratio of 2:1 at all possible confidence threshold. To study the effect of count density on the detectability of 8-mm lesion at lesion contrast ratio of 2:1, the AUCs of count density of ~5 M counts and ~10 M counts were 0.6119 and 0.7160, respectively. The ROC curves of two different count densities were shown in Figure 8. The plot showed that the curves did not cross each other implying that the detectability of count density of ~10 M counts was better than the count density of ~5 M counts at all possible confidence thresholds.

Table 1 The AUC in lesion detection for factors affecting lesion detectability in hepatic SPECT images such as lesion size, lesion contrast ratio and count density.

Lesion Size (mm)	Lesion Contrast Ratio	Count Density	AUC
8	2:1	~5 M	0.6119
8	2:1	~10 M	0.7160
8	5:1	~5 M	0.9308
10	2:1	~5 M	0.7176
15	2:1	~5 M	0.9795

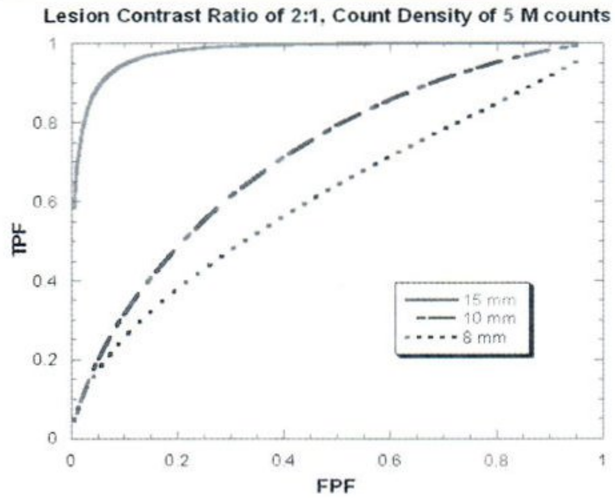

Fig.6 The ROC curves of three different lesions; 8-mm, 10-mm and 15-mm with lesion contrast ratio of 2:1 for projection data of ~5 M counts.

DISCUSSION

In this study, the application of CHO results of this study showed that the 15-mm lesion was clearly seen, the detectability of 10-mm lesion was fair and the 8-mm lesion was difficult to be detected with lesion contrast of 2:1 at count density of ~5 M counts. The results agreed with Dromain et al.[6] They found that the trend of the detection of liver metastases was better when the lesion size was more than 15 mm. Similarly, Gabriel et al[1] found that all of lesion sizes that were seen in the liver were in the range of 10 mm.

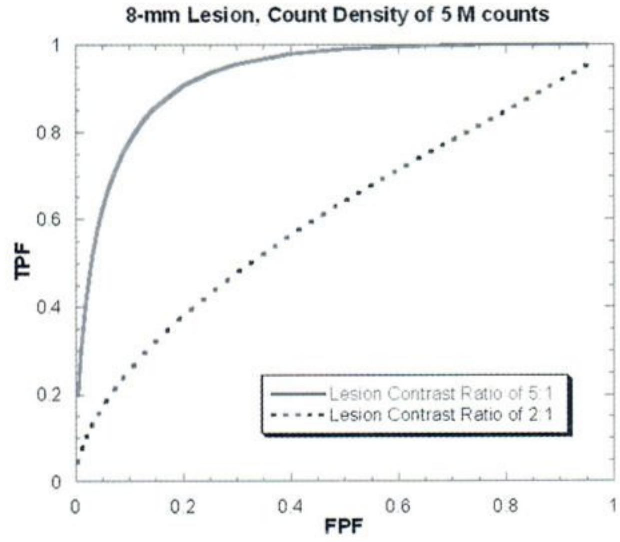

Fig.7 The ROC curves of two different lesion contrast ratios; 2:1 and 5:1 of 8-mm lesion for projection data of ~5 M counts.

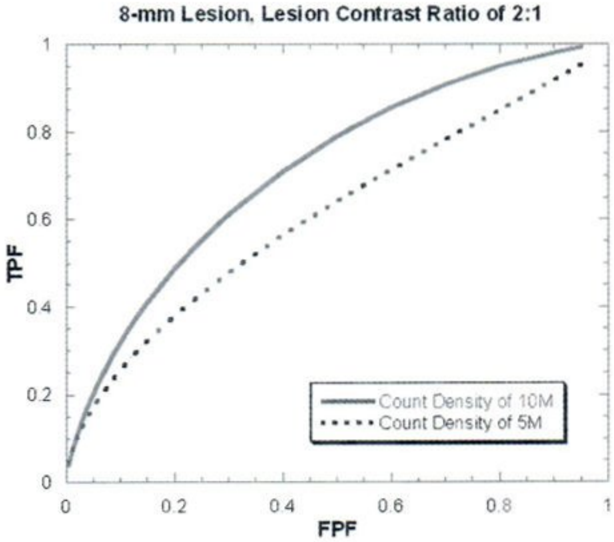

Fig.8 The ROC curves of ~5 M counts and ~10 M counts of 8-mm lesion with lesion contrast ratio of 2:1.

For the effect of lesion contrast ratio on lesion detectability, the detectability of 8-mm lesion was improved when the lesion contrast ratio was increased from 2:1 to 5:1. This result agreed with Meisetschlager et al.[9] They investigated the tumor contrast ratios in the liver and the result revealed that the mean tumor contrast ratio was approximately to 5:1. Moreover, this study showed that the lesion detectability of 8-mm lesion with count density of ~5 M counts was poor, the lesion detectability was slightly better when increasing the number of count density to ~10 M counts. The detectability may be borderlined for this SPECT system, regarding the range of 5.6 mm to 11.1 mm of the system resolution. That means the 8-mm lesion detectability can be seen with noise -free data. In clinical situation, to increase count density can be achieved by increasing either injection dose or scanning time or both. Good patient cooperation should be aware.

Another aspect of this study was to demonstrate the application of CHO for lesion detectability. Although, CHO needs a large number of images, computational time is short and repetition of the experiment is easily to perform. Furthermore, it is very useful tool for a preliminary study.

Therefore, CHO is a good research tool for lesion detectability.

Limitations of This Research

The data used in this study were simulated based on clinical studies. However, there were several limitations in this study. Firstly, the effects of attenuation, collimator-detector response and scatter were not modeled. Secondly, the variation of lesion locations was not sufficient (3 locations), it may affect the results in terms of over-estimated AUC. Thirdly, CHO provides only the relative AUC and human observers give absolute AUC. For these reasons, the results of this study can be served as guidelines in the clinical situation. Although, CHO becomes the good research tool for lesion detectability, the human observer study is still needed for the reliable and acceptable method to evaluate the image quality and the performance of diagnostic test.

ACKNOWLEDGEMENTS

The authors would like to thank Professors Benjamin M.W. Tsui and Eric C. Frey, Dr. Xin He and Dr. William Paul Segars, Department of Radiology, Johns Hopkins University, USA for CHO software program, phantom and the valuable advices. The authors also thank to the University of Washington, USA for SIMSET software program and the staffs at Division of Nuclear Medicine, Department of Radiology, Siriraj Hospital for their help in the preliminary study of ^{99m}Tc-HYNIC-TOC imaging.

REFERENCES

1. Gabriel M, Decristoforo C, Donnemiller E, Ulmer H, Rychlinski CW, Mather SJ, et al. An intrapatient comparison of ^{99m}Tc-EDDA/ HYNIC-TOC with 111In-DTPA-Octretide for diagnostic of somatostatin receptor -expressing tomors. J Nucl Med 2003; 44: 708-16.
2. Decristoforo C, Mather SJ, Cholewinski W, Donnemiller E, Riccabona G, Moncayo R. ^{99m}Tc-EDDA/HYNIC-TOC: a new ^{99m}Tc -labelled radiopharmaceutical for imaging somatostatin receptor-positive tomours: first clinical results and intra-patient comparison with ^{111}In-labelled octreotide derivatives. Eur J Nucl Med 2000; 27: 1318-25.
3. Bangard M, Béhé M, Guhlke S, Otte R, Bender H, Maecke HR, et al. Detection of somatostatin receptor-positive tumors using the new ^{99m}Tc-tricine-HYNIC-D-Phe-Try^{3}-octreotide: first results in patients and comparison with ^{111}In-DTPA-D-Phe-octretide. Eur J Nucl Med 2000; 27: 628-37.
4. Dydejczyk AH, Baron KF, Mikolajczak R, Maecke HR, Huszno B, Pach D, et al. ^{99m}Tc-EDDA/HYNIC-octreotate scintigraphy, an efficient method for the detection and staging of carcinoid tumours: results of 3 years' experience. Eur J Nucl Med Mol Imaging 2006; 33: 1123-33.
5. Schillaci O, Spanu A, Scopinaro F, Falchi A, Danieli R, Marongiu P, et al. Somatostatin receptor scintigraphy in liver metastasis detection from gastroenteropancreatic neuroendocrine tumors. J Nucl Med 2003; 44: 359-68.
6. Dromain C, de Baere T, Lumbroso J, Caillet H, Laplanche A, Boige V, et al. Detection of liver metastases from endocrine tumors: a prospective comparison of somatostatin receptor scintigraphy, computed tomography, and magentic resonance imaging. J Clin Oncol 2005; 23: 70-8.
7. Gifford HC, King MA, de Vries DJ, Soares EJ. Channelized Hotelling and human observer correlation for lesion detection in hepatic SPECT imaging. J Nucl Med 2000; 41: 514-21.
8. Smith WE, Barrett HH. Hotelling trace criterion as a figure of merit for the optimization of imaging systems. Opt Soc Am 1986; 3: 717-25.

9. Meisetschlager G, Poethko T, Stahl A, Wolf I, Scheidhauer K, Schottelius M, et al. Gluc-Lys ([^{18}F]FP)-TOCA PET in patients with SSTR-positive tumors: biodistribution and diagnostic evaluation compared with [^{111}In] DTPA-octreotide. J Nucl Med 2006; 47: 566-73.
10. SimSET homepage [Homepage on the internet]. USA: Washington University; [cite 2008 Mar 20]. Available from: URL: http://depts.washington.edu/~simset/html/simset_main.html.
11. Frey EC, Gilland KL, Tsui BMW. Application of task-based measures of image quality to optimization and evaluation of three-dimensional reconstruction-based compensation methods in myocardial perfusion SPECT. IEEE Trans Med Imag 2002; 20: 1040-50.
12. Metz CE, Herman BA, Shen JH. Maximum likelihood estimation of receiver operating characteristic (ROC) curves from continuously -distributed data. Statist Med 1998; 17: 1033-53.

VALIDATION OF EJECTION FRACTION OBTAINED FROM GATED SPECT IMAGING USING NCAT PHANTOM

Soontaree SRIWONGTA, MSc,[1] Chiraporn TOCHAROENCHAI, PhD,[1] Pawana PUSUWAN, MD[2]

OBJECTIVE: The purpose of this study was to validate the accuracy of three quantification software packages for assessing left ventricular ejection fraction (LVEF) using NURBs-based Cardiac Torso (NCAT) phantom.

MATERIALS AND METHODS: The populations of NCAT phantom with 10 different anatomical heart parameters and 12 different LVEFs were used. The Simulation System for Emission Tomography (SimSET) Monte Carlo simulation code was used to simulate myocardial gated single photon emission tomography (SPECT) projection data with matrix size of 128x128 and 60 views over 180 degrees and gating at 8 frames/cardiac cycles. The projection datasets were reconstructed using ordered subset expectation maximization (OS-EM) algorithm with 6 subsets, 2 iterations and Butterworth filter at cutoff frequency of 0.52 cycles/cm and order of 10. The percentages of LVEF were determined using three quantification software packages; the Emory Cardiac Toolbox (ECTb), 4D-MSPECT and Myovation. Then the accuracy and the correlation of LVEF obtained from each software package were calculated. A two tailed pair t-test was used to test statistically significant differences in LVEFs obtained from 3 packages with p-value <0.05.

RESULTS: The results showed that for LVEF <45%, the percentages of accuracy were 44.59, 11.11 and 54.41 and the correlation coefficients were 0.77, 0.80 and 0.66, while LVEF ≥45%, the percentages of accuracy were 21.06, 7.48 and 15.55 and the correlation coefficients were 0.74, 0.91 and 0.97 for ECTb, 4D-MSPECT and Myovation, respectively. There were statistically significant differences in LVEF (p-value <0.001) among 3 packages.

CONCLUSION: In conclusion, LVEF obtained from 4D-MSPECT was the most accurate and had good correlation with true LVEF for the full range of LVEF. The LVEF obtained from Myovation was less accurate but was well correlated with true LVEF for LVEF ≥45%. While the accuracy of LVEF obtained from ECTb was the least and the correlation with the true LVEF was poor. The LVEFs obtained from 3 software packages were not interchangeable.

Keywords: Ejection Fraction, Gated SPECT, NCAT phantom, Monte Carlo Simulation

The left ventricular (LV) function and myocardial perfusion are the important predictors in nuclear cardiology for diagnosis and prognosis in patients with coronary artery disease (CAD). Myocardial perfusion study has been widely used to determine the adequacy of blood flow to the myocardium, whereas equilibrium-gated blood pool study is widely used for assessment the ventricular

[1] Department of Radiological Technology, Faculty of Medical Technology, Mahidol University
[2] Department of Radiology, Faculty of Medicine Siriraj Hospital, Mahidol University

function such as ventricular volume, ejection fraction (EF), and regional wall motion. Early nuclear cardiology, the assessment of myocardial perfusion and ventricular function were separated. Recently, the development of myocardial gated single photon emission tomography (SPECT) has allowed for the quantitative assessment of LV function simultaneously with the evaluation of the LV perfusion from a single procedure. This development has accelerated the utilization of this procedure for the diagnostic and prognosis associated with CAD. Myocardial gated SPECT has now been routinely used to assess, in addition to myocardial perfusion, global and regional left ventricular function. The main parameter of global function is left ventricular ejection fraction(LVEF).[1-3]

For quantitative analysis of LV functions, several kinds of quantification software packages have been developed and applied to clinical practices. The software packages available in nuclear medicine are the Emory Cardiac Toolbox (ECTb, Emory university, Atlanta, GA), 4D-MSPECT (University of Michigan Medical Center, Ann Arbor, MI) and Myovation (GE healthcare, Haifa). Due to different characteristics of algorithms to determine the LVEF of each software, the same patient could get different LVEFs when different packages were applied. Therefore, the accuracy of three software packages was studied.[4-5]

MATERIALS AND METHODS

Phantom Generation

The NURBs-based Cardiac Torso (NCAT) phantom with various LVEFs developed by Segars[6] was used. Ten different anatomical parameters of male and female hearts were generated. Several parameters were varied to model the realistic variations in the size, shape, orientation and position of the heart (from Emory thorax model database). From each heart model, the ejection fraction of the NCAT phantom was varied from 25% to 75%, in 5% increments.[7] After phantoms were generated, the true LVEFs were computed from the end diastolic volumes and end-systolic volumes. Totally, there were 120 (10x12) NCAT phantoms using this study. Each NCAT phantom was generated in a 128x128x128 array with a pixel size and slice thickness of 0.345 cm. The cardiac cycle of the NCAT phantom was divided into 8 frames.

Gated Projection Data Simulation

Projection data of gated SPECT of each phantom were generated using Simulation System for Emission Tomography (SimSET) Monte Carlo Simulation code[8] and parameterized according to the clinical protocol as followed. A single head thallium activated sodium iodide (NaI(Tl)) detector SPECT system with energy resolution of 9% at 140 keV and a low-energy high resolution (LEHR) collimator with a thickness of 3.5 cm, a hole radius of 0.07875 cm, and a septa thickness of 0.020 cm were used. The radius of rotation was 25 cm and the energy window was set at 20% of 140 keV. The gated projection data were simulated with matrix size of 64 x 64, 60 views over from left posterior oblique (LPO) to 45^{0} right anterior oblique (RAO). For gated mode, the cardiac cycle was divided into 8 frames/cycle, the total of projection data was 960 images (8 frames x 60 views). Finally, there were 120 sets of gated projection data used in this study.

Image Reconstruction

Each projection data was reconstructed using the iterative ordered subset expectation maximization (OS-EM) with 2 iterations and 10 angles per subset and this number was used because it gave the most accurate inferior wall thickness. The images were reconstructed into 64x64 arrays with a pixel width and slice thickness of 0.69 cm. The reconstructed images were post-filtered with Butterworth filter with cutoff frequency of 0.52 cycles/cm and order of 10.

Gated SPECT Analysis

To compute the LVEF, three quantification software packages: ECTb, 4D-MSPECT and Myovation on a GE Xeleris workstation were used. The ECTb software uses cylindrical coordinates to sample from the basal wall to the distal wall and spherical coordinates to sample the apex.[9-10] The model for 4D-MSPECT also uses a cylindrical-spherical coordinate system and uses weighted spline and thresholding techniques to refine surface estimates. To estimate wall position and thickness, a gaussian function was used.[11] The Myovation models the heart by automatically detecting the location of center-of-mass left ventricular, a gaussian function was applied to determine the mid-myocardial surface associated with the ellipsoid shape. Then, the endocardial and epicardial surface points were calculated using the standard deviation of a gaussian function. To determine the valve plane, the basal rim of the sampled mid-myocardial was detected. Although all three packages are semi-automatic, all calculations were performed with the default configurations of each package.

Data Analysis

The LVEF of each phantom was determined from three packages and the accuracy of each package was calculated as shown in equation 1.

$$\text{Accuarcy}(\%) = \frac{(\text{LVEF}-\text{LVEF}_{\text{NCAT}})}{\text{LVEF}_{\text{NCAT}}} \quad (1)$$

Furthermore, the linear regression analysis was also applied to determine the correlation of LVEF between those three software packages and the true value from NCAT phantom. For the comparison of the LVEF obtained from ECTb, 4D-MSPECT and Myovation, a two-tailed pair t-test was used to test statistical significant in the mean difference for each pair of software packages.

RESULTS

Table 1 showed the mean, maximum, minimum and standard deviation of the LVEFs obtained from ECTb, 4D-MSPECT and Myovation. The results demonstrated that the average LVEF obtained from ECTb was higher than that from the true value. While the average LVEF obtained from Myovation was lower and the average LVEF from 4D-MSPECT was slightly higher than the true value. Table 2 showed the average accuracies for all ranges of LVEF, LVEF ≥45% and LVEF <45%. The results showed that the overall average accuracies of ECTb, 4D-MSPECT and Myovation, were 30.86%, 8.99% and 31.74%, respectively. For LVEF <45%, the average accuracies of ECTb, 4D-MSPECT, and Myovation were 44.59%, 11.11% and 54.41%, respectively. While LVEF ≥45%, the average accuracies were 21.06%, 7.48% and 15.35% for ECTb, 4D-MSPECT and Myovation, respectively.

Table 1 The mean, standard deviation, maximum and minimum of LVEF for ECTB, 4D-MSPECT and Myovation compared with the true LVEF.

	%LVEF			
	Mean	**SD**	**Min**	**Max**
True Value	47.36	16	20	72
ECTb	59.24	18.30	11	90
4D-MSPECT	48.42	18.60	12	89
Myovation	36.05	21.94	5	80

Table 2 The average of the accuracy of LVEF for ECTb, 4D-MSPECT and Myovation.

LVEF	Accuracy (%)		
	ECTb	**4D-MSPECT**	**Myovation**
All Ranges	30.86	8.99	31.74
<45%	44.59	11.11	54.41
≥45%	21.06	7.48	15.55

The correlation of LVEF between the true LVEF and each software package was studied and divided into two groups: for LVEF <45% and LVEF ≥45%. For LVEF <45%, The correlation between LVEF obtained from ECTb and the true LVEF was shown in Fig.1 and the correlation coefficients was 0.77. Fig.2 showed the correlation between the

LVEF from 4D-MSPECT and the true value with the correlation coefficient of 0.8. The correlation between the LVEF obtained from Myovation and the true LVEF was plotted and shown in Fig.3 with the correlation coefficient of 0.66. The results demonstrated that LVEF obtained from 4D-MSPECT and ECTb were well-correlated and that obtained from Myovation was poor-correlated.

For LVEF ≥45%, the correlation coefficients between the LVEF of true LVEF obtained from those three software packages were 0.74, 0.91 and 0.97 for ECTb, 4D-MSPECT and Myovation, respectively. Fig.4 showed the correlation between the LVEF of true LVEF and that from ECTb. The plot revealed that the correlation was poor. While the true LVEFs and that obtained from 4D-MSPECT and Myovation were well-correlated as shown in Fig.5 and 6, respectively.

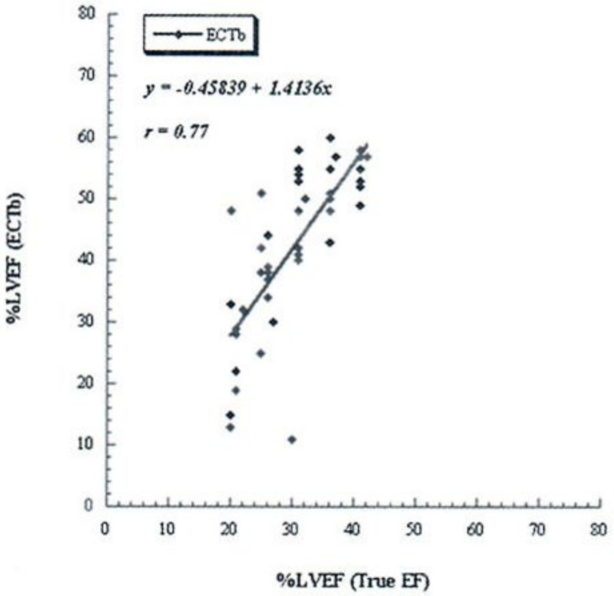

Fig.1 The correlation analysis of LVEF between true LVEF and ECTb for LVEF <45%

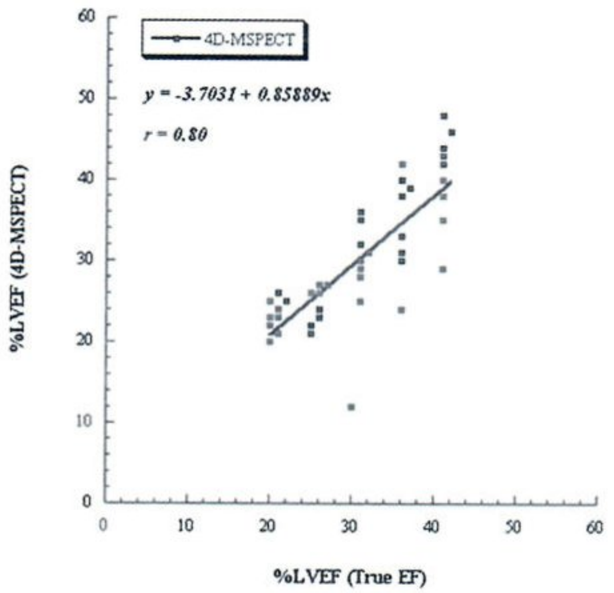

Fig.2 The correlation analysis of LVEF between true LVEF and 4D-MSPECT for LVEF <45%

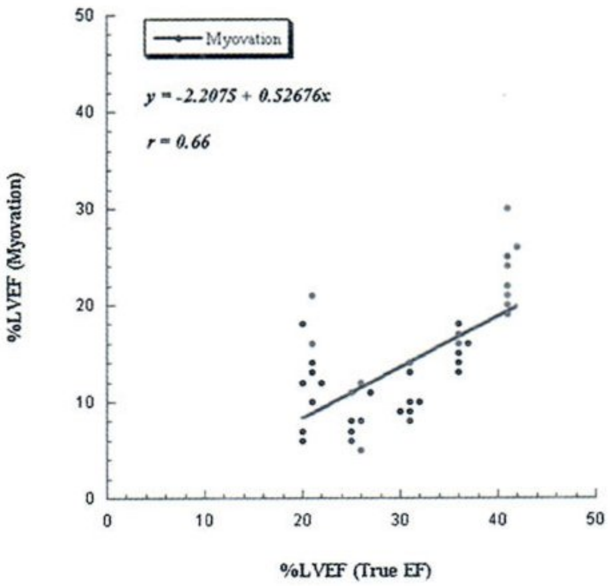

Fig. 3 The correlation analysis of LVEF between true LVEF and Myovation for LVEF <45%

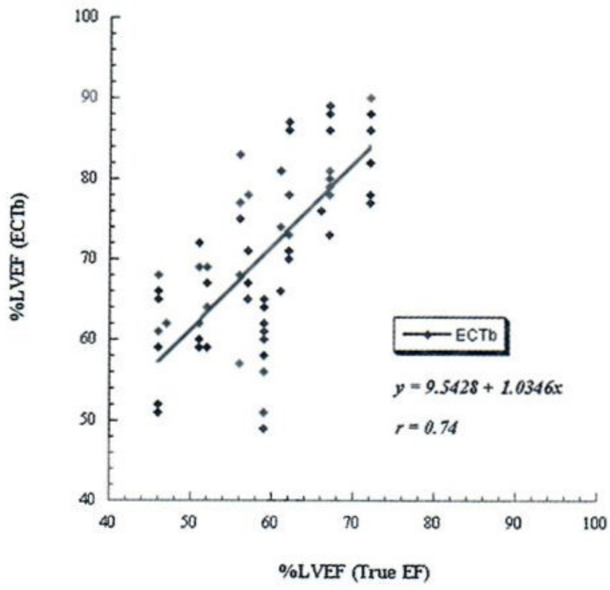

Fig.4 The correlation analysis of LVEF between true LVEF and ECTb for LVEF ≥45%

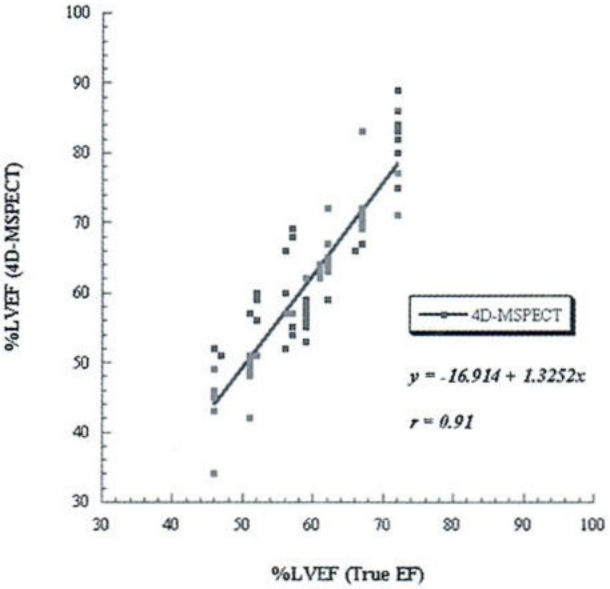

Fig.5 The correlation analysis of LVEF between true LVEF and 4D-MSPECT for LVEF ≥45%

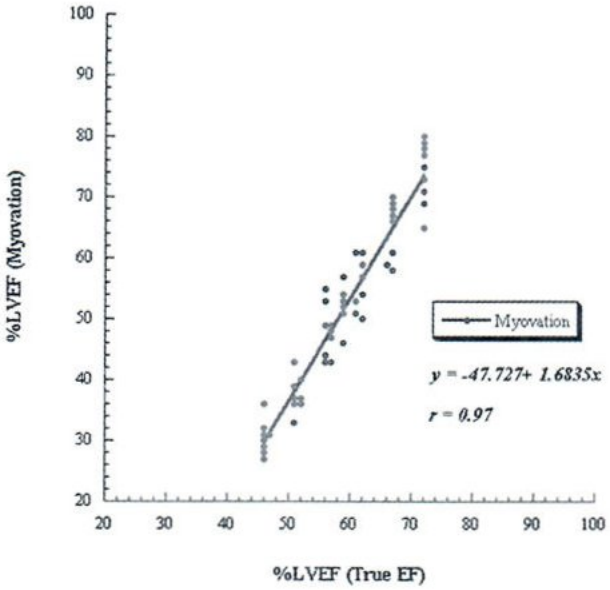

Fig.6 The correlation analysis of LVEF between true LVEF and Myovation for LVEF ≥45%

Table 3 The mean of difference, standard deviation, and p-value for each pair of software packages.

	Mean Difference	SD	P-value
ECTb - 4D-MSPECT	10.83	8.21	<0.001
ECTb - Myovation	23.19	11.34	<0.001
4D-MSPECT - Myovation	12.37	6.81	<0.001

To study the differences between LVEFs obtained from each package, a two-tailed pair t-test was used. Table 3 reported the mean difference of the LVEF, standard deviation and p-value for each pair. The mean difference between LVEF obtained from ECTb and that from 4D-MSPECT was 10.83 and they were statically significantly different with 95% confident interval (p<0.001). The mean difference of LVEF obtained from ECTb and Myovation, was 23.19 and they were statically significantly different with 95% confident interval (p<0.001). Similarly, the mean difference of LVEF obtained from 4D-MSPECT and Myovation was 12.37 and they were statistically significant different with 95% confident interval (p<0.001).

DISCUSSION

From the results of this study, LVEF obtained from 4D-MSPECT was the most accurate than that from the others for all ranges of LVEF. For LVEF <45%, Myovation gave less accuracy than 4D-MSPECT and ECTb. While for LVEF ≥45%, ECTb gave the largest error. The correlation of LVEF between the true LVEF for each software packages was studied using linear regression analysis. The LVEF obtained from 4D-MSPECT was well correlated, the LVEF obtained from ECTb was poor correlated with true LVEF for all ranges of LVEF. The LVEF obtained from Myovation was well correlated with the true LVEF for LVEF ≥45% but poor correlated when LVEF <45%. Schaefer et al.[12] studied the accuracy of QGS, ECTb and 4D-MSPECT in assessment of LVEFs using cMRI as a gold standard. They found that LVEF determined by ECTb, 4D-MSPECT, and QGS from gated ^{99m}Tc-MIBI SPECT agreed over a wide range of clinically relevant values with cMRI. The LVEFs calculated from ECTb and 4D-MSPECT did not differ significantly from cMRI. Nagajima et al.[13] compared the accuracy of LVEFs from 4 software packages: QGS, ECTb, 4D-MSPECT and Perfusion and Functional Analysis for Gated SPECT (pFAST: Sapporo Medical University, Sapporo, Japan) with that from gated blood pool (GBP). They found that all 4 software programs showed well correlations between LVEF and the GBP study. The LVEFs estimated from ECTb and 4D-MSPECT were slightly higher than that obtained from by GBP study. The QGS, ECTb, and 4D-MSPECT gave over estimated LVEF in patients with small hearts.

Although LVEF can be obtained from commercially available software package but the accuracy of LVEF should be considered. The results of this study indicated that the accuracy of LVEF obtained from 4D-MSPECT was high, while that from ECTb was low. The Myovation gave a fairly accurate LVEF. In this study, the accuracy was computed using NCAT phantoms and the heart models of the phantoms might not be exactly similar to the real hearts. However, the results from this study can be used as a guideline for clinician when having follow-up patients that the LVEF should be obtained from the same software packages.

ACKNOWLEDGEMENTS

The authors would like to thank Dr. William Paul Segars for the NCAT phantom, Profs. Benjamin MW Tsui and Eric C. Frey, Johns Hopkins University for all the programs that used in this study and Dr. Glenn SY, GE Healthcare, for information of Myovation. The authors also thank Taratip Narawong and the staff of Section of Nuclear Medicine at Rajavithi Hospital, for all the supports about the software applications.

REFERENCES

1. Garcia EV, Santana C, Faber TL, Cooke Dl. Methods for evaluating left ventricular function computed from ECG-Gated myocardial perfusion SPECT [document on the Internet]. 2nd virtual congress of cardiology; [cited 2007 Aug 9]. Available from: http://www.fac.org.ar /scvc/llave/ image/ garcia/garciai.htm.
2. Paul AK, Nabi HA. Gated myocardial perfusion SPECT: basic principles, technical aspects, and clinical applications. J Nucl Med Technol 2004; 32: 179-187.
3. Germano G, Kiat H, Kavanagh PB, Moriel M, Mazzanti M, Su HT, Van Train KF, Berman DS. Automatic quantification of ejection fraction from gated myocardial perfusion SPECT. J Nucl Med 1995; 36(11): 2138-2147.
4. Go V, Bhatt MR, Hendel R. The diagnostic and prognostic value of ECG-Gated SPECT myocardial perfusion imaging. J Nucl Med 2004; 45: 912-921.
5. Nichols K, Santana CA, Folks R, Krawczynska E, Cooke CD, Faber TL et al. Comparison between ECTb and QGS for assessment of left ventricular function from gated myocardial perfusion SPECT. J Nucl Cardiol 2002; 9: 285-293.
6. Segars WP. Medical imaging simulation techniques and computer phantoms [Homepage on the internet]. Department of Radiology Johns Hopkins University. Available from: http://dmip.rad.jhmi. edu/people/faculty /Paul/.
7. Feng B, Sitek A, Gullberg GT. Calculation of the left ventricular ejection fraction without edge detection: Application to small hearts. J Nucl Med 2002; 43: 786-794
8. University of Washington. SimSET homepage [Homepage on the internet]. 1999 [updated 2006 Jan 19; cited 2007 Dec 3]. Available from: http://depts.washington.edu/~simset/ html/simset_main.html.
9. Faber TL, Cooke CD, Peifer JW, Pettigrew RI, Vansant JP, Leyendecker JR, et al. Three-Dimensional displays of left ventricular epicardial surface from standard cardiac SPECT perfusion quantification techniques. J Nucl Med. 1995; 36: 697-703.
10. Cooke CD, Garcia EV, Cullom Si, et al. Determining the accuracy of calculating systolic wall thickening using a fast Fourier transform approximation: a simulation study based on canine and patient data. J Nucl Med. 1994; 35: 1185-I192.
11. The INVIA, LLC and the Regent of the University of Michigan. Reference manual for 4D-MSPECT v.4.2: comprehensive and flexible software for quantitative assessments of cardiac function and perfusion using emission tomography. 2006.
12. Shaefer WM, Lipke C, Standke D, Kuhl HP, Nowak B, Kaiser H, et al. Quantification of left ventricular volumes and ejection fraction from gated 99mTc-MIBI SPECT: MRI validation and comparison of the Emory Cardiac Toolbox with QGS and 4D-MSPECT. J Nucl Med 2005; 46:1256-63.
13. Nakajima K, Higuchi T, Yaki J, Kawano M, Tonami N. Accuracy of ventricular volume and ejection fraction measured by gated myocardial SPECT: comparison of 4 software programs. J Nucl Med 2001; 42: 1571-78.

ACCURACY OF ULTRASONOGRAPHY COMPARED TO UNENHANCED HELICAL COMPUTERIZED TOMOGRAPHY IN SCREENING OF SMALL KIDNEY STONES IN A COMMUNITY

Amorn PREMGAMONE,[1] Eim-on MAIRIANG,[2] Pote SRIBOONLUE,[3] Petcharakorn HANPANICH,[2] Wattana DITSATAPORNCHAROEN[1]

ABSTRACT

OBJECTIVE: To determine the sensitivity and specificity of ultrasonography for screening of small kidney stone by comparison with unenhanced helical computerized helical tomography (UHCT). Our community in the North-Easthern part of Thailand have a prevalence of kidney stone which is the main public health problem. Our ultrasonography (US) survey found a prevalence of hyperechoic (HYF) with or without acoustic shadowing mimicing with small kidney stones (KS). Since small stone is relatively easy to manage but difficult to be diagnosed. It will be most beneficial to study this project in order to be able to manage the kidney stones in the epidermic area since the stones are still small and easier to be managed.

METHOD: Participants were 164 subjects (328 kidneys) randomly sampled from our community survey, with and without HYF in 118 and 210 kidneys, respectively. Within 48 hours, the subjects were transferred to the university hospital for UHCT by the radiologists.

RESULT: By comparison with UHCT, the sensitivity and specificity of US in screening for KS was 81.1% and 72.7%. The respective sensitivity and specificity of microhematuria and micropyuria were 53.7% and 57.9%, and 36.6% and 52.9%.

CONCLUSION: The screening of small kidney stones by US in community had moderate sensitivity and specificity.

Key words: hyperechoic foci, small kidney stone, unenhanced helical computed tomography, microhematuria, micropyuria

HYF = Hyperechoic Foci
KS = Kidney Stones
HYF = Hyperechoic Foci
UHCT = Unenhanced Helical Computerized Tomography

INTRODUCTION

Kidney stones (KS) are a common health problem among the rural community of Northeast Thailand. The prevalence of KS vary, particularly when different diagnostic techniques are employed. In a survey of known stone cases, confirmed by plain radiography (KUB) in an area of Khon Kaen province, the prevalence was 0.38%.[1] Using ultrasonography (US) in two community surveys, the prevalence was 9%[2] and 16%,[3] vs. 5% by KUB.[4] These differences may partly reflect the difference in sampling techniques

[1] Department of Community Medicine, Faculty of Medicine, Khon Kaen University, Khon Kaen, Thailand 40002
[2] Department of Radiology, Faculty of Medicine, Khon Kaen University, Khon Kaen, Thailand 40002
[3] Department of Biochemistry, Faculty of Medicine, Khon Kaen University, Khon Kaen, Thailand 40002

and/or the real situation in the studied communities, or the accuracy of the technique (s) used. All of these surveys might not be able to detect the small kidney stone.

Stone size is the crucial factor in determining the accuracy of US where the diagnosis of stones >5 mm has the accepted accuracy.[5,6] However, all of these previous studies were hospital-based using high quality equipment in an optimally-controlled environment; mostly, on cases with radio-opaque stones.[5,6] Unenhanced helical computed tomography (UHCT) is highly sensitive in detecting ureteral stone. The UHCT has replaced emergency urography and became the modality of choice for imaging patients with ureteral colic.[7-9] Our study was designed to determine the sensitivity and specificity of US in screening of KS in community level done by a general practitioner. UHCT was used as the gold standard.

UHCT = Unenhanced Helical Computed Tomography

MATERIALS AND METHODS

Sampling Method and Estimation of Sample Size

To answer the question about sensitivity and specificity of US as compare to the UHCT, we made the assumption that the sensitivity and specificity was 0.75 and 0.65, respectively. When we allowed the 0.10 difference, the sample size for detection of the sensitivity and specificity was 73 and 88 kidneys, so we needed at least 88 normal kidneys (or 44 negative subjects) and 88 positive kidneys to enrolled in the study. We decided to use 100 subjects with HYF and 64 normal subjects in this study.

Free kidney stone checking, by a mobile ultrasound unit, was announced about one week in advance by local health volunteers. During the 20-month study period (2003-2005), participating subjects were underwent US examination. From the result of US, we performed the simple random sampled 5-6 subjects whose HYF size not over10.0 mm and 3-4 normal subjects for each village. These subjects were sent for UHCT in the university hospital within 48 hours after screening by US. The radiologist was blind for the US result.

US Examination and Criteria for Hyperechoic Foci (HYF)

After the interview and urinalysis, the subjects were examined for the presence of significant HYF by an US machine curved phased array transducers, with frequencies ranging from 3.0- 4.0 MHz.(Fukuda Denchi, UF4000, 256 grey scale). Multiple anatomic approaches were used in the imaging of kidneys (from the supine and decubitus views, both transverse and longitudinal planes). Standard views of the kidneys using the liver and spleen as acoustic windows were also employed. Performing each US examination lasted about 8-10 minutes. Due to time constraint, we did not count the number of multiple stones. Only the longest diameter of the largest stone or HYF was measured and recorded for comparison with the results of other methods. The significant HYF or KS by US in our study were demonstrated as the characteristic highly echogenic foci with or without acoustic shadowing. If it appeared without acoustic shadowing, it was diagnosed as a HYF when it met all of the criteria, namely: 1) the focus was denser than normal vascular or collecting tissues, and 2) was in an unusual place when compared with the distribution of vascular or collecting tissues, and 3) showed some calyectasis or chronic inflammation such as the scar of the nearby tissues.

Urinalysis

The participants were tested for urine abnormalities after the interview. A spot urine sample was collected from each subject and tested with a urine strip for the presence of red blood cells (microhematuria) and white blood cells (micropyuria), which were read by a reflectance photometer (Urilux-S). Urine collection in female who were in (or less than 48 hours after) the menstruation period was omitted.

UHCT Examinations

Within an interval of 48 hours after the US examination, the participating subjects were transferred to the university hospital for UHCT examination. The radiologist who performed UHCT was blinded for the US results. The UHCT examinations were performed with a helical CT scanner (Toshiba, model Exvision). The exposure settings were 120 kVp and mAs 200. Helical data acquisition consisted of 5 mm thick sections with 3 mm reconstruction.

RESULTS

A total of 1,423 subjects from 20 rural villages were enrolled in the field survey. 1,423 subjects underwent US examination with 581 subjects had the HYF size not over 10.0 mm (Details of the survey would be in another report). From the result of US, we performed the simple random sampled 100 and 64 subjects with and without HYF, respectively, to undergo the UHCT exam (Fig.1). Of the 164 subjects (328 kidneys) enrolled in the study, 78.1% of them were females, 86.6% were ?40 years old. There were 118(36%) kidneys contained significant HYF by US, 88 (74.6%) of which had the longest diameters between 2.1-5.0 mm and 25 (21.2%) of them were between 5.1-7.5 mm (Table 1). The acoustic shadow could not detect for HYF size less than 7.5 mm.

Fig. 1 Details of patients enrolled in the study

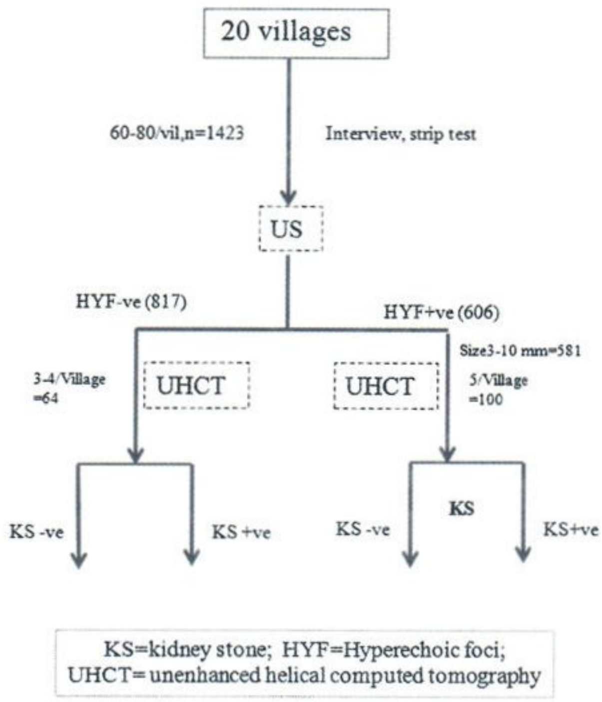

Table 1 Characteristic of subjects participated in the study and stone sizes by US

Variables		Number	Percent
Sex	Male	49	29.9
	Female	115	70.1
Age	<40	22	13.4
(years)	40-49	45	27.4
	50-59	58	35.4
	≥60	39	23.8
HYF sizes (US)	2.1 - 5.0 mm	88	†74.6
	5.1 - 7.5 mm	25	†21.2
	7.6 -10.0 mm	5	†4.2
Total kidney with significant HYF		118	36.0
No. of kidney without HYF		210	64.0

US, ultrasonography; HYF, Hyperechoic focus(foci); †, Percent distribution from total kidney with HYF

The positive KS by US (or the significant HYF) were 118 (36%) kidneys, while the positive KS by UHCT were 53(16.2%). Both US and UHCT demonstrated stones in 43 kidneys, and neither could find stone in 200 kidneys. For the positive stones (significant HYF) by US (118 kidneys), UHCT demonstrated stones in 36.4% (43 kidneys). For the negative stone by US (210kidneys), UHCT find stone in 4.8 % (10 kidneys) (Table 2).

The average size of HYF and KS measured by US and by UHCT [mean (SD)] were 4.8(1.4) and 4.4(3.2) mm, respectively (data no showed). The average size discrepancy of HYF and KS by UHCT in our study was 0.6 4.3 mm, of which US was slightly larger. The distribution of stones by size as measured by US and UHCT were different as shown in Table 3.

Table 4 shows the percentage positive for stones by UHCT from the US positive. Percent of stone positive by UHCT were significantly increased (p-value<0.05 Chi square for trend) with the increase in sizes of the HYF, i.e., 29.5% for the smallest (2.1-5.0 mm), 48% for the small (5.1-7.5 mm) and 100% for the mid-size (7.6-10.0 mm) (Table 4).

Accuracy of Each Method

Using UHCT as gold standard, the sensitivity and specificity for stone detection by US and urine findings are shown in Table 5. From 118 positive kidney by US, 53 subjects were confirmed as positive KS by UHCT. The kidneys with normal US was 210 of which 10 kidneys was positive by UHCT.

For HYF size 2.1-10mm, the sensitivity and specificity for US were 72.2% and 76.3%. When microhematuria and micropyuria was used as screening methods, both sensitivity (53.7% and 36.6 %) and specificity (57.9% and 52.9%) were lower than US.

Based on a stone prevalence of 16.1% by UHCT [positive kidneys (53)/total kidneys (328) x 100, Table 2] in our study, the positive predictive values (PPV) for HYF, the presence of RBC and WBC in urine were 36.4%, 30.1% and 20.8%, respectively.

The respective negative predictive values (NPV) for HYF, and the presence of microhematuria and micropyuria were 95.2%, 78.7% and 71.1%. The presence of pyuria and hematuria in urine had 56.8% and 48.8% accuracy in predicting the existence of KS, both were lower than the HYF (74.1%). Compared with other methods, the micropyuria or microhematuria, the HYF by US had the higher sensitivity (81.1%), accuracy (74.1%), NPV (95.2%) but the PPV was quite low(36.4%), however, the interpretation of HYF as small kidney stone were to be improved.

Table 2 Diagnosis of kidney stone by the methods of US, and urine findings as compared to UHCT

Method (Number)	Result	UHCT Pos (%)	UHCT Neg (%)	Total (%)
US† (n=328)	Pos	43(81.1)	75(27.3)	118(36)
	Neg	10(18.8)	200(72.7)	210(64)
	Total	53(100)	275(100)	328
Microhematuria ‡				
(n=162)	Pos	22(53.7)	51(42.1)	73(45.1)
	Neg	19(46.3)	70(57.9)	89(54.9)
Micropyuria ‡ (n=162)	Pos	15(36.6)	57(47.1)	72(44.4)
	Neg	26(63.4)	64(52.9)	90(55.6)

US, ultrasonography ; RBC, urine red blood cells ; WBC, White blood cells;
UHCT, Unenhanced helical computerized tomography;
† Number of total kidneys(328);
‡ Number of total subjects was 164 but 2 subjects being in menstruation period.

Table 3 Numbers of stones by sizes as estimated by US and UHCT

Stone size by UHCT (mm)	Size of HYF by US (mm) 2.1-5.0 R(L)	5.1-7.5 R(L)	7.6-10.0 R(L)	US positive R(L)	US negative R(L)	Total R(L)
≤2	9(4)	2(1)	0(0)	11(5)	5(1)	16(6)
2.1-5.0	4(5)	1(1)	0(1)	5(7)	2(2)	7(9)
5.1-7.5	0(1)	1(0)	1(1)	2(2)	0(0)	2(2)
7.6-10.0	1(2)	1(1)	0(0)	2(3)	0(0)	2(3)
>10	0(0)	4(0)	0(2)	4(2)	0(0)	4(2)
UHCT positive	14(12)	9(3)	1(4)	24(19)	7(3)	31(22)
UHCT negative	37(25)	7(6)	0(0)	44(31)	89(111)	133(142)
Total kidney	51(37)	16(9)	1(4)	68(50)	96(114)	164(164)

US, Ultrasonography ;UHCT, Unenhanced helical computed tomography;
HYF, Hyperechoic foci ; R, right kidney ; L, left kidney ;

Table 4 Percentage of stone detection by UHCT in kidneys with positive and negative HYF by US

No. of kidney with HYF(US)	Size of HYF by US (mm)	No. of kidney with stone by UHCT	% Detected by UHCT*
88	2.1-5.0	26	29.5
25	5.1-7.5	12	48.0
5	7.6-10.0	5	100.0
118	Total detect	53	44.9
210	Not detected	10	4.8

UHCT, Unenhanced helical computerized tomography;
HYF, Hyperechoic foci; US, Ultrasonography ;
* p-value<0.05 (Chi square for trend)

Table 5 Sensitivity , Specificity, PPV , NPV and Accuracy of detection of KS by US , urine findings when the gold standard was UHCT

Method	**Sens (%)**	**Spec (%)**	**PPV (%)**	**NPV (%)**	**Acc (%)**
US (HYF=2.1-10.0mm)	81.1	72.7	36.4	95.2	74.1
Micro-hematuria	53.7	57.9	30.1	78.7	56.8
Micro-pyuria	36.6	52.9	20.8	71.1	48.8

KS, Kidney stone; Sens, Sensitivity; Spec, Specificity; PPV, Positive predictive value ; NPV, Negative predictive value; Accu, Accuracy; HYF, Hyperechoic foci(focus); US, Ultrasonography; UHCT, Unenhanced Helical Computed Tomography

DISCUSSION

Summary of Main Findings

About 30% and 50% of the HYF of the sizes 3-5.0 and 5.1-7.5mm, respectively, was confirmed by UHCT as kidney stones, while the false negative by US in KS not larger than 10 mm was 5%. Ultrasonography can be used as screening test for small kidney stone in patient with suspected nephrolithiasis with the awareness of the moderate sensitivity (72-81%) and specificity (72.7-76.3%). The US scanning by multiple anatomical approaches, the significant HYF in this studied was fulfilled with the 3 criteria: denser, unusual place, and nearby calyectasis.

Where This Fits with Other Literature

The present study found the ability of US to detect stones depends upon stone size as described by Middleton.[5] In reported literature the sensitivity of US is reported to be 96 % for kidney stones and the specificity is 100% for stones larger than 5 mm [5, 12]. Vrtiska and coworker[6] reported the sensitivity of US was as high as 98% in radiopaque stone patients who had undergone ESWL when compared abdominal radiographs and renal tomograms. Ather MH[12] reported that when compared US with UHCT in the patients with serum creatinine ≥1.8 mg/dl, the sensitive and specific for kidney stones was 81 and 100%, respectively. US is highly sensitive and specific for renal stones in patients with renal failure, it lacks sensitivity for ureteric calculi particularly when they are in the middle ureter. In patients with acute flank pain diagnosed for the presence of ureteric stones in previous reports the sensitivity of US varies between 37 and 64 %.[14-16]

In our study, for detection of the KS not larger than 10 mm, US had sensitivity and specificity of 81 and 72%.

Some investigators reported that stone sizes were overestimated by US in 22% of all detected stones. Middleton[5] described that the causes of the difference may be opaque uric acid mantle or proteinaceous matrix around the central radiopaque nidus. In our study the mean (SD) of the size discrepancy of HYF and KS by UHCT was 0.6 (0.3) mm, of which US was slightly larger (data not shown).

The HYF detected by US but were not diagnosed as stones by UHCT might be the renal sludge, pericalyceal fat, crystal laden calyceal sub-mucosal plaques, milk of calcium or uric acid in the calyceal diverticula or arterial calcification as mentioned earlier by Vrtiska.[6]

Strengths and Limitations

This is the first attempt in Thailand to study the reliability of the screening small kidney stones with simple available machine by a general practitioner who had 5 year- experience in US scanning. The result of the study, performed in the practical environment in rural community, can be applied to the actual circumstances. This study based on the facts that radiologist is extremely rare and does not work in the remote communities. However, if the US screener was a radiologist with a new generation US, the study result might be more attractive.

Because of time limitation and a large numbers of participants in the field survey, the position of the largest stones in this study were not definitely located, so the difference in stone size by US and UHCT may due to measuring different stones in cases of multiple stones.

Implications

Screening for small KS is crucial for effective control. The treatments of large KS by surgical removal or shockwave lithotripsy (SWL) have a high rate of recurrence, which increases with age and observation time. The average recurrence rate is 30- 40 %.[17,18] Since small stones can pass spontaneously, the earlier the diagnosis the easier and more successful stone management, by promoting the passage of stones.[11,12] The presence study revealed that the US had a positive predictive value of 36.4%, which is quite low but it is better than the urine strip exam for screening of small KS in the community.

ACKNOWLEDGMENTS

We thank Khon Kaen University for the grant support and Mr. Bryan Roderick Hamman assistance with the English-language presentation.

REFERENCES

1. Sriboonlue P, Prasongwatana V, Chata K, Tungsanga K. Prevalence of upper urinary tract stone disease in a rural community of north-eastern Thailand. Br. J. Urol. 1992; 69: 240-4.
2. Premgamone A, Khantikaew N, Kessomboon P. Prevalence of nephrolithiasis in three districts of Khon Kaen province using the mobile ultrasound unit. Srinagarind Med. J. 1995; 10: 272-86.
3. Yanagawa M, Kawamura J, Onishi T, et al. Incidence of urolithiasis in northeast Thailand. Int. J. Urol. 1997; 4: 537-40.
4. Aimpetcharapong C, Chuasatuchon C, Pongsapritr N. Prevalcence of urinary tract stone in rural communities in north-east Thailand: A research reported to the Ministry of Public Health. 1994.

5. Middleton WD, Dodds WJ, Lawson TL, Foley WD. Renal calculi: sensitivity for detection with US. Radiology 1988; 167: 239-44.
6. Vrtiska TJ, Hattery RR, King BF, et al. Role of ultrasound in medical management of patients with renal stone disease. Urol. Radiol. 1992; 14: 131-8.
7. Abramson S, Walders N, Applegate KE, Gilkeson RC, Robbin MR. Impact in the emergency department of unenhanced CT on diagnostic confidence and therapeutic efficacy in patients with suspected renal colic: a prospective survey. AJR 2000; 175: 1689-95.
8. Katz DS, Lane MJ, Sommer FG. Non-contrast spiral CT of patients with suspected renal colic. Eur Radiol 1997; 7: 680-5.
9. Smith RC, Varanelli M. Diagnosis and management of acute ureterolithiasis: CT is truth. AJR 2000; 175: 3 -6.
10. Bovornpadungkitti S, Sriboonlue P, Tungsanga K. Post operative renal stone recurrence in Khon Kaen Regional Hospital. Thai J. Urol. 1992; 13: 21-6.
11. Motola JA, Smith AD. Therapeutic options for the management of upper tract calculi. Urol. Clin. North Am. 1990; 17: 191-206.
12. Ahmed NA, Ather MH, Rees J: Unenhanced helical computed tomography in the evaluation of acute flank pain. Int J Urol 2003, 10: 287-292.
13. O'Flynn JD. The treatment of ureteric stones: report on 1120 patients. Br. J. Urol. 1980; 52: 436-8.
14. Sinclair D, Wilson S, Toi A, Greenspan L. The evaluation of suspected renal colic: ultrasound scan versus excretory urography. Ann. Emerg. Med. 1989; 18: 556-9.
15. Aslaksen A, Gothlin JH. Ultrasonic diagnosis of ureteral calculi in patients with acute flank pain. Eur. J. Radiol. 1990; 11: 87-90.
16. Deyoe LA, Cronan JJ, Breslaw BH, Ridlen MS. New techniques of ultrasound and color Doppler in the prospective evaluation of acute renal obstruction. Do they replace the intravenous urogram? Abdom. Imaging 1995; 20: 58-63.
17. Sudah M, Vanninen RL, Partanen K, et al. Patients with acute flank pain: comparison of MR urography with unenhanced helical CT. Radiology. 2002; 223: 98-105.
18. Pearle MS, Watamull LM, Mullican MA. Sensitivity of non-contrast helical computerized tomography and plain film radiography compared to flexible nephroscopy for detecting residual fragments after percutaneous nephrostolithotomy. J Urol. 1999; 162: 23-6.

DISTRIBUTION OF THE SIZES OF KIDNEY STONES IN A COMMUNITY

Amorn PREMGAMONE,[1] Eim-on MAIRIANG,[2] Srinoi MASKASEM,[1] Vitoon PRASONGWATANA,[3] Wattana DITSATAPORNCHAROEN[1]

ABSTRACT

Background: Small stone is easy to manage but difficult to diagnose. We aimed to determine the size distribution of kidney stones (KS) in rural community using 256-grey-scale ultrasonography (US) with multiple anatomical approaches.

Method: The modified fist test (MFT) and urine strip test by the urine analyzer(UriluxS S) was performed. The presence of hyperechoic foci (HYF) were considered to be significant when fulfilled with the 3 criteria: i.e., denser, unusual place, and nearby calyectasis.

Results: A total of 1,423 subjects, aged between 18 and 72 years were enrolled and HYF were detected in 606 subjects (42.6%). HYF findings were significantly associated ($p < 0.05$, Pearson Chi-Square) with eight chronic health complaints: myofascial pain, back pain, dyspepsia, arthralgia, fatigue, frank paresthesia, dysuria and any of these aggravated by purine-rich foods. Another four significantly associated variables including: [1] a positive MFT, [2] blood relative with KS, [3] age >45, and [4] the presence of red blood cells. We calculated the expected number of KS in each size by the number of HYF and the figures from part 1. The expected percentage distribution of KS was 54.3, 23.9, 13.1, 4.5, 1.7, 1.4 and 1.1 % percent in stone size 5.0, 5.1-7.5, 7.6-10.0, 10.1-12.5, 12.6-15.0, 15.1-20.0 and >20.0 mm, respectively.

Conclusions: We concluded that nine from ten of the KS detected in the community were small (≤10 mm), thus active management at the community level should be the prime concern.

Key words: dyspepsia, hyperechoic foci, myofascial pain, purine rich food, ultrasound

INTRODUCTION

Worldwide, regional differences in the incidence of urolithiasis have resulted in certain high incidence areas being called stone belts1.[1] In Thailand, epidemiological analysis has indicated that stone belts lay over the northern and northeastern regions where incidence is 3 to 5 times higher than in other parts of the country.[2] The patterns of urinary stone disease in Thailand, as in other parts of the world, have changed from a predominance of lower urinary tract or bladder stones to upper urinary tract or kidney stones (KS).[3-5] However, preliminary studies and anecdotal evidence suggests that the burden of stone disease at the community level is more extensive than evidenced in the hospital records. In one epidemiological survey for

[1] Department of Community Medicine, Faculty of Medicine, Khon Kaen University, Khon Kaen, Thailand 40002
[2] Department of Radiology, Faculty of Medicine, Khon Kaen University, Khon Kaen, Thailand 40002
[3] Department of Biochemistry, Faculty of Medicine, Khon Kaen University, Khon Kaen, Thailand 40002

the prevalence of bladder stones indicated that, for every patient hospitalized for stone removal three persons pass their stones spontaneously and eight have presumptive symptoms.[3] The sizes of stone are the major determinant for the choice of treatment. Stones < 5 mm in diameter have a high chance of passing spontaneously, in comparison with only 50% for those 5-7 mm. KS over 7 mm in diameter usually require urological intervention.[6] Most hospital admitted cases having open stone surgery (OSS) or extracorporeal shock wave lithotripsy (ESWL) represent for only those stones >10 mm. ESWL has become the treatment of choice for most calculi of the upper urinary tract and the need for OSS has declined considerably. However, stone recurrence is often encountered as a long-term problem requiring re-treatment. The rate of recurrence after ESWL varies according to the stone types but the higher is the infected stone. If stone fragments are retained, the re-growth rate is about 33% at 3.6 years.[7] Kosar *et al.*[8] reported that the rate of recurrence was 31.8% within a mean of 40 months in the OSS group, whereas this figure was 13.9% with a mean interval period of 46 months in the ESWL group. However, the mean diameter of KS in both groups reported by Kosar et al. were different (29±8 *vs.* 14±11 mm, respectively). A study in the Northeast Thailand reported a recurrence of 25 and 49 percent at 12 and 24 months respectively after OSS.[9] To gain more understanding of the size distribution of KS and their associated symptoms, we conducted a field survey in 20 rural villages. By simple random sampling, some of these subjects with or without HYF by ultrasonography (US) were sent to the university hospital for unenhanced helical computed tomography(UHCT) for comparisons, and the figures obtained were use to calculate the expected number of different sizes of KS.

MFT	=	Modified Fist Test
KS	=	Kidney Stone
HYF	=	Hyperechoic Foci
US	=	Ultrasonography
ESWL	=	Extracorporeal Shock Wave Lithotripsy
UHCT	=	Unenhanced Helied Computed Tomography
OSS	=	Open Stone Surgery
HYF	=	Hyperechoic Foci

METHODS

Sampling Method and Estimation of Sample Size

The sample size was calculated based on the purpose to demonstrate the percent distribution of the sizes of small KS, ≤ 5.0, 5.1-7.5 and > 7.5 mm, in the community. We assumed that the 5.1-7.5 mm group was 25% and the worst acceptable value was 20%, so we needed at least 263 KS to answer the question. We estimated that about 50% of HYF detected by US were confirmed as KS, so we had to study at least 526 subjects with HYF. The previous study revealed that the prevalence of HYF in voluntary villager seeking for free examination of urinary stones by ultrasonography was not less than 40%. So the sample size for ultrasonography screening was 1,315 persons (400/0.35). To answer the question about sensitivity and specificity of US as compared to the UHCT, we made the assumption that the sensitivity and specificity was 0.75 and 0.65, respectively. The sample size for detection of the sensitivity and specificity was 73 and 88 kidneys, if we allowed the 0.10 difference. So we needed at least 88 normal kidneys (or 44 negative subjects) and 88 positive kidneys to enrolled in the study. We decided to use 100 subjects with HYF and 64 normal subjects in step 2 of the study.

Data Collection Step1: Screening for HYF

Free US checks for kidney abnormality were offered through the village health volunteer network in 2 districts of Khon Kaen Province in the Northeast Thailand. There were 20 rural villages willing to participate in all the 2 step of the study. Participants in the study joined voluntarily and were interviewed for demographic information and the presence of 9 common multiple chronic health complaints (MCHC), including: [i] myofascial pain, [ii] back pain or lower abdominal pain, [iii] dyspepsia, [iv] arthralgia, [v] headache, [vi] fatigue, [vii] frank paresthesia, [viii] dysuria, and [ix] any of these variables aggravated by the consumption of purine-rich foods (PRF) or alcoholic beverages. Participants had their costo -vertebral angle area repeatedly percussed with equal force by the examiner's fist to see which side had more dull pain (i.e., a positive fist test). Then each subject underwent a spot urinalysis for the presence of red blood cells (hematuria) and white blood cells (pyuria) using a strip (Combur^{10} Test M, Roche, Basel, Switzerland) read by a portable urine analyzer (UriluxS, Roche, Basel, Switzerland). The presence of significant hyperechoic focus (HYF) was determined using 256-grey-scale US scanner with a multiple anatomical approach, which included the prone, decubitus and supine views obtained in the transverse, longitudinal and oblique planes. Characteristically, small stones diagnosed in the present study appeared as a significant HYF with or without acoustic shadowing. It was denser than the renal vascular tissue and its location was not coincide with the distribution of vascular tissue and had related calyectasis. The longest diameter of the biggest HYF was measured and recorded when there were multiple foci.

Fig 1 Details of patients enrolled in the study

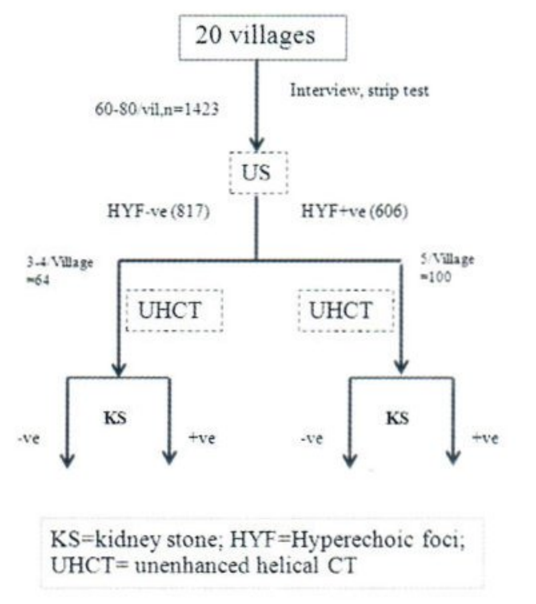

Step 2: UHCT for KS (Unenhanced Helical Computed Tomography for Kidney Stone)

From the 20 villages willing to participate in step1, we performed the simple random sampling of 5-6 subjects who had the HYF size < 10.1 mm and 3-4 normal subjects for each village for step 2. These subjects were sent for UHCT in the university hospital within 48 hour after screening by US. The radiologist was blind for the US result. The Details of the results in step2 would be in another report. We extracted the rate of positive KS at different sizes of HYF to calculate the expected numbers of KS in the survey. The results are presented as the percents, means (SD). For comparison between groups, the Student-*t* tests and χ^2-test were used. A probability of $p < 0.05$ was considered statistically significant. Logistic regression models were use to investigate the variables associated with HYF.

This study was funded by Khon Kaen University. The protocol was approved by the Ethics Committee of Khon Kaen University (HE 450309).

HYF = Hyperechoic Foci
MCHC = Multiple Chronic Health Complaints
PRF = Purine Rich Foods

RESULTS

Participants

A total of 1,423 subjects (65.8% females) were enrolled in step1. The subjects were between 18 and 72 years of age and were divided into three groups: under 30, 30-59 and $\geq$ 60 years old. Those between 30 and 59 constituted the largest group (79.2%) (Table1).

HYF findings

US imaging detected significant HYF in 606 subjects (42.2%). When a comparison was made among the groups for the prevalence of HYF, the 60 and over group was the highest (53.7%) while those under 30 was the lowest (18.7%) (Table1). For step 2, we random sampled 103 subjects who had HYF in their kidneys and 3 subjects were unavailable at the appointed time. The total subjects in step 2 was 164, 100 subjects were positive for HYF in at least one kidney (118 positive kidneys HYF and 82 normal kidneys) and 64 subjects without HYF (128 kidneys with negative HYF) were willing to join.

Table 1 Age and sex distribution of participants and ultrasonography findings

Character	Negative n (%)	Positive For HYF n (%)	Total (%)
Sex Male	280(60.3)	193(39.7)	486 [34.2]
Female	497(55.9)	413(44.1)	937 [65.8]
Total	817(57.4)	606(42.6)	1,423 [100]
Age < 30	109(81.3)	25(18.7)	134 [9.4]
30-59	633(56.2)	494(43.8)	1,127 [79.2]
≥ 60	75(42.3)	87(53.7)	162 [11.4]
Total	817(57.4)	606(42.6)	1,423 [100]

( ), % within row; [ ], % within column; HYF, hyperechoic foci

Distribution of HYF sizes and kidney stone sizes

At first we arranged the distribution of the HYF, and then calculated the expected number of KS. The HYF were classified into seven groups according to their sizes (range, ≤ 5.0 to > 20.0 mm in diameter). The average (SD) size of the detected HYF was 5.22 (4.7) mm in diameter: 66.0, 23.6, 6.3, 2.1, 0.8, 0.6 and 0.5 percent were 5, 5.1-7.5, 7.6-10.0, 10.1-12.5, 12.6-15.0, 15.1-20.0 and >20.0 mm. Two-third of the HYF were ≤ 5.0 mm and less than 5% were > 10.0 mm (column 5, Table 2). The step 2 data revealed the rates of detection of KS from the finding of the HYF depend on their sizes, which was 29.5, 48.0 and 100.0% for stone size 5, 5.1-7.5, and >7.5 mm, respectively (column3, Table 2). The percentage of positive KS despite negative HYF was 4.7%. From these figures, we calculated the expected number of stones for each size (column 4, Table 2). After the adjustment, the expected percentage stone size distribution was 40.8, 23.9, 13.1, 4.5, 1.7, 1.4 and 1.1 % in 5, 5.1-7.5, 7.6-10.0, 10.1-12.5, 12.6-15.0, 15.1-20.0 and > 20.0 mm, respectively. For the negative HYF, 39 stones (13.5%) were expected. Only 8.7% of the KS was bigger than 10 mm. From one kidney stone of the size bigger than 1.0 mm found there were more than ten KS or twenty KS existed in the community. The distributions of KS by size after the adjustment are presented in Figure 2.

Association between chronic symptoms and HYF

Our results showed that eight of the nine MCHC parameters, except headache, were significantly associated with the finding of HYF i.e., myofascial pain (odds ratio(OR) = 1.82, 95% confidence interval (CI): 1.44, 2.30), back pain or lower abdominal pain (OR=1.71, 95%CI: 1.36, 2.16), dyspepsia (OR=1.55, 95%CI: 1.25, 1.92), arthralgia (OR=1.43, 95%CI: 1.16, 1.77, dysuria (OR=2.33, 95%CI: 1.84, 2.97), fatigue (OR= 1.32, 95%CI: 1.05, 1.65), frank paresthesia (OR=1.75, 95%CI: 1.35, 2.26) and MCHC aggravated by PRF (OR= 2.34, 95%CI: 1.9, 2.92) (Table 3). Besides the MCHC parameters, there were four other variables which were significantly associated with HYF. These four variables were: the fist test, blood relative with KS, age over 45, and urine RBC. When logistic regression models were performed only two MCHC variables and three other variables were significantly associated with the finding of stones. These were [i] dysuria [(adjusted OR =1.69 (95%CI:1.26 ,2.26)], [ii] MCHC aggravated by PRF [adjusted OR=1.59 (95%CI:1.21,2.09)], [iii] positive fist test [adjusted OR= 2.32(95% CI: 1.76 ,3.04)], [iv] at least one kidney-stone blood relative [adjusted OR=1.81 (95% CI:1.33,2.47)] and [v] age over 45 years [adjusted OR=1.55 (95%CI: 1.15,2.01)]. MCHC were significantly associated with HYF and pyuria. Subjects with HYF had more chronic symptoms than the ones without HYF ($p<0.0001$, Student-t tests). The respective mean (SD) of MCHC parameters in subject with and without HYF was 5.1(2.2) and 3.9(2.0). Subjects with pyuria also had significantly ($p<0.0001$, Student-*t* tests) more chronic symptoms than the one without urine WBC (Table 4). Subjects with HYF had a higher rate hematuria (46.5%) than those without (41.1%); however, the difference was not significant (Table 3).

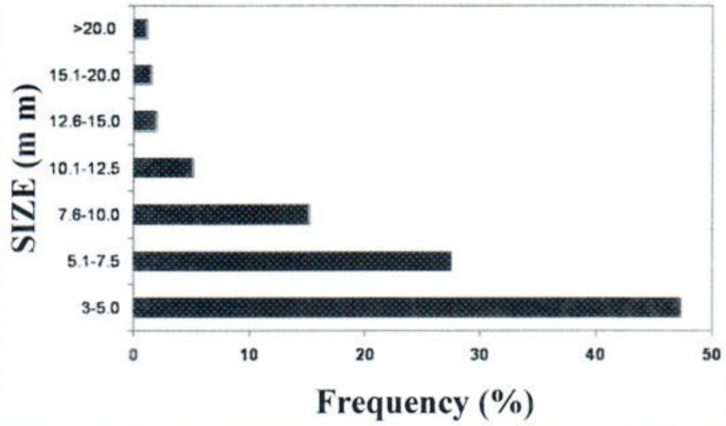

Fig.1 Distribution of the sizes of kidney stones by US (adjusted by UHCT)

Table 2 Distributions of the sizes of hyperechoic foci (HYF), kidney stones

HYF size (mm)†	No. with HYF, n (%)	%KS (UHCT)‡	Expected No. of KS, n (%)	% Cum. of HYF	%Cum. of KS
Not found	817	4.7	39 (13.5)	0	13.5
? 5.0	400 (66.0)	29.5	118 (40.8)	66.0	54.3
5.1-7.5	143 (23.6)	48	69 (23.9)	89.6	78.2
7.6-10.0	38 (6.3)	100	38 (13.1)	95.9	91.3
10.1-12.5	13 (2.1)	100	13 (4.5)	98.0	95.8
12.6-15.0	5 (0.8)	100	5 (1.7)	98.8	97.5
15.1-20.0	4 (0.7)	100	4 (1.4)	99.5	98.9
> 20.0	3 (0.5)	100	3 (1.1)	100.0	100
Total	06 (100)		§289 (100)		

†, Mean SD = 5.22 4.7 mm;
‡, When unenhanced helical computed tomography (UHCT) is the reference ;
KS, kidney stones; %Cum, Cumulative percent;
§ Prevalence of KS = (100x289)/1423 = 20.3%

Table 3 Association between chronic health complaints, urinary findings, other variables and hyperechoic foci (HYF)

Variable	HYF (%)			OR(95%CI)	Adj OR† (95%CI)
	Neg	Pos	All		
Myofascial pain	61.9	74.8	67.5	1.82(1.44,2.30)	1.28(0.95,1.72)
Back pain	61.5	73.3	66.7	1.71(1.36,2.16)	
Dyspepsia	45.3	56.1	50.0	1.55(1.25,1.92)	
Arthralgia	41.4	50.4	45.3	1.43(1.16,1.77)	
Dysuria	20.1	37.0	27.6	2.33(1.84,2.97)	1.69(1.26,2.26)
Fatigue	28.4	34.3	31.0	1.32(1.05,1.65)	
Frank paresthesia	17.9	27.6	22.1	1.75(1.35,2.26)	
Aggravated by PRF‡	30.6	50.8	39.5	2.34(1.90,2.92)	1.59(1.21,2.09)
Headache	52.8	57.6	54.9	1.22(0.98,1.51)	
Positive MFT§	23.4	45.8	32.6	2.77(2.15,3.57)	2.32(1.76,3.04)
Blood-relative with KS	16.8	27.7	21.4	1.90(1.43,2.53)	1.81(1.33,2.47)
Age >45 years	46.5	60.9	52.9	1.77(1.42,2.21)	1.55(1.15,2.01)
Pyuria	40.3	48.0	43.7	1.37(1.11,1.70)	1.28(0.99,1.65)
Hematuria	41.1	46.5	43.7	1.24(0.99, 1.53)	

† By multiple logistic regression;
‡ Purine rich food; ? Modified fist test

Table 4 Hyperechoic foci (HYF), pyuria and multiple chronic health complaints (MCHC)

Variable		Subjects	No. of MCHC mean (SD)	p-value †
HYF	positive	606	5.1(2.2)	<0.001
	negative	817	3.9(2.0)	
Pyuria	positive	603	4.9(2.1)	<0.001
	negative	780	4.2(2.1)	

†, Student-t tests

DISCUSSION

Summary of Main Findings

The percentage of KS size 5, 5.1-7.5, 7.6-10.0, 10.1-12.5 and 12.6-15.0 mm were 54.3, 23.9, 13.1, 4.5 and 1.7%, respectively. For ten KS in the community, only one was bigger than 10.0 mm, so this showed that the diagnosed KS in the hospital based treatment was only the tip of iceberg when compared with the burden of the disease. More than half of the HYF size < 7.5 mm found in this study was not the KS. The HYF was associated with purine-rich food problems, pyuria, and multiple chronic complaints (dyspepsia, arthritis, myofascial pain, back pain, fatigue and positive Modified Fist Test). The

HYF which was not the KS may be the sludge and can be the nest of bacterial infection.

Where This Fits with Other Literature

The finding also suggesting that the number of nephrolithiasis admitted to the hospital represents a small fraction of the real burden in community. This is similar to a report on bladder stones in the region.[3] The HYF in this study was associated with pyuria and the MCHC. Vrtiska and coworker10 postulated that the HYF might be sludge or milk for uric acid or calcium. The HYF could be a nest for microorganisms and chronic infection, which may be the cause of symptoms in the MCHC. One study reported that all MCHC subsided when treated kidney stones presenting with antibiotic plus Orthosiphon grandiflorus.[11]

The distribution of KS size in this study can explain the variation in the figure of stone prevalence when different instruments were used. If we can use the gold standard UHCT in a survey to detect KS of all sizes, the prevalence rate will be higher than ordinary instruments. The increasing intensity in arthralgia, myofascial pain and dyspepsia after consuming purine-rich foods or alcoholic beverages suggested the subjects might be suffering from uric acid over-production. Hyperuricosuria as a consequence of uric overproduction can promote stones formation by heterogeneous nucleation of calcium oxalate by uric acid crystals or reduction of urine crystal growth inhibitors. Uric acid stones are known to form because of dehydration, excessive sweating, intestinal alkali loss and purine overload or overproduction.[11-13] A study found that 38.4% of urolithiasis in Kuwait had abnormal mineral metabolic screen of which hyperuricosuria accounted for 79.8% of those abnormalities.[14] Primary gout, where urinary pH is low, is associated with uric acid crystallization and stone formation15. In the present study, although the symptoms of gouty arthritis were aggravated by PRF, joint pain was less severe than in overt gouty arthritis and most of the patients were female. Further study about the composition of the kidney stones and purine metabolism in this group of subjects should be undertaken. There was a strong association between the finding of HYF and the pain on percussion at the CVA. Our Modified Fist Test (MFT) was performed as follows: the examiner lightly percussed with his fist 4-5 times on the costo-vertebral area of one side then switched to the other and repeats at least 4-5 times. The subjects who were positive for MFT felt only a small difference in dull pain between sides. The severity of pain was less intense than acute pyelonephritis. The authors want to name this technique the "modified fist test" (MFT). A positive MFT showed the strongest association with HYF (adjusted OR 2.32, 95%CI: 1.76, 3.04).

Strengths and Limitations

This study was the first attempt to reveal the important of small KS and the HYF. The 256 grey -scale US used in this study was widely used in clinics and community hospitals in Thailand, so the result can be generalized for the general practitioners who regularly use the machine. On different point of view, the high resolution US and the better surrounding in the scanning may be more accurate and may alter the percentage distribution of the KS. The authors agreed with this idea and it should be performed where the resources and technologies are available.

This study did not aim to report the stone prevalence, so we did not randomly select the subjects in the enrollment. The 42.6% of HYF (Table 1) and 20.3 % of KS (Table2) in this study does not represent the real prevalence because of the selection bias. The mean (SD) MCHC variables in the subjects with HYF and without HYF in this study was 5.1(2.2) and 3.9(2.0) (Table 4). The participants might choose to join the project because they already had some symptoms of MCHC, which were perhaps related to the presence of stones or HYF in the urinary tract. The true prevalence may therefore be lower if a rigorous sampling technique is implemented.

Implications

The majority of community kidney stones were small, more than half under 5 mm and 90%

under 10 mm, which is crucial for the control of kidney stone via health education in the community level. Subjects with multiple chronic symptoms (MCHC) might have sludge/small kidney stones, so clinicians encountering patient with MCHC should consider the appropriate investigations or treatments.

A history of chronic symptoms aggravated by PRF, the new finding in the present study, should not miss in the history taking process.

MCHC = Multiple Chronic Health Complaints

ACKNOWLEDGEMENTS

The authors thank the Faculty of Medicine, Khon Kaen University for its funding support, Prof. A J Hedley for his valuable comments and Mr. Bryan Roderick Hamman for assistance with the English -language presentation of the manuscript.

REFERENCES

1. Swift Joly J. The etiology of stone. J Urol 1934; 32:541.
2. Unakul S. Urinary stones in Thailand: A statistical survey. Siriraj Hosp Gaz 1958; 13: 199-214.
3. Halstead SB, Valyasevi A. Studies of bladder stone disease in Thailand: III Epidemiologic studies in Ubol province. Am J Clin Nutr 1967; 20:1329-39.
4. Sriboonlue P, Prasongwatana V, Chata K, Tungsanga K. Prevalence of upper urinary tract stone disease in a rural community of north-east Thailand. Br J Urol 1983; 55: 353-5.
5. Yanagawa M, Kawamura J, Onishi T, Soga N, Kameda K, Sriboonlue P, Prasongwatana V, Bowornpadungkitti S. Incidence of urolithiasis in northeast Thailand. Int J Urol 1997; 4: 537-540.
6. Coe FL, Evan A and Worcester E. Kidney stone disease J. Clin. Invest (2005). 115: 2598-2608.
7. Lahme S, Wilbert DM, Schneider M, Bichler KH. Fate of clinically insignificant residual fragment (CIRF) after ESWL. In: Rodgers AL, Hibbert BE, Hess B, Kahn SR, Preminger GM, editors. Urolithiasis 2000. Proceedings of the 9th International Symposium on Urolithiasis; 2000 Feb 13-17; Cape Town (South Africa). Rondebosch (South Africa): University of Cape Town Publishers; 2000. P.748-9.
8. Kosar A, Sarica K, Aydos K, Kupeli S, Turkolmez K, Gogus O. Comparative study of long-term stone recurrence after extracorporeal shock wave lithotripsy and open stone surgery for kidney stones. Int J Urol 1999 Mar; 6 (3): 125-9.
9. Bowornpadungkitti S, Sriboonlue P, Tungsanga K. Post operative kidney stone recurrence in Khon Kaen Regional Hospital. Thai J Urol 1992; 13: 21-6.
10. Vrtiska TJ, Hattery RR, King BF, Charboneau JW, et al. Role of Ultrasound in Medical Management of Patients with Renal Stone Disease.Urol Radiol14: 131-138(1992)
11. Premgamone A, Sriboonlue P, Ditsatapornjaroen W, Maskasem S, Sinsupan N and Apinives C. A long-term study on the efficacy of a herbal plant, Orthosiphon grandiflorus, and sodium potassium citrate in treatment renal calculi. Southeast Asian J Trop Med Public Health 32: 654-60.
12. FL, Moron E, Kavalieh AG: The contribution of dietary purine over consumption to hyperuricosuria in calcium oxalate stone formers. J Chronic Dis 1976; 29: 793-800.
13. FL, Kavalich AG: Hypercalciuria and hyperuricosuria in patients with calcium nephrolithiasis. N Engl J Med 1974; 291: 1344-1350.
14. Reshaid K, Mughal H, Kapoor M, Epidemiological profile, mineral metabolic pattern and crystallographic analysis of urolithiasis in Kuwait.Eur J Epidemiol 1997;13(2):229-234
15. Gutman AB, Yu TF. Uric acid nephrolithiasis. Am J Med1995; 45: 756-779.

UTERINE FIBROID EMBOLIZATION(UAE): CHANGE IN VOLUME OF FIBROID AND THE UTERUS

Krisdee PRABHASAVAT, Pattamapun ANANTAPONG, Chutakiat KRUATACHUE, Trongtum TONGDEE, Saowanee HOMSUD, Weeasak WONGTIRAPORN, Chanchai VANTANSIRI[1]

ABSTRACT

Purpose: For evaluation the effectiveness of bilateral uterine arterial embolization, (UAE) in the treatment of fibroids, in aspect of changes in volume of fibroid and the uterus.

Material and Method: Retrospective study of pre and post UAE MRI in 8 Thai women, mean age 36 years who were to undergo bilateral UAE of uterine fibroids, from January, 2006-January, 2008. The follow up MRI was 15d, 1month, 3months(3 pts), 6months(2pts) and 2 yrs(1pt). Bilateral UAE was performed by injecting 500-700 micron polyvinyl alcohol (PVA) or 700-900 micron Beadblock. Two radiologists interprete MRI by consensus. The volume of fibroid and the uterus was calculated by the formula;lengthxdepthxwidth x 0.523. The signal intensity change in MRI after UAE was observed.

Result: Technical results Bilateral embolization of uterine arteries was accomplished in all patients(100%). Patients had multiple fibroids(range 1-6 lesions). 26 fibroids were noted. The volume of fibroids varied from 3.6-512.4 cm3(mean=94.1 cm3). The mean volume reduction of fibroids after bilateral UAE was 36.75%. The mean volume reduction of intramural lesions was 44.54%. The mean volume reduction of subserosal and submucosal lesions were 28%and 25% respectively. No major complication, no mortality was occurred.

Conclusion: Significant volume reduction of fibroid after bilateral uterine artery embolizatiòn for treatment of fibroid with good clinical outcomes.

UAE = Uterine Artery Embilization
pts = patients

Uterine fibroid is the most common gynecologic tumor in reproductive age, being symptomatic about 25-30% of women but present in as many as 70-80% of women by age 50. Uterine fibroids are caused by abnormal growth of sex steroid-responsive muscle cells in the myometrium. Although benign, fibroids can grow at very rapid rates and cause a constellation of symptoms, including menorrhagia (excessive menstrual bleeding), pelvic pressure, infertility, pregnancy loss and abdominal distension. Symptomatic fibroids have generally been treated by hysterectomy. Other treatment including myomectomy, myolysis, cryoablation and hormone therapy have been used in selected cases. The common hysterectomy carries complications about 10-15% of surgery with several days of hospital stay and long recovery time. Myomectomy has similar associated risks and approximately 20-25% of women undergoing

[1] Radiology Dept, and OB-GYN Dept.. Siriraj Hospital Faculty of medicine, Mahidol University.

myomectomy will have a recurrence of symptoms, requiring further intervention. Myolysis and cryoablation both also require laparotomy or laparoscopy and general anesthesia, and reported results have been mixed. Hormonal therapy is effective for short-term control but requires continued medication and has associated side effect, such as hot flashes, mod swings, insomnia and dyspareunia.

Uterine arterial embolization (UAE), a recognized treatment of acute pelvic hemorrhage, has become accepted as an effective and safe treatment for fibroids. This minimally invasive procedure requires a recovery of days rather than weeks but has results similar to those of other uterine-saving therapy.

The purpose of the study is to evaluate the effectiveness of bilateral uterine arterial embolization the in treatment of fibroids, in aspect of change in volume of fibroid and the uterus.

MATERIAL AND METHOD

Retrospective study of MRI of 12 consecutive women, age ranged 27-41 years (mean age, 36 years) who were to undergo bilateral UAE of uterine fibroids, from January, 2006-January, 2008.

8 patients were Thai women and the other 4 patients were foreigners. We studied only the imagings and clinical informations of Thai patients.

Every patients underwent MRI of lower abdomen before and after bilateral UAE, by using 3 T system (Achieva, Phillips). The MRI included sagittal T2W/TSE, coronal SSH/TSE, axial T2W/TSE/SPAIR, axial T2W/TSE, axial T1FFE/Inphase and THRIVE/GD/FS.. The follow up MRI was 15d, 1 month, 3 months (3 pts), 6 months (2pts) and 2 yrs (1pt).

Embolization was performed via unilateral femoral approach. Bilateral uterine arteries were selective catheterized in all cases. We used Robert pre-shape uterine catheter or 4 F. cobra-head giding catheters. Embolization was achieved by injecting 500-700 micron polyvinyl alcohol (PVA) or 700-900 micron Beadblock into each uterine artery until the flow had ceased before refluxing of contrast media into anterior division of internal iliac artery.

Conscious sedation with combination of narcotics (morphine sulfate, fentanyl citrate, or both) and benzodiazepines (midazolam hydrochloride) was used in all patients.

The volume of fibroid and the uterus was calculated by the formula; lengthxdepthxwidth x 0.523. The signal intensity change in MRI after UAE was observed. The signal intensity of fibroid was compared to myometrium.

Two radiologists interpreted all MRI by consensus. Statistic analysis was performed using average value.

RESULT

Technical results:

Bilateral embolization of uterine arteries were accomplished in all patients(100%)

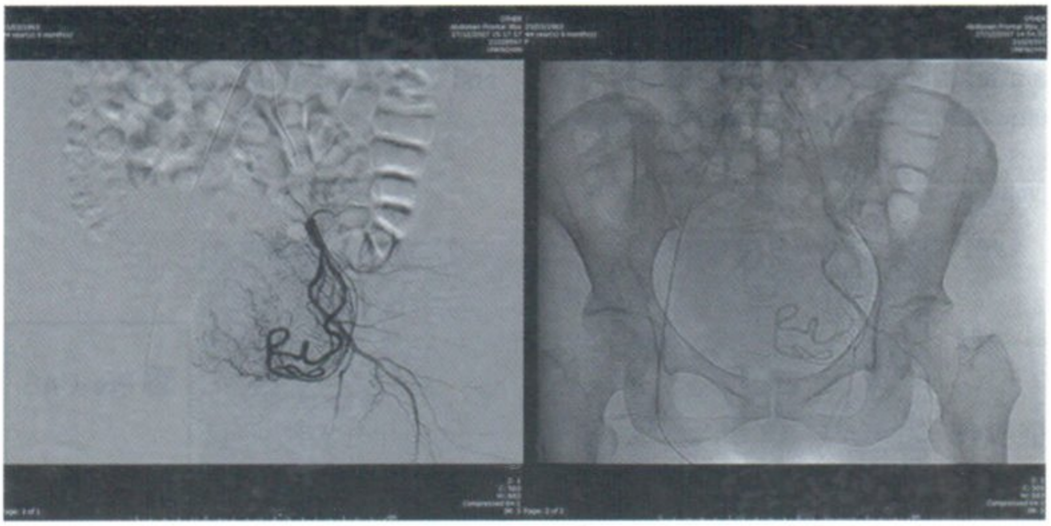

A B

Fig.1 Uterine arteriogram of a patient, presented with a feeling of having a big mass in the pelvis. A. Pre-UAE arteriogram revealed tortuous enlarged Lt. uterine artery with hypervascular mass at Lt. side of uterus. B.After Lt. uterine artery embolization with 500-700 micron PVA, disappearance of hypervascular mass and cessation of blood flow of ascending part of Lt.uterine artery was seen.

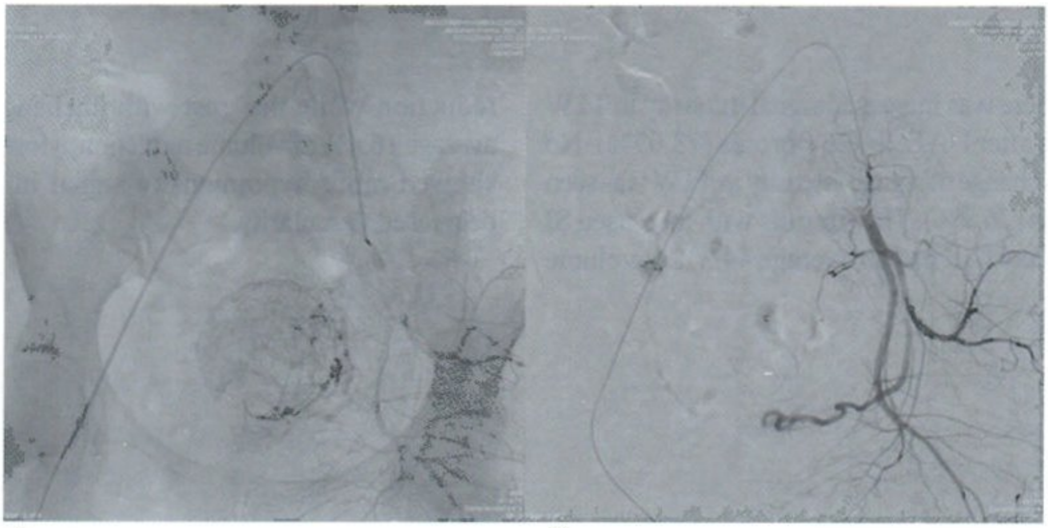

A B

Fig.2 Lt.uterine arteriogram of patient presentation with menorrhagia. A. Pre-UAE arteriogram revealed diffuse hypervasularity area at Lt. lateral fundus. B.After Lt. uterine embolization with 500-700 micron PVA, disappearance of hypervascularity was noted.

Imaging Follow up:

Patients had multiple fibroids(range 1-6 lesions). 26 fibroids were noted. 15 intramural, 7 subserosal and 4 submucodal fibroids were identified. The volume of fibroids varied from 3.6-512.4 cm3 (mean = 94.1 cm3). 24 of 26 fibroids (92.3%) showed volume reduction. The mean volume reduction of fibroids after bilateral UAE was 36.75%. The mean volume reduction of intramural lesions was 44.54%. The mean volume reduction of subserosal and submucosal lesions were 28%and 25% respectively. The fibroid with intermediate-high signal intensity in T1W before UAE were 41.07% reduction of volume after UAE. Those lesions with pre-UAE isointensity and hypointensity in T1W showed 31.8% and 34.5% of volme reduction.

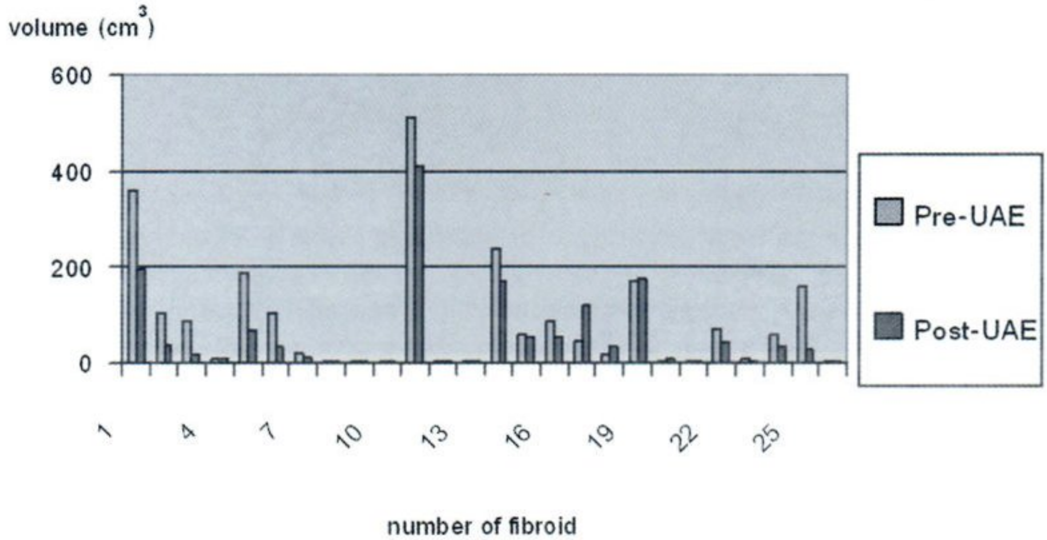

Fig.3 Graph illustrates a comparison of fibroid volume before and after bilateral UAE

There was increased signal intensity in T1W of fibroids after UAE, 24/26 fibroids (73.07%). No significant change of signal intensity in T1W was seen in 7 lesions (26.9%). The fibroids with increased SI in T1W after UAE had an average 44.3% of volume reduction while the rest with unchanged SI had average 16.4% of volume reduction. Most of fibroids showed more hypointensity signal in T2W and decreased vascularity.

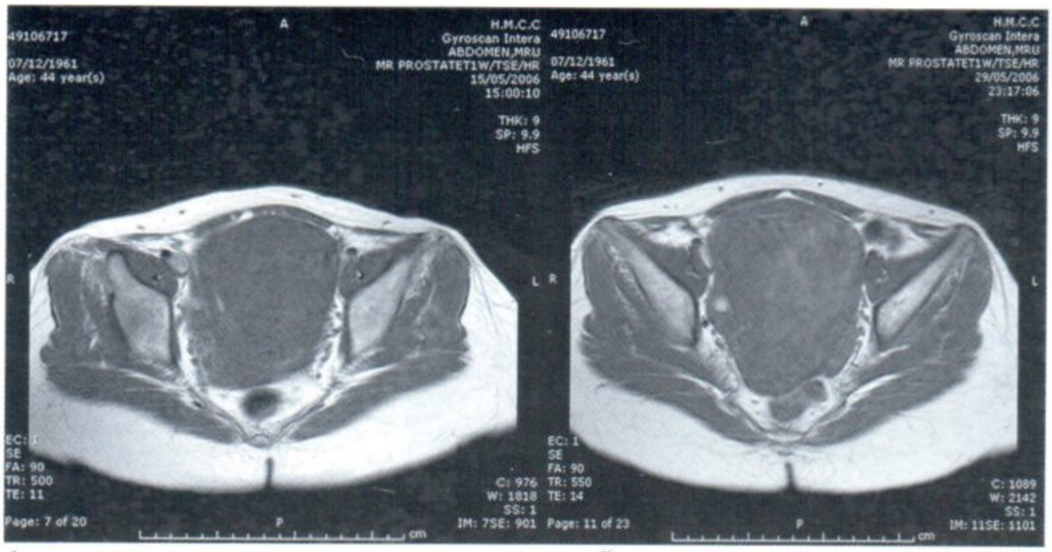

A B

Fig.4 T1-weighted axial image of the uterus. A:Prior to UAE. Large intramural fibroid with isosignal intensity. B:15 days post-UAE image revealed heterogenous increased signal intensity, represents hemorrhagic infarction.

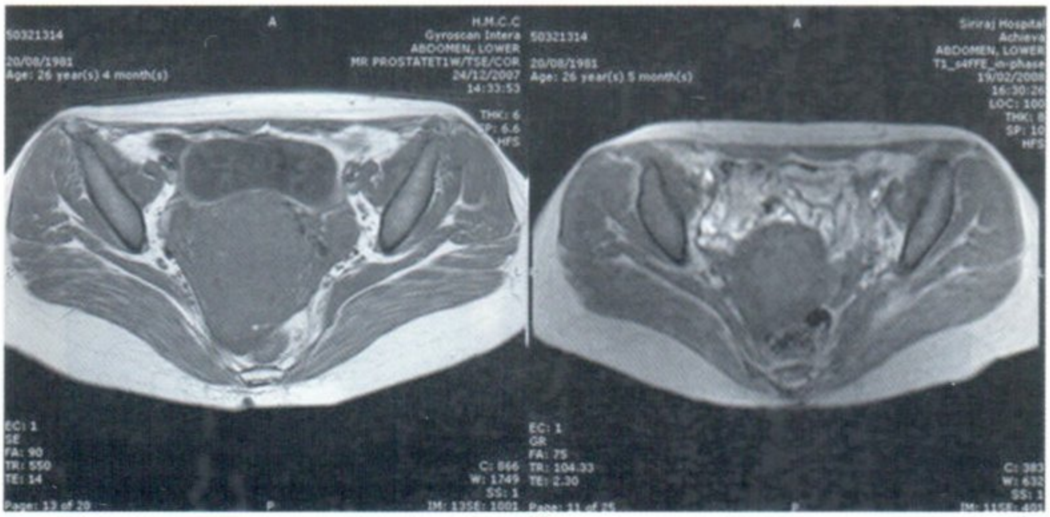

A B

Fig.5 Axial T1W of uterus with fibroid. A. Prior to UAE. B.3 months post-UAE. There was decreased in size of fibroid and the uterus. Increased signal intensity of fibroid was noted.

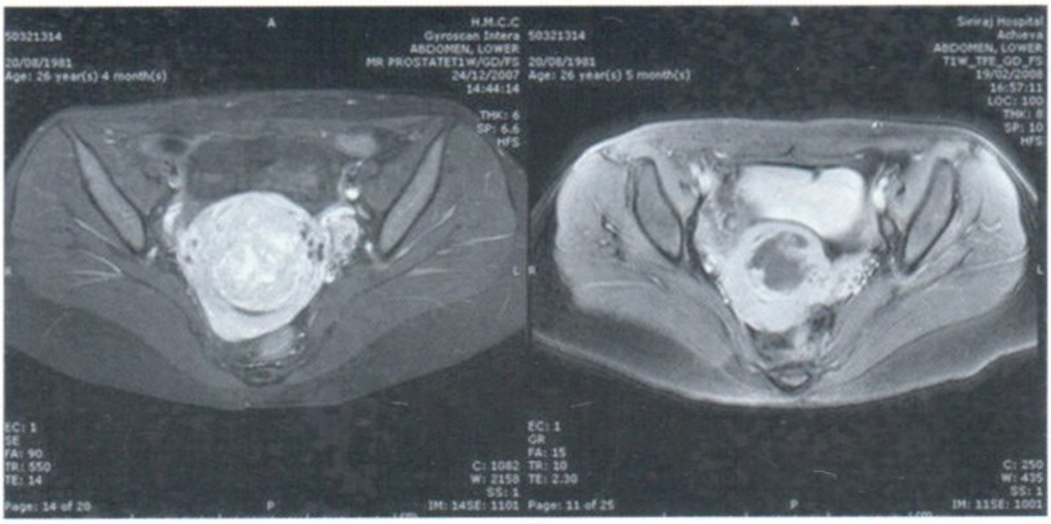

A B

Fig.6 Axial T1W Gd-enhanced images. A.Prior to UAE showed hypervasular fibroid at fundus. B.3 month post-UAE image revealed degeneration of fibroid with decreased size and vascularity.

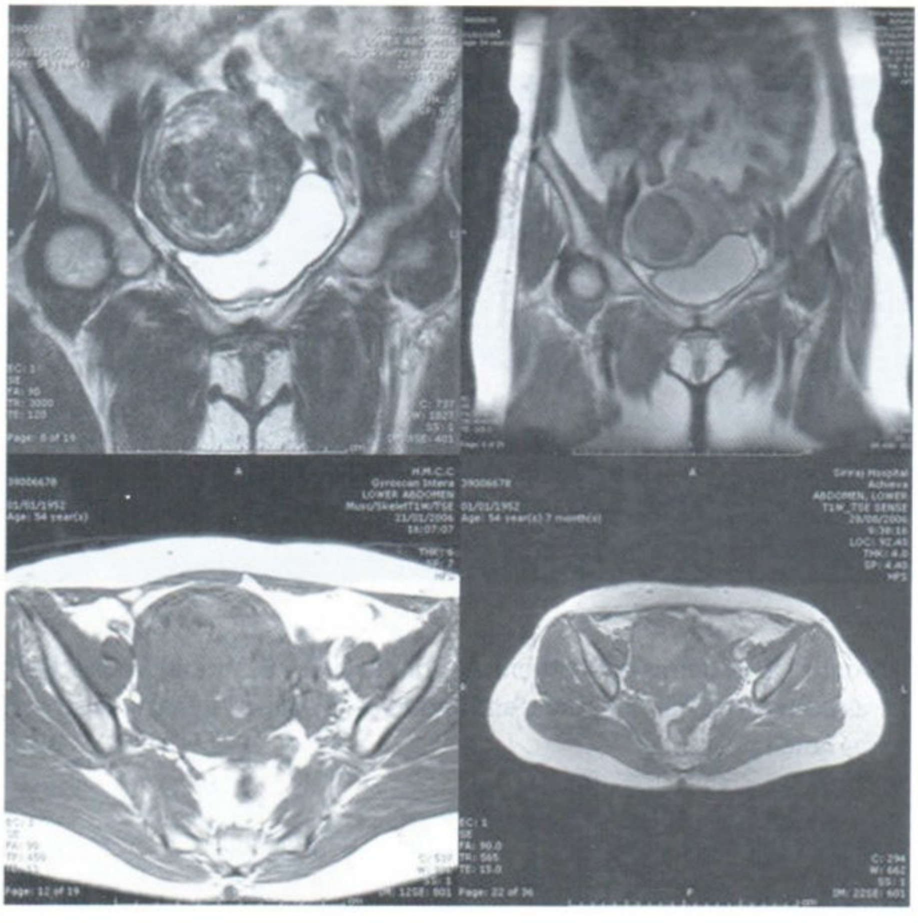

Fig.7 Coronal and axial MRI images in pre-UAE (A,B) and 1 month post -UAE (C,D) Post-UAE images revealed significant decreased size of fibroid with hemorrhagic infarction.

The volume of the uterus was calculated by total volume of the uterus-total volume of fibroids. The volume reduction of the uterus after UAE was 32.1% (range 17.2-47.4%). The greater volume reduction was observed in patients at 3 and 6 months (3 and 2 pts) after UAE, 30.9% and 41.7% respectively. One patient at 2 yrs post-UAE had 10.9% of uterine volume reduction and 37.7 % of fibroid volume reduction.

Clinical Follow Up:

The patient clinical presentations were menorrhagia (4 pts), bulk-related symptoms (3 pts), dysmenorrhea (3 pts), infertility (2 pts). 48 hrs follow up revealed moderate pelvic pain in 2 pts with recovery in few days by using of narcotics. Abnormal bleeding and dysmenorrheal were significant improved in 3 of 4 pts (75%) and minimal improved in 1 pt. Bulk-related symptoms were improved in all 3 pts. (100%) All patients (8pts) (100%) were satisfied with clinical results. The average hospital stay was ranged 2-3 days (mean = 2.2 days)

DISCUSSION

Findings from this study demonstrated significant volume reduction of fibroid after UAE at 1, 3, 6 month and 2 years (36.9%, 34.5%, 39.2% and 37.7 % respectively) The volume reduction of the uterus was obviously, 28.9%, 30.9%, 41.7% and 10.9% at 1, 3, 6 month and 2 years after UAE. A significant decreased in size of the uterus and fibroids has been described by various investigators. Laurent et al. reported the 23% mean size reduction of fibroids in series during the first 3 months after embolization whereas reported by Worthington-Kirsch et al 46% and that by Burn et al 43%. The volume reduction of the dominant fibroid is greater than that of the uterus. The follow up ultrasound has shown a reduction in uterine size of upto 40% with the dominant fibroid decreasing in size by upto 70%. The majority of fibroid shrinkage occurs within 6 month period following embolization with further reduction in size occurring between 6 and 12 months.[12-14]

The immunohistochemical data showed that the myometrium had a significant greater microvascular density than a small or large fibroid.[7] Farrer-Brown et al reported greater average vascular diameter in myometrium than in fibroid. Nandita et al reported that at 4 months after bilateral UAE, myometrium perfusion had returned to normal whereas fibroid perfusion suppressed.

Burn et al reported poor response in patients with fibroid of high signal on T1W before UAE. We found that intermediate-high SI on T1W had 41.1% volume reduction and that of hypo-and isointensity were 34.5 % and 31.8 %. The intramural fibroids had greater volume reduction (44.5 %) than those of submucosal and subserosal lesions (28 % and 25 %). James et al reported that submucosal location and a high correlation with size reduction.

Post-UAE fibroids also showed signal change. In this study there were 19 fibroid (73.1 %) increased signal intensity on T1-weighted with 45.2% of volume reduction. 7 fibroids (26.9%) with no significant signal intensity change after UAE showed 17.9 % volume reduction. The increased signal intensity on T1W in post-UAE is consistent with **hemorrhagic infarction.** Treated fibroids typically show more homogenous dark signal on T2W and diminished vascularity.

All of our 8 patients are satisfied with treatment. Abnormal uterine bleeding and dysmenorrheal are significant improved in 3 of 4 patients. Bulk-related symptoms are also improved in post-UAE of all 3 pts. Worthington-Kirsch et al reported 46 of 52 pts (88%) with marked improvement of abnormal uterine bleeding, 29/31 pts (94%) with substantial improvement of bulk-related symptoms and 90 % of pts returned to normal activity within. 10 days. The mean time for resolution of all postprocedural symptoms was 13 days. 79% of pts would choose this procedure again.

CONCLUSION

This study reveals significant volume

reduction of fibroid after bilateral uterine artery embolization for treatment of fibroid with good clinical outcomes. We suggest that UAE is an effective and safe alternative treatment for uterine fibroid.

REFERENCES

1. Cramer SF, Patel A. The frequency of uterine leiomyomas. Am J Clin Pathol 1990; 94: 435-438.
2. Baird DD, Dunson DB, Hill Mc et al. High cumulative incidence of uterine leiomyoma in black and white women: Ultrasound evidence. Obset Gynecol 2003; 188; 100-107.
3. Wilcox LS, Koonin LM, Pobras R, et al. Hysterectomy in the united states,1998-1990. Obstet Gynecol 1994; 83: 549-555.
4. Burn p, McCall JM, Chinn r,et al. Embolization of uterine fibroids. Br J Radiol 1999; 72: 159-161
5. Jha RC, Ascher SM, Imaoka I et al. Syumptomatic fibroleiomyomata: MR imagin of the uterus before and after uterine embolization. Radiology 2000; 217: 228-231.
6. Tetsuya Katsumori, Kazuhiro Nakajima, et al Is large fibroid a high risk factor for uterine artery embolization. AJR; 2003: 181: 1309-1314
7. Nandita M. deSonza et al. Uterine arterial embolization for leiomyomas: Perfusion and volume change at MR imaging and relation to clinical outcome. Radiology; Feb 2002: 365-373
8. Casey R, Rogers PA, Vollenhoven BJ. An immunohistochemical analysis of fibroid vasculature. Hum Reprod 2000; 15: 1469-1475
9. Pelage JP, Le Dref O, Soyer P, et al. Fibroidrelated menorrhagia: treatment with superselective embolization of the uterine arteries and midterm follow up. Radilogy 200; 215: 428-431
10. James B. Spies, Jean -Pierre Pelage. Uterine artery embolization and synecologic embolotherapy 2004; 6-7, 41-45
11. Walker WJ, Pelage JP. Uterine artery embolization for symptomatic fibroids: clinical results in 400 women with imaging follow up. BJOG 2002; 109: 1262-1272
12. Worthington-Kirsch RL, Popky GL, Hutchins FL Jr. Uteine arterial embolizatiion for the management of leiomyomas, quality of life assessment and clinical response. Radiology 1998; 208: 625-629
13. Molly T., Johanna L., et al. Cost-effectiveness of uterine artery embolization and hysterectomy for uterine fibroids. Radiology 2004; 230: 207-212
14. Haney AF. Clinical decision making regarding leiomyomata; what we need in the next millennium. Environ Health Perspect 2000; 108: 835-839

SPLENIC CALCIFICATIONS

Dr. M.A. Taher & Dr.Shakila Zaman Rima [1]

ABSTRACT

A lady of age 55 years came with upper abdominal pain for ultrasound examination. No abnormality was found except absence of gallbladder which was removed surgically 3 years before and small bright dots scattered all over the spleen (Figure 1). As there was no evidence of infection we suspected hemosiderosis of the spleen as the diagnosis.

INTRODUCTION

Punctate, irregular calcification in spleen is seen following tuberculous or histoplasma infection and occasionally in cysticercosis. Tuberculous calcification of the spleen is usually associated with hepatic and nodal calcification and a similar type of coarse, irregular or punctate calcification may be seen in splenic venous phleboliths. As elsewhere in the body, phleboliths are seldom clinically significant and they appear as oval or irregular foci between 2 and 5 mm in diameter. Diffuse or granular calcification may be associated with previous infarction and is particularly seen in patients with sickle cell disease. Excessive hemosiderin deposition in the spleen produces a diffuse increase in radiodensity, but focal deposition may also occur, in which case multiple dense nodules up to 3 mm in diameter may be seen.[1] Multiple echogenic areas are seen throughout the spleen consistent with chronic granulomata due to past infection with histoplasmosis (H. capsulatum).[2] The patient is almost always unaware of the H. capsulatum infection. Less common causes of diffuse splenic calcification are Brucella species and the formation of phleboliths in splenic veins.[3]

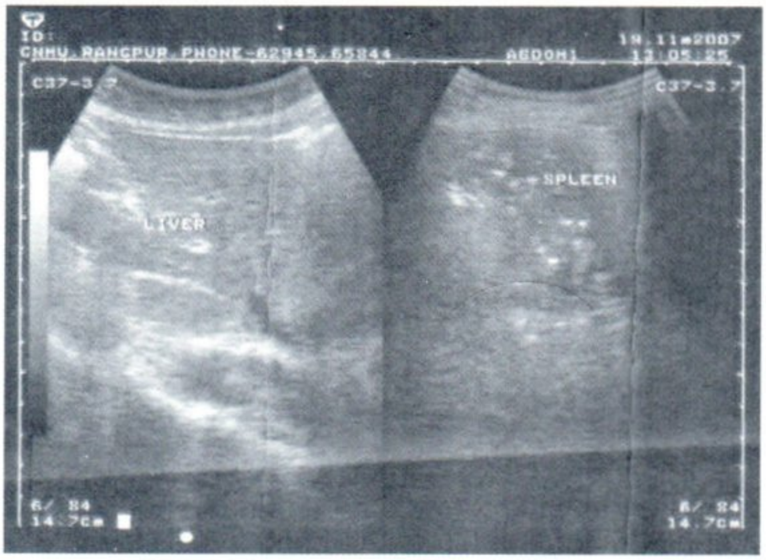

Fig.1 Tiny calcifications in spleen.

[1] Centre for Nuclear Medicine & Ultrasound, Rangpur, Bangladesh.

REFERENCES

1. King DM. The Spleen. In Wilkins RA & Nunnerley HB (Eds.): Imaging of the Liver, Pancreas and Spleen, 1990 Blackwell, Oxford pp. 445-472.
2. Taylor KJW, Aronson D. Spleen. In Goldberg BB (Ed.): Textbook of Abdominal Ultrasound, 1993 Williams & Wilkins, Baltimore pp. 202 -220.
3. Zwiebel WJ. The Spleen. In Zwiebel WJ & Sohaey R: Introduction to Ultrasound, 1998 W.B. Saunders Company, Philadelphia pp. 115-120.

SKELETAL AND HEPATIC METASTASIS IN BREAST CARCINOMA

Dr. M. Abu Taher[1]

ABSTRACT

A post-mastectomy follow-up for infiltrating ductal carcinoma. Of breast reveale multilple skeletal and cyst-like hepatic metastases in a lady aged 45 years.

Key words : Breast carcinoma, skeletal metastases, hepatic metastases.

INTRODUCTION

Breast carcinoma patients are followed-up by radionuclide and ultrasound scans to detect bony and hepatic metastases for proper staging and optimum therapy.

CASE REPORT

A lady of age 45years came to this centre for radionuclide whole-body bone scan and ultrasonography of whole abdomen. She had a nodule in her right breast for the last three and a half years. Post-mastectomy biopsy revealed infiltrating ductal carcinoma. Technetium diphosphonate ($Tc^{99}m$ HDP) bone scan 3 hours after intravenous injection of 20 milli-Curies showed multiple skeletal metastases: 4th cervical vertebra, right shoulder, 1st sacral vertebra, head of the right femur (Fig.1) and shaft of right humerus (Fig.2). Three hypoechoic cyst-like areas were seen in hepatic parenchyma(Fig.3).

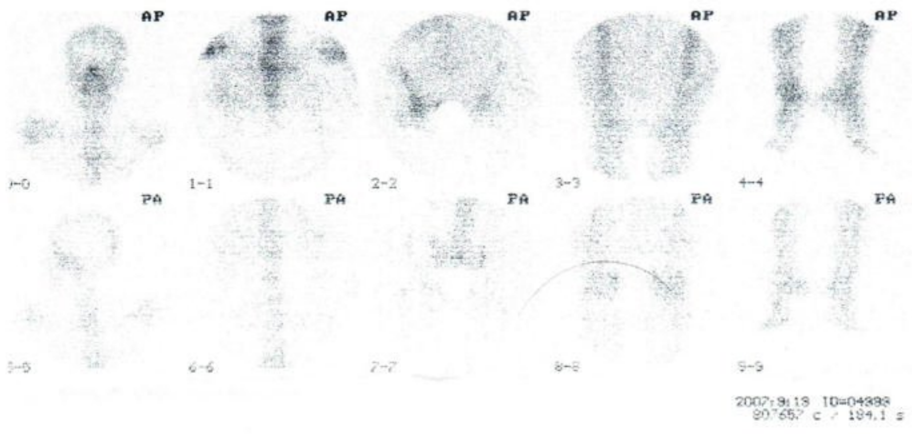

Fig.1 Multiple bony lesions seen in bone scan.

[1] Director, Centre for Nuclear Medicine & Ultrasound, Box 16 Rangpur 5400 Bangladesh.

Fig.2 Spot-view of fractured right humerus in bone scan.

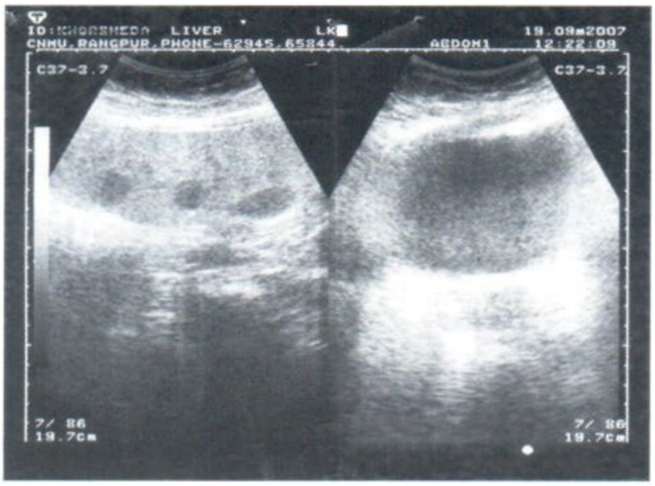

Fig.3 Ultrasonography of liver showing three cyst-like metastases.

DISCUSSION

Breast cancer is the most common cause of death from cancer in women from the age of 15 to 75 years.[1] It is generally accepted that in patients of breast cancer, bone scans should be done in patients with symptoms of bone metastases, soft tissue metastases and locally advanced disease for prognostic purposes.

Five ultrasonographic patterns have been described for hepatic metastases: (a) discrete, anechoic masses; (b) discrete, hypoechoic masses; (c) discrete, hyperechoic masses; (d) discrete target lesions; and (e) diffuse nonhomogeneity of the hepatic parenchyma.[2] Delay in diagnosis and treatment should be avoided as happened in this patient.

REFERENCES

1. McKillop JH. Bone scanning in metastatic disease In: Fogelman I (ed.): Bone scanning in clinical practice, Springer-Verlag, London, 1987, pp.41-60.
2. Zwiebel WJ. Solid-Appearing Hepatic Masses. In: Zwiebel WJ & Sohaey R.(eds.) Introduction to Ultrasound. W.B. Saunders Company, Philadelphia, 1998; pp.81-93.

ANTENATAL SONOGRAPHY OF A SIAMESE TWIN

Dr. M. A. Taher, [1]

ABSTRACT

Antenatal ultrasonographic findings of a conjoined (Siamese) twin is presented as it is a rare phenomenon.

Key words : Twin pregnancy, Conjoined(Siamese) twin, Ultrasonography.

INTRODUCTION

Antenatal ultrasound is becoming popular in many countries of the world including Bangladesh to monitor fetal growth and to detect congenital anomalies. However, to the best of the author's knowledge this is the first report of sonographic findings of cephalopagus conjoined twin from Rangpur, a small town in northern Bangladesh.

CASE REPORT

A lady of age 28 years, gravida 2nd with unspecified period of amenorrhea came for antenatal ultrasound. The sonographic findings were two fetal heads located high up on right side and joined together in a small area of fetal skulls (Fig.1), biparietal diameter (BPD) was 86.1mm, femur length (FL) was 57.2 mm, average fatal age was 33.5 weeks, two placentae were placed anteriorly and posteriorly. Both fetal hearts were beating regularly. A diagnosis of cephalopagus conjoined twin was made and follow- up is being done.

Fig.1 Two fetal heads joined together in small area of fetal skulls.

[1] Director & CMO, Centre for Nuclear Medicine & Ultrasound, Box 16 Rangpur-5400, Bangladesh.

DISCUSSION

The term Siamese twin means congenitally united twins. It is coined after Chang and Eng (1811-1874), joined Chinese twins born in Siam.[1] In some cases the individuals are joined in a small area and are capable of activity, but the extent of union may be so great that survival is impossible. Nevertheless, ultrasonography can detect it before birth and modern surgical techniques have made it possible to separate infants who in the past would not have been expected to survive and have a good prognosis. Twin Pregnancies and the evaluation of twin growth are difficult topics, considering the variables in types of twinning and the methods of growth evaluation.[2]

REFERENCES

1. Taber's Cyclopedic Medical Dictionary. Thomas CL(ed.) 1993 Jaypee Brothers, New Delhi.
2. Harrison SD, Cyr DR, Patten RM, Mack LA. Twin Growth problems: Causes and Sonographic Analysis. Seminars in Ultrasound, CT, and MRI 1993; 14: 56-67.

HYDRANENCEPHALY IN A PRIMIGRAVIDA

Dr. M. Abu Taher[1]

ABSTRACT

A case of hydranencephaly in a primigravid woman seen in our centre by ultrasonography is presented considering its rarity.

Key words : Hydranencephaly, Ultrasonography, Congenital anomaly.

INTRODUCTION

Hydranencephaly is the complete or nearly complete destruction of the cerebral cortex and basal ganglia.[1] Usually, the thalami and lower brain centers are preserved although the thalami may also be involved in the destructive process. The choroid plexus may also be preserved, thus although the head is often small, with functioning choroid plexus, hydrocephalus may ensue. In hydranencephaly, the telencephalon is replaced by fluid-filled cavities covered only by leptomeninges. The abnormalities seen sonographically in hydranencephaly are so striking that detection is not a problem.

CASE REPORT

A woman of age 25 yrs., came to CNMU, Rangpur for antenatal ultrasound. She was a primigravida with a history of 25 wks. of amenorrhea. Sonographic findings were polyhydramnios, large fluid-filled fetal cranium, cerebral mantle was deficient, brain stem, basal ganglia and thalami were visualized, but falx was not intact (fig.1), however, fetal heart movement was present and regular. Other fetal parts were normal apparently. The patient was admitted under Prof.Dr. Ferdousi Sultana in Rangpur Medical College Hospital. The patient was counseled about the poor prognosis of the baby and she agreed to terminate the pregnancy.

Fig.1 Ultrasonography of fetal head showing deficient cerebral mantle and fluid-filled fetal cranium.

[1] Director & Chief Medical Officer and Dr. Shakila Zaman Rima, Medical Officer.
Centre for Nuclear Medicine and Ultrasound(CNMU), Box-16, Rangpur-5400, Bangladesh.

DISCUSSION

In hydranencephaly, cerebrum is entirely replaced by cerebrospinal fluid (CSF). Prognosis is poor, most of the babies die within first year.[2] Multiple causes are described, occlusion of internal carotid arteries or intracranial cerebral artery[3] of developing cerebrai hemispheres and infection. Skull and meninges are normal. Cerebellum and midbrain are intact.

REFERENCES

1. Filly RA. Ultrasound evaluation of the fetal neural axis. In Callen PW(ed.): Ultrasonography in Obstetrics and Gynecology,2nd ed. 1988, W.B. Saunders Company, Philadelphia, pp.83-135.
2. Hall R. The Ultrasound Handbook. 2nd ed. 1993, J.B. Lippincott Co. Philadelphia.
3. Sohaey R. The fetal head, neck and face. In Zwiebel WJ, Sohaey R. Introduction to Ultrasound, 1998, W.B. Saunders Co. Philadelphia, pp. 395-413.

RENAL TRAUMA DETECTION-ROLE OF ULTRASONOGRAPHY

Dr. Md. Murshed Ali. MB, BS; M-Phil(NM);Ph.D. [1]

INTRODUCTION

Renal injuries are the most common injuries of the urinary system. Although well protected by lumbar muscles, ribs, vertebral bodies and viscera, the kidneys have a limited mobility, consequently, parenchymal damage and vascular injuries can easily occur.

Trauma is generally caused by falls, road traffic accidents, blows, sporting accidents, stab wounds and gunshot wounds. Spontaneous rupture of the kidney is uncommon; nevertheless most urologists will have seen at least two or three cases during a lifetime of urological practice.[1]

Renal trauma can be classified as either blunt (non penetrating) or penetrating, and both can be divided into two major classifications, the major and minor injuries.[2]

CASE NO.1

A young men aged about 22 years was admitted into the hospital with a history of blunt trauma in the left upper abdomen followed by hugely distended abdomen and frank haematuria.

On examination patient pulse was 100 beats/min, B.P. was 125/75 mm of Hg. The patient was severely anaemic with a severe tenderness in the left upper abdomen. His temperature was normal. He was sent to the Centre for nuclear medicine and ultrasound, Rangpur for renal scan. Ultrasounds were performed by using Toshiba Just Vision-400 Ultrasound machine using 3.5 to 5 MHz probes. Ultrasound revealed huge haemoperitonium and huge enlarged left kidney with altered size, shape with loss of normal cortico-medullary differentiations and mild free echogenic fluid collection around the left kidney. Retained clot was present in urinary bladder along with a retained catheter. Right kidney was normal in size, shape and position. Cortex, medulla and sinuses were well outlined.

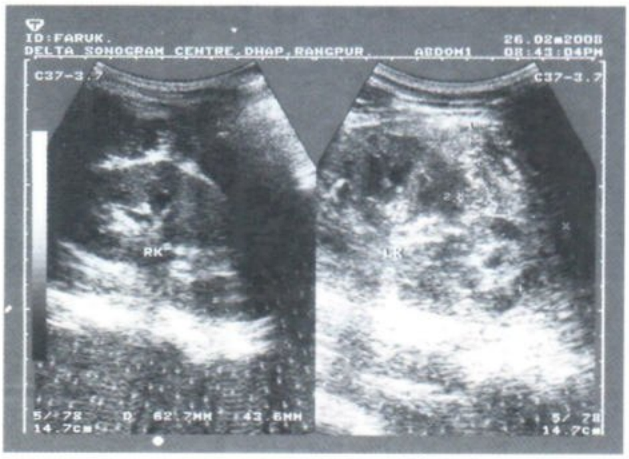

CASE NO.1

CASE NO.2

A young female aged about 18 years was admitted into the hospital with a history of blunt injury in the right upper abdomen for 15 days, having a severe rise of temperature with features of acute abdomen and frank haematuria.

On examination patient pulse was 105 /min,

[1] Senior Medical Officer and Director (Acting) Centre for Nuclear Medicine & Ultrasound, Dinajpur, Bangladesh.

B.P was 120/70mm of Hg. The patient was severely anaemic with a severe tenderness in the right upper abdomen. Her temperature was 103^0. She was sent to the Centre for nuclear medicine and ultrasound, Rangpur for scanning. Ultrasounds were performed by using Toshiba Just Vision-400 Ultrasound machine using 3.5 to 5 MHz probes. Ultrasound reveals huge haemoperitonium and hugely enlarged right kidney with altered size, shape and loss of normal cortico-medullary differentiations and mild free echogenic fluid collection around the right kidney. Retained clot was present in urinary bladder along with a retaining catheter. Left kidney was normal in size, shape and position.Cortex, medulla and sinuses were well outlined.

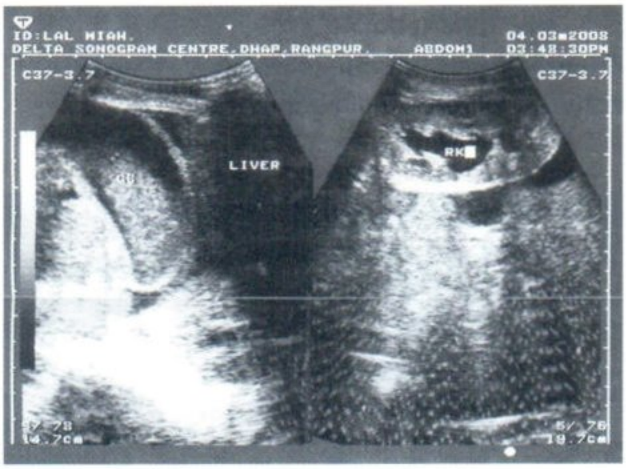

CASE NO.2

MODE OF INJURY

Blunt renal trauma can be classified according to the severity of injury and the most common is the renal contusion. Blunt trauma in the region of 12^{th} rib compresses the kidney against the lumbar spine, and the injuries will commonly involve the waist or lower pole of the kidney, where the 12^{th} rib makes its impact. The kidney can be damaged from a blow in the abdomen anteriorly, just below the rib cage, particularly in road traffic accidents, e.g. the victim is thrown onto the steering column or some other projecting object. Abdomonal injuries due to seat belts include 11% which involve the urinary tract and half of those are renal.[3]

Penetrating injuries (usually from gunshot or stab wounds) account for 20% of renal traumas in an urban setting. The damage from a bullet will depend not only on direction, but also on the velocity of the missile. Low-velocity missiles will penetrate all structures in their path. With high-velocity missiles it is necessary to assume that the shock wave will have damaged an area around the track of the missile. A knife or stilleto stab can readily cut the cortex of the kidney if the weapon is driven more than 3 inches into the victim. Although a peri-renal hematomas usually develops, the patient may not show haematuria unless the weapon has reached the calvces or renal pelvis.[4]

There is also the possibility of iatrogenic injuries, that can occur in the passage of a catheter up the ureter (damage of renal pelvis), when a renal biopsy is done or when there is an infection carried indirectly into the renal pelvis.

Frequency

In United States Renal trauma is the most frequent urologic trauma, occurring in 8-10% of patients with considerable blunt or penetrating abdominal trauma. Blunt trauma is the overwhelming cause of 80% of renal injuries.[5] Among patients with gross hematuria, notable renal trauma is present in 25%; however, less than 1% of patients with microhematiria have substantial renal injury.[6,7]

In other countries, particularly in the developed countries, the most common cause of renal trauma is motor vehicle accidents with significant blunt abdominal trauma accounting for most renal injuries.[8]

But in developing countries main cause of renal trauma is accidental fall and Blunt trauma.

DISCUSSION

Mortality and morbidity rates for renal injuries vary with the severity of renal injury, the degree of injury to other organs, and the treatment plan utilized. Thus, treatment options must be weighed against related mortalities and morbidities. In the evaluation for treatment options, the injury grade is correlated with the apparent need for surgery to repair or remove the injured kidney.[9]

Ultrasonography is the initial diagnostic choice for the detection of renal anatomy and many pathology. The ability of the kidney ultrasound to detect its normal anatomy, congenital variants as well as different pathological conditions depends on the size, shape & type of the lesions.10

Kidney ultrasound is very good at discovering kidney cysts, renal mass, congenital variants of the kidneys, polycystic kidney diseases, peri/para-nephric abscess and perinephric haematoma resulting from ruptured of the kidney.

Now a days ultrasound is available almost all the corners of the country. The opportunity of diagnosis of kidney details has now increased in many folds. Though traumatic rupture of the kidney is rare but tends to be very serious and progress rapidly, resulting in end-stage even death in many undiagnosed cases.[11]

Traumatic rupture of the kidney is fortunately for the doctors and the patient a rare entity.

Although sonography can depict free fluid in the abdomen and pelvis, it cannot be used to make the clinically important distinction between extravasated urine, blood, or other types of fluid. Moreover, ultrasonography cannot depict the source of the bleeding. A variety of groups also have proposed the use of ultrasound to search for solid-organ injury, but sufficient sensitivities and specificities have not been demonstrated to data.[12,13]

Ultrasonography may demonstrate renal laceration, a change in echogenicity of an injured kidney, or a decrease in the usual perinephric echogenicity if perinephric fluid or hemorrhage is present. However, if sonograms are negative and if noteworthy hematuria is present, or if the sonogram is positive, CT is still indicated for evaluation of the injury if the patient is stable.14 For this reason, the use of sonography is probably best reserved for the rapid evaluation for intraperitoneal fluid in the unstable patient who may require urgent surgery.

CONCLUSION

The ultrasonography is easier, cost effective, hazardless initial method of investigation for kidney details. Some authors believe that every patient should undergo an ultrasonic scanning because it may show the size of a possible perirenal hematoma and monitor whether its extending or resolving.

REFERENCES

1. Altman AL, Haas C, Dinchman KH. Selective nonoperative management of blunt grade 5 renal injury. *J Urol.* Jul 2000; 164(1): 27-30; discussion 30-1.
2. Baverstock R, Simons R, McLoughlin M. Severe blunt renal trauma: a 7-year retrospective review from a provincial trauma centre. *Can J Urol.* Oct 2001; 8(5): 1327-6.
3. Bertini JE, Flechner SM, Miller P. The natural history of traumatic branch renal artery injury. *J Urol.* Feb 1986; 135(2): 228-30.
4. Blankenship B, Earls JP, Taher LB. Renal vein thrombosis after vascular pedicle injury [clin conference]. *AJR Am J Roentgenol.* Jun 1997; 168(6): 1574
5. Bode PJ, Niezen RA, van Vugt AB. Abdominal ultrasound as a reliable indicator for conclusive laparotomy in blunt abdominal trauma. *J Trauma.* Jan 1993; 34(1): 27-31.
6. Boone TB, Gilling PJ, Husmann DA. Ureteropelvic junction disruption following blunt abdominal trauma. J Urol. Jul 1993; 150(1): 33-6.
7. Brandes SB, McAninch JW. Reconstructive surgery for trauma of the upper urinary tract. *Urol Clin North Am.* Feb 1999; 26(1): 183-99,x.
8. Bretan PN, McAninch JW, Federle MP. Computerized tomographic staging of renal trauma: 85 consecutive cases. J Urol. Sep 1986; 136(3): 561-5.

9. Bruce LM, Croce MA, Santaniello JM. Blunt renal artery injury: incidence, diagnosis, and management. Am Surg. Jun 2001; 67(6): 550-4; discussion 555-6.
10. Campbell EW, Filderman PS, Jacobs SC. Ureteral injury due to blunt and penetrating trauma. Urology. Sep 1992; 40(3): 216-20.
11. Carroll PR, McAninch JW, Klosterman P. Renovascular trauma: risk assessment, surgical management, and outcome. J trauma. May 1990; 30(5): 547-52; discussion 553-4.
12. Cass AS, Luxenberg M, Gleich P. Clinical indications for radiographic evaluation of blunt renal trauma. *J Urol.* Aug 1986; 136(2): 370-1.
13. Cass AS, Luxenberg M. Traumatic thrombosis of a segmental branch of the renal artery. J Urol. Jun 1987; 137(6): 1115-6.
14. Corr P, Hacking G. Embolization in traumatic intrarenal vascular injuries. Clin Radiol. Apr 1991; 43(4): 262-4.

RETAINED SURGICAL SPONGE: DIAGNOSIS WITH SONOGRAPHY-A CASE SERIES

Dr. Md. Murshed Ali. MBBS; M-Phil(NM); Ph.D [1]

INTRODUCTION

A retained foreign body in the abdominal cavity following surgery is a continuing problem. Despite precautions, the incidence is grossly underestimated.

Retained foreign objects after surgery are associated with multiple major surgical procedures being performed at the same time and an incorrect instrument or sponge count.

The diagnosis of a retained surgical sponge was made by sonography in three patients. The plain abdominal radiograph were normal in all cases. In each of the three cases. Sonography disclosed a well-defined hypoechoic mass containing highly echogenic foci with a strong posterior shadow. In these cases, sonographic findings, together with a history of surgery, permitted the correct preoperative diagnosis of a retained foreign body.

There are many causes of pain in the abdomen which ultrasonography play a vital role to find out the causes.

This study was performed in the Centre for Nuclear Medicine and Ultrasound, Rangpur to find out the post-operative intra-abdominal foreign body.

CASE 1

A young lady of about 20 years admitted into the hospital with the complaint of constant pain of variable nature in the right lower abdomen and generalized weakness, weight loss, constipation, nausea and intermittent fever for the last six months. She had abdominal laparotomy for appendicular pathology. Her pulse was 76 min, B.P. was 115/70 mm of Hg. The patient was mild anaemic, but non icteric.

On palpation, deep tenderness was present in the right lower abdomen but no definite lump/mass felt in right lower abdomen. Her menstrual cycle was regular. Her plain x-ray of abdomen reveals nothing contributory. She was send for ultrasound scan. After adequate bowel preparation, ultrasound scan reveal a bright semi lunar echogenic structure casting dense posterior acoustic shadow in the right lower abdomen which does not consistent with others abdomino-pelvic organs.

[1] Senior Medical Officer and Director (Acting) Centre for Nuclear Medicine and Ultrasound, Dinajpur, Bangladesh.

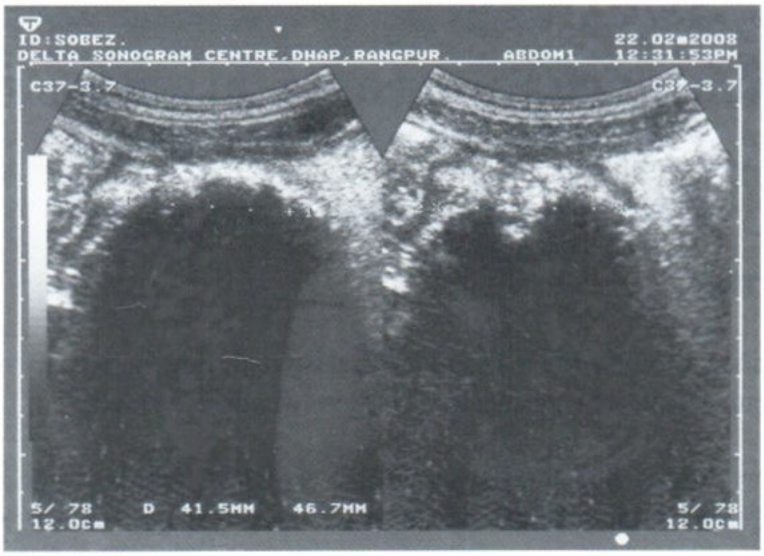

CASE 1

CASE 2

An women age about 39 years admitted into the hospital for abdominal hysterectomy and hysterectomy done accordingly. From the 7th post operative day she suddenly developed features of acute abdomen. Her pulse was 88 beat/min, B.P. was 145/85 mm of Hg, temperature 102^0 F. She was dehydrated, mild anemic but no jaundice. On palpation abdomen was distended, severely tender, more marked in the left para-umbilical region. Her plain x-ray abdomen reveals sub-acute intestinal obstruction She was sent for ultrasound examination. Ultrasound scan reveals a large bright echogenic structure with a thin rim of hypoechoic collection around which does not consistent with other abdominal organ and was associated with distended loops of intestine.

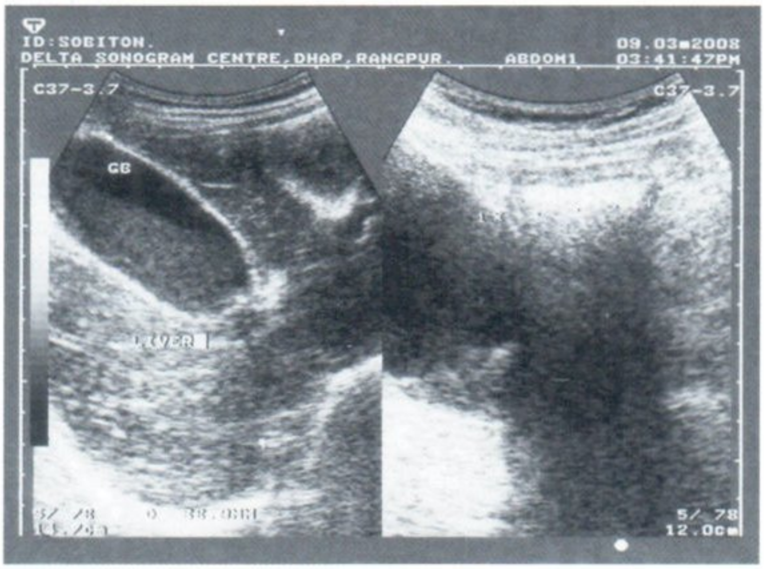

CASE 2

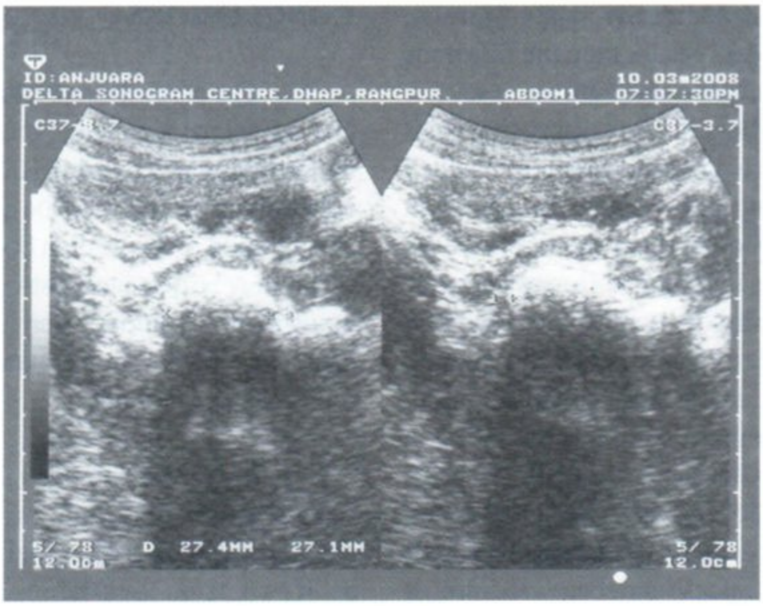

CASE 3

CASE 3

A man aged about 45 years admitted into the hospital with complaints of generalized weakness, gradual weight loss, nausea, and constant pain in right lower abdomen. He had a history of laparotomy for repairing of the perforation of abdominal hallow viscus in the last 3 months.His pulse was 78 /min, B.P. 130/80 mm of Hg, temperature was 99^0 F. He was mild anaemic but non-icteric. On palpation deep tenderness was present in the right lower abdomen. His plain x-ray abdomen reveals nothing contributory. He was sent for ultrasound scan. Ultrasound scan revealed a large irregular bright structure casting strong posterior acoustic shadow in the right lower abdomen above the level of umbilicus which does not consistent with other abdominal solid organs.

MATERIALS AND METHODS

A detailed history was obtained and physical examination carried out. Ultrasounds were performed by using Toshiba Just Vision-400 Ultrasound machine using 3.5 to 5 MHz probes. Most of the patient had adequate bowel preparation for abdominal ultrasound.

DISCUSSION

Retained surgical foreign body is seldom reported due to medicolegal implications. Awareness of this problem among surgeons and radiologists is essential to avoid unnecessary morbidity.

The diagnosis of retained surgical foreign body will continue to be a problem as long as nonabsorbable materials are used. The most common surgically retained foreign body is gauze.[1]

Since cotton sponges are inert. They do not undergo any specific decomposition of biomedical reaction.[2] Pathologically, however, two types of foreign-body reactions occur.[3] One is an aseptic fibrinous response that creates adhesions and encapsulation, resulting in a foreign-body granuloma. This occurred in one of our three cases. In the other variety, the response is exudative in nature and leads to abscess formation with or without secondary bacterial invasion. The development of an abscess represents an attempt by the body to extrude the foreign material, either externally or into a hollow viscus. This may lead to postsurgical complications such as fecal fistula or erosion and perforation into adjacent viscera.[1,2] The exudative type of foreign -body granuloma appears earlier than the fibrinous type, because symptoms and signs are more severe. Radiologically, a whirl-like pattern on plain radiographs has been described as being characteristic of retained sponges.[4] This finding may be due to gas of an intestinal orgin trapped between the fibers of the sponges. However, this finding is not always present. In this series, no abnormality was detected on plain abdominal radiographs of the two cases and another had features of sub-acute intestinal obstruction. In foreign-body granulomas, sonography shows a raniform mass with an echogenic center and hypoechoic rim. A central echogenic area represents the retained foreign body, which strongly attenuates the sound waves, thus creating an intense and sharply delineated acoustic shadow.[5] In these cases, a retained surgical sponge with granuloma or abscess formation must be differentiated from abscesses due to other causes.[6]

Despite the rarity of the reporting of a retained surgical sponge, this occurrence appears to be encountered more commonly than generally appreciated. Operating teams should ensure that sponges be counted for all vaginal and any incisional procedures at rick for retaining a sponge. In addition, the surgeon should not unquestioningly accept correct count reports, but should develop the habit of performing a brief but thorough routine post operative wound/body cavity exploration before wound closure. The strikingly similar outcome for most patients would argue for a standardized indemnity payment being made without the need for adversarial legal procedures.

Ultrasonography has paramount importance in investigating the cause of pain in the abdomen. Apart from its noninvasiveness nature and lack of radiation exposure, ultrasound can provide the information on the presence of post-operative intra -abdominal retained foreign body.[7]

CONCLUSIONS

The clinical manifestations ranged from mild abdominal pain, palpable mass, persistent drainage and granuloma to intestinal obstruction secondary to adhesions or occlusion of the intestinal lumen because of migration of the foreign body and intraabdominal sepsis may be detected post-operatively. Despite this being a rare situation, when it happens it presents as a very serious problem to patients with high rates of morbidity and mortality.

Prevention remains the key to the problem. Ultrasound is the initial procedure of choice for detection of intra-abdominal retained foreign body, as it is easier, available, hazardless and cost effective.

REFERENCE

1. Williams RG, Bragg DG, Neison JA. Gossypoboma- The problem of the retained surgical sponge, *Radiology* 1978; 129: 323-326.
2. Sturdy JH, Baird RM, Gerein AN. Surgical sponges: a cause of granuloma and adhesion formation *Ann Surg* 1967; 165: 128-134.
3. Olnick HM, Weens HS, Rogers JV Jr. Radiological diagnosis of retained surgical sponges. *JAMA* 1955; 159: 1525-1527.
4. Robinson KB, Levin EJ, Erosion of retained surgical sponges into the intestive. *AJR* 1966; 96: 339-343.
5. Mason LB. Migration of surgical sponges into small intestine. JAMA 1968; 205: 938-939.
6. Kressel HY, Filly RA. Ultrasonographic appearance of gas-containing abscesses in the abdomen, AJR 1978; 130: 71-73.
7. Chan MY, Tan C, Chiu MT, et.al; Alvarado score: an admission criterion in patients with right iliac fossa pain. Surgeon. 2003 Feb; 1(1): 39-41.[abstract]

CARCINOMA OF NASOPHARYNX, A RACIAL GENITICAL TRANSMITTED DISEASE.

Professor Dr. Kawee TUNGSUBUTRA, M.D., F.R.C.R. (ENGLAND)

Pharynx means "pass way". Nasopharynx means pass way of Air through the nose into the lungs. Air and Food are the two things which are necessary for life. Life can not be continued without Air and Food.

The essential Air for life is Oxygen, while the food must contain both water and other foods and Vitamins which are necessary for life. Life can not be survive without Air, foods and water.

Pharynx in Human beings consisted of 3 parts.

1. Nasopharynx is the Air passage through the noses.
2. Oropharynx is the passage of both the Air and Foods.
3. Laryngopharynx is the passage of foods through the posterior part of the larynx, or the Voice Box with its function for passage of the Air into the lungs and for speaking or making noises.

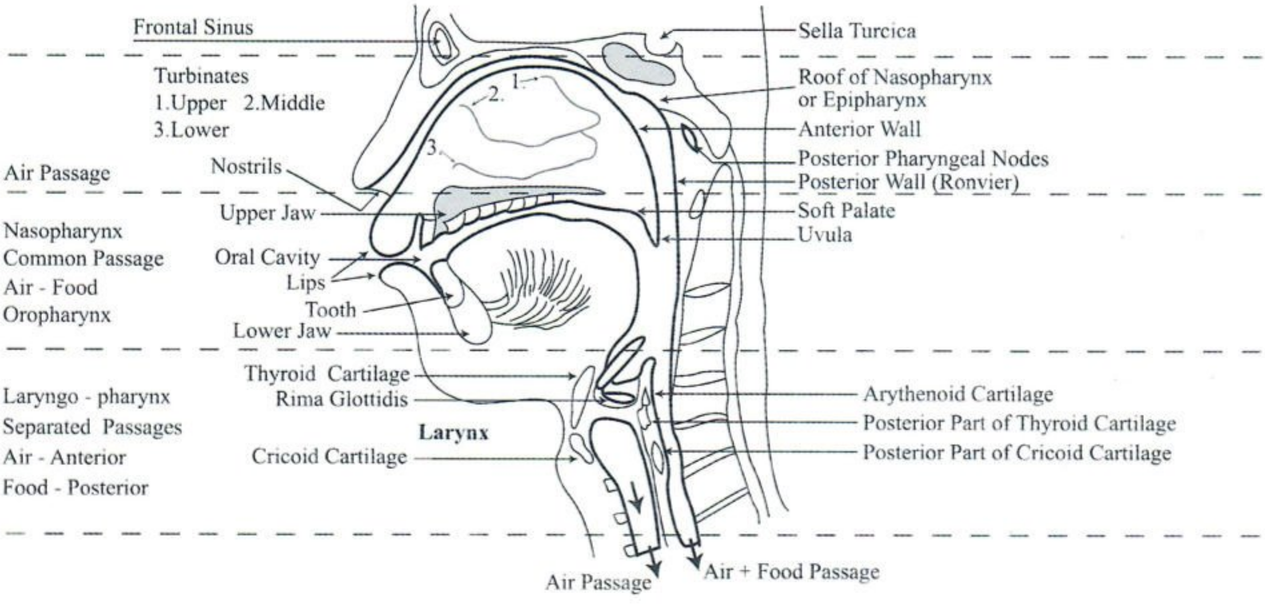

Fig.1 Picture showing Anatomy of Air and Foods passage into the body.

[1] Professor, Radiotherapy, Kaweevej, 318, Tarksin road, Dhonburi, Bangkok, Thailand, 10600. Tel. 0-2465-8518

Air passage starting from Nasopharynx, the air passed through both nostrils. The roof of Nasopharynx is the base of skull. Oropharynx is the common passage of air and food. Laryngopharynx is also the common passage of air and food. Laryngopharynx is divided into **air passage anteriorly** and **food passage posteriorly.** In swallowing of food the tongue will be moved posteriorly. Epiglottis will also be moved posteriorly to close the air passage and push the food into the laryngopharynx, and oesophagus respectively and finally into the stomach. While swallowing the food, epiglottic which is at the root of tongue will do the duty of closing the larynx to prevent the food droping into the trachea and pushing the food either solid or liquid into the oesophagus. If there is any food or water happened to drop into the larynx, and further into the air way, there remain the cough reflex to expel either solid or liquid out from the air passage before having a chance of getting into the bronchus and finally getting into the lungs. This is a natural defence mechanism which is responsible by the Autonomic Nervous System, to prevent food and water getting into the lungs causing pneumonia.

The Natural Defense Mechanism will control the food and water when swallowing to go into the right tract, i.e., Oesophagus and stomach not to go into the bronchus and lungs, and at the same time the breathing air into the air passages to have the exchanges of O_2 and CO_2 in the alveoli of the lungs, automatically. If there is excess of air entered into the stomach, it will be expelled out by Antiperistalisis automatically.

Before going into the detail of the disease, the normal anatomy of the Nasopharynx will be described briefly. Nasopharynx is an air passage shaped as 4 sided tube which have the roof as the base of skull. There are two anterior opening called the nostrils. The posterior end of the nasopharynx is also consisted of two opening, called the posterior nares. The air will be breathed through the anterior nares from both sides of the nose passing through the posterior nares into the Oropharynx, Larynx and both Lung. The posterior end of the Nasopharynx is continued by the Oropharynx. The posterior Nasopharyngeal wall is infront of the Anterior surface of the upper Cervical Vertebrae which is covered with the nasopharyngeal mucosa, there are two dimples one on the right and another one on left, which are called the Rosenmuller Fossae. On the lateral sides of these fossae, there is a small opening which is called the Rosenmuller Fossa,which is the opening of the connection between the middle ear and the Nasopharynx by a Eustachian tube. This special tube one on each side is very useful in keeping the equilibrium of the pressure in the middle ear with the Atomospheric pressure.

If there is cancer, benign tumour, inflammation with sticky pus causing obstruction of this Eustacian opening or canal, it will cause some strange noises called "Tinnitus". This condition if not properly treated, will end up with infection of the middle ear with pus known as "Otitis Media".

Symptoms: The symptoms of Ca. Nasopharynx may be classified according to the symptoms due to the position of the tumour mass.

1. Symptoms due to the tumour mass.

1.1. Air way obstruction causing difficulty in breathing:
Ask the patient to press his thumb on one of his nostril and take a deep breath through the other nostril once on each side. If there is a tumour mass obstreucted in one nostril, there will no air passing through the nostril of that side.

1.2. Epitaxis or Bleeding through the nostril of the affected side, from time to time.

1.3. Foul smell discharge or pus running through the nose or the throat from time to time, or coughing with blood and pus expectoration.

2. Symptoms due to Infiltration or Local invasion of Ca. Nasopharynx making obstruction of the Eustachian tube of

the affected side.

2.1. Impairment of hearing in the affected side of the tumour.
2.2. Tinnitus.
2.3. Partial Loss of Hearing.
2.4. Chronic Otitis Media of the affected side.

3. Symptoms due to Cranial Nerves Involvement.

3.1. Symptoms due to Paresis of Extrinsic Muscles making limitation of movement of the eye ball in the affected side, or Ptosis of the eyelid. The involvement of different cranial nerves cause different symptoms as followed:

Nerve II., making Ptosis due to paralysis of Levator Palpebrae.

Nerve III., paralysis making limitation of movement of eye ball.

Nerve IV., paralysis of lateral Rectus Muscle making Internal Squint.

Nerve VI., paralysis of Superior Oblique making the patient not be able to move the eye ball to see the object superiorly and obliquely above the head.

3.2. In having the paresis of the muscles which control the movements of eye ball, the eyes have to be accommodated in compensation all the time involuntarily which make the subject always have symptoms of headache.
3.3. Patient may have double visions.
3.4. In having the Internal Squint, making the patient lost the lateral visual field of the eye of that side.
3.5. The patient can speak some words not clearly due to the involvement of N. IV., Glossopharyngeal Nerve, making the paralysis of Pharynx and Uvula of that side.

If we ask the patient to open his mouth widely and say "Ah" the Uvula will be deviated to the side, opposite to the side of the paralytic nerve. Ask the patient to pushed out his tongue, the tip of tongue will be deviated to the side which the branch of N. VII. was pressed by the tumour.

4. The involvement of local lymph nodes.

Primary station of metastasis of Ca. Nasopharynx is the Node of Ronvier or Posterior Pharyngeal Nodes. These lymph nodes were located at the posterior wall of Nasopharynx which may be seen by nasopharyngeal mirror or direct nasopharyngoscopy and may be confirm by direct palpation by gloved finger at the posterior pharyngeal wall. It will be found that the posterior pharyngeal wall is lobulated with bulging enlargement of the posterior pharyngeal lymph nodes. Secondary station is the lymph follicles which is in the Inner Wal-de-year's Ring which may be palpable at the posterior triangle of neck and is the posterior group of Jugulo-Digastric and Jugulo-Omohyoid.

The next step of metastases is the spreading upward to the upper 1/3 of neck region and then spread downward to the lower cervical nodes, down to the clavicle and supraclavicular region.

5. Symptoms due to distant metastasis.

The predilection sites of distant metastasis of Nasopharyngeal cancer are Brain, Liver and Lungs. The general and local symptoms are the same as the Metastatic carcinoma which spread from the other primary sites of Cancer such as Head and Neck Cancer to the same metastatic sites.

Diagnosis. The diagnosis of Ca. Nasopharynx can be given only by a positive tissue biopsy reported from a qualified pathologist from the tissue biopsy taken from the mass in the nasopharynx, seen in the mirror or from a mass seen by direct nasopharyngoscopy. The Negative histological section does not mean that the patient have no cancer of the nasopharynx, if the clinical symptoms of the patient and the result of clinical examination indicated that the patient is suffering from Ca. nasopharynx, e.g. there are multiple Cranial Nerves involvement. Re-biopsy should be done even the first biopsy is negative. There is a high percentage of Primary tumour of the Ca. Nasopharynx with a primary tumour very small, difficult to be seen or can not be palpable. Blind Biopsy is recommended to be done at least at the 3 predilected sites, namely at the Rosenmuller fossa and the opening of Eustachian Tube, secondly at the Posterior Wall and thirdly, the Lateral wall of the Nasopharynx, The physical examination of the Nasopharynx can be done easily by passing a catheter into one nostril and ask the patients to open his mouth widely and use a long forceps to pull the end of the catheter through the mouth and keep stabilized by a forceps, holding the two ends of the catheter together. Slowly pull the soft palate to one side, to open the clear view of Nasopharynx seen by the mirror examination without making the patient too much trouble. To avoid coughing or sneezing of the patient, local spraying of local anesthetic agents may be used at the nose and oral cavity.

Histological Types.

1. The most common histological type is Squamous cell Carcinoma with a varying degree of differentiation from well differentiated type to Undifferentiated or Anaplastic type.
2. Adenocarcinoma.
3. Adeno-acanthoma.
4. Lympho-epithelioma.
5. Lymphoma or Lymphosarcoma.
6. Tumour of Ectopic Salivary gland.
7. Plasmocytoma or Plasma cell sarcoma.

Treatment.

Ca. Nasopharynx is the central organ which surrounded by bony cages. The treatment by surgery is inadequate and impossible to take the primary lesion and its submucosal spreading adequately and remove en bloc., for curative treatment. Surgical procedure can be employed only for biopsy to prove that the lesion is cancer and what histological type with malignancy grading only. The adequate treatment or curative treatment could be done only by Radiation. The type of Radiation which aims at curative could be done only by External Radiation alone with high dosage wide and adequate fields of radiation covering the primary lesion and potential areas of lymph nodes in the head and neck region. Chemotherapy is recommended to use only in Lymphoma histological types only. Intracavitary Brachytherapy is recommended only, as an additional treatment in residual primary lesion in certain histological type such as Adenocarcinoma or Adeno -acanthoma. We recommended to use external radiation only using 6 MeV linear accelerator to have a high cure rate by delivering adequately high doses of radiation into the primary tumour area and the potential areas of metastasis in the head and neck.

Chemotherapy may be used as supplementary treatment or palliative treatment in rather late stages or palliative for recurrent cases according to general condition of the patient and the radiotherapist's decision that it is appropriate.

Principle of Radiotherapy.

Radiotherapy should cover by two lateral opposing fields from the Base of Skull down to clavicle, the upper border from the anterior end above the eye brow, the lower border down to cover the supraclavicular region. The posterior border of the radiation field, at the anterior border of Cervical vertebrae avoiding the cervical spinal cord so as the radiation field will cover the posterior pharyngeal wall to include lymph nodes and lymph follides at the posterior pharyngeal wall.

The third field may be added anteriorly to cover from the base of skull down to the hard palate for another 1000 rads. The addition radiation may be added in the cases of some histological types or grades which are known to be rather radioresistant. The supplementary radiation may be given either by External radiation, anterior direct field or by Intracavitary Brachytherapy to prevent or minimize the complication of Radiation Myelitis and yet be able to diliver adequate doses to the tumour which is in the **bones cage.**

Total Doses of radiation depend on Histologic Sections. Squamous cell or Adenocarcinoma, the total dose may be high about 6500-7500 rads or centigray in 6.5 to 7.5 weeks. If still there is residual growth, followed up after 6-8 weeks after finished the first course of external radiation, Intracavitary Brachy therapy may be given as additional course by high dose rate, after loading applicators through the oropharynx.

The technique of radiotherapy for Ca. Nasopharynx aim to cover the Primary lesion and the Neck nodes to cover the potential areas of local spreading on bloc. The chemotherapy will be given or not depend on the decision of the physician and the histologic section, e.g. Lymphoma or lympho-epithelioma may be followed up by Chemotherapy.

The total doses of radiation in cases of Lymphoma may be given 4500 rads or cgy but lympho -epithelioma the radiation dose still have to be high up to 6500 rads, at least, the same as Squamous cell carcinoma followed by Chemotherapy or not, is up to the decision of the physician or the radiotherapist.

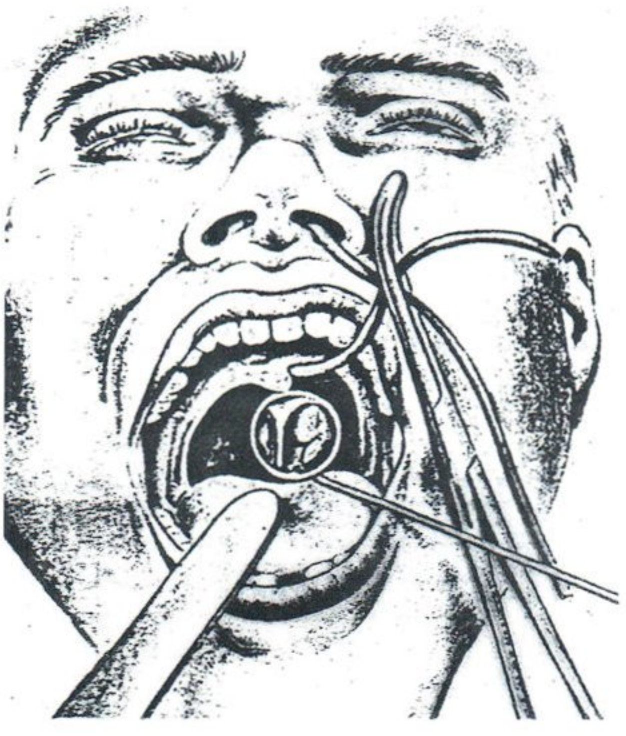

Fig.2 The examination of the Nasopharynx can be done easily by introducting a catheter into one nostril and ask the patient to open his mouth and use a long forceps to pull the other end of the catheter out from the mouth. The prevent the patient coughing or sneezing, use the local anesthesia to spray into the nasal and oral cavity before introducing the catheter into the nose.

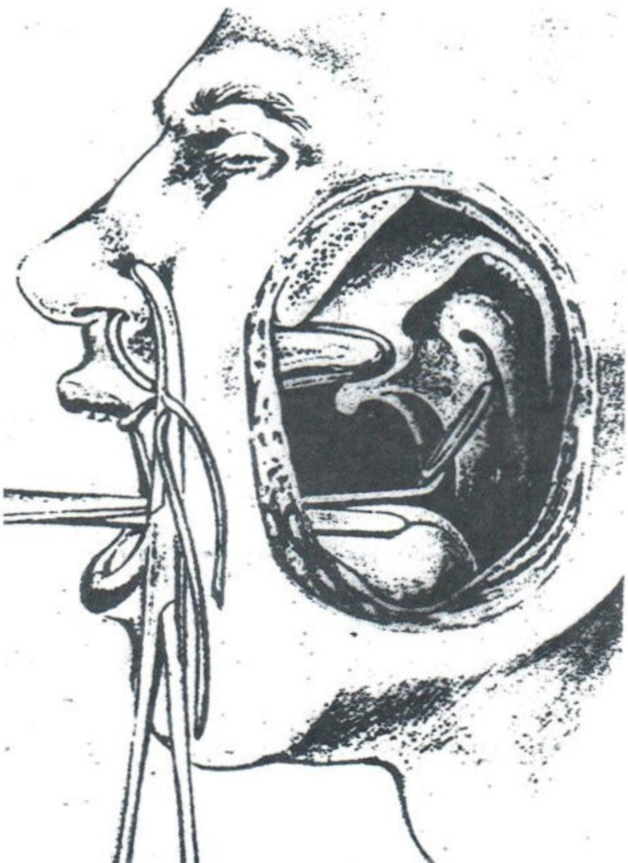

Fig.3 Hold both ends of the catheter to one side to open the clear view of the Nasopharynx without making too much trouble to the patient. Make a thorough examination of the Nasopharynx by the mirror as shown in the figure.

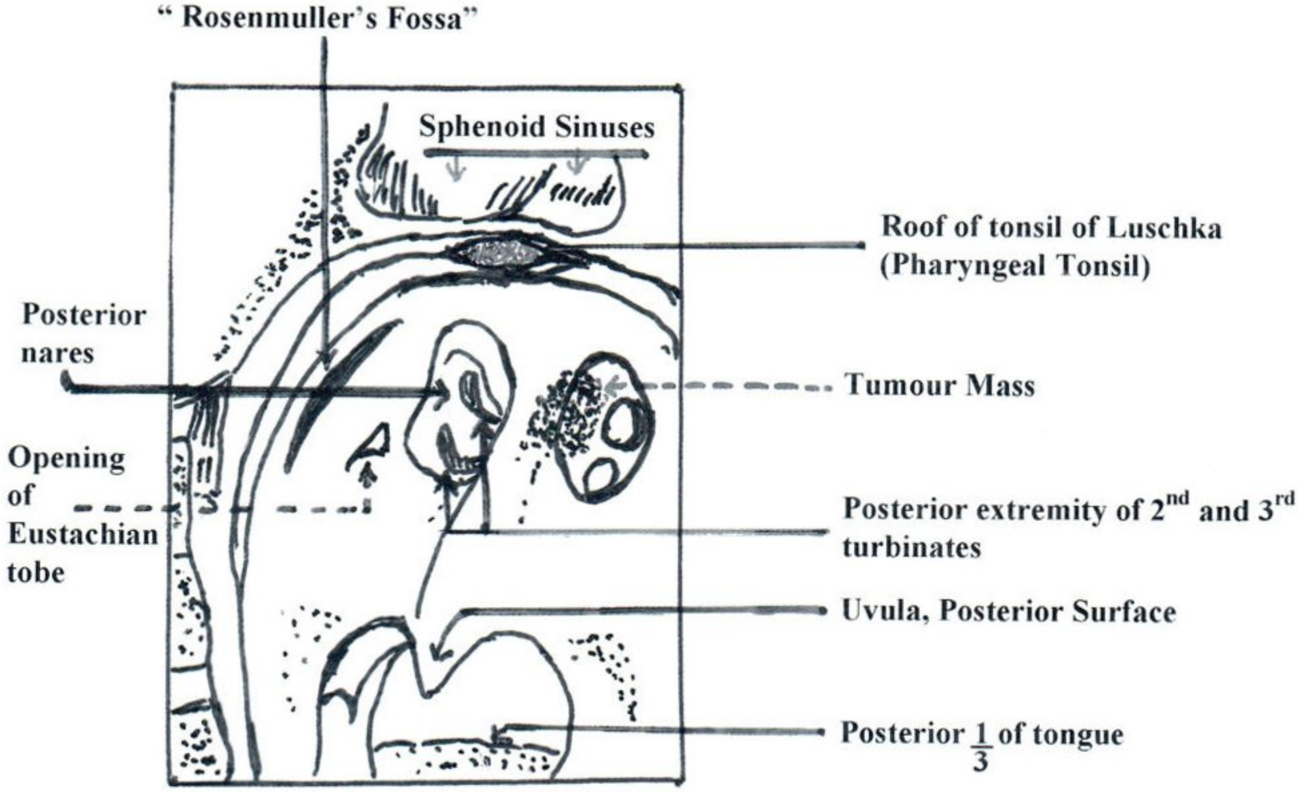

Fig.4 Nasopharynx seen by Nasopharyngoscope or mirror examination showing posterior nares, posterior extremities of 2nd and 3rd turbinates and opening of eustachian tube

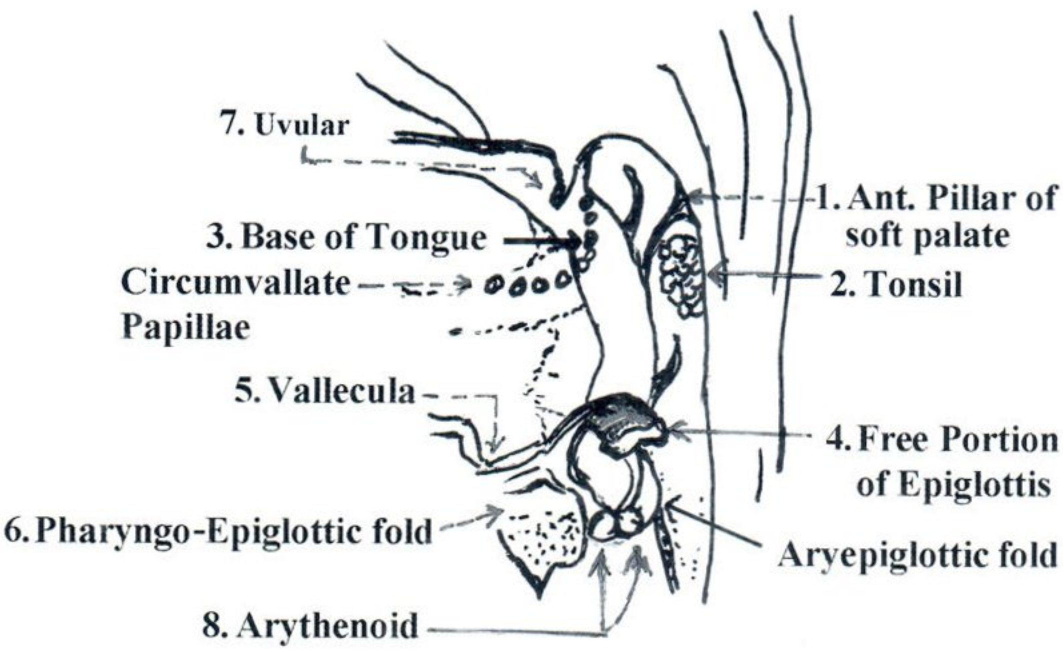

Fig.5 Postero-Lateral view of oropharynx

1. Anterior pillar of soft palate
2. Tonsil
3. Base of tongue
4. Free portion of epiglottis
5. Vallecula
6. Pharyngo-epiglottic fold
7. Uvala
8. Arythenoids

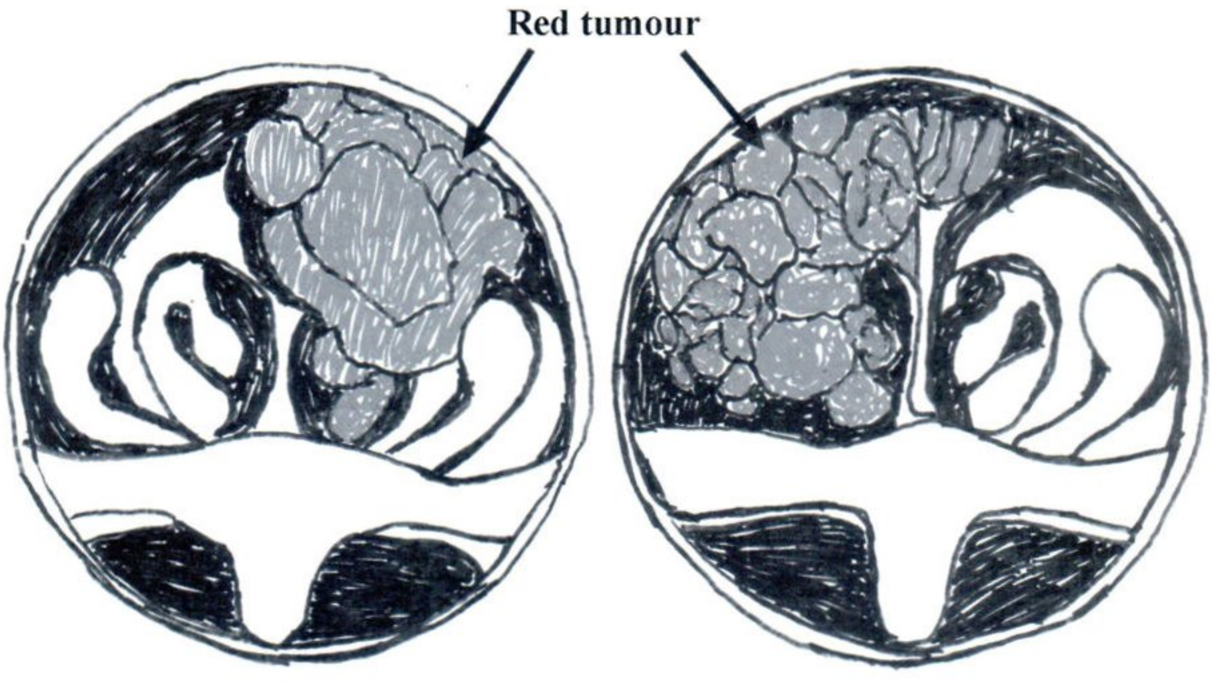

Fig.6A Fig.6B

Fig.6 Nasopharynx seen by Nasopharyngoscope or mirror examination showing posterior nares, posterior extremities of 2nd and 3rd turbinates. Red tumour is seen in each side of Nasopharynx.

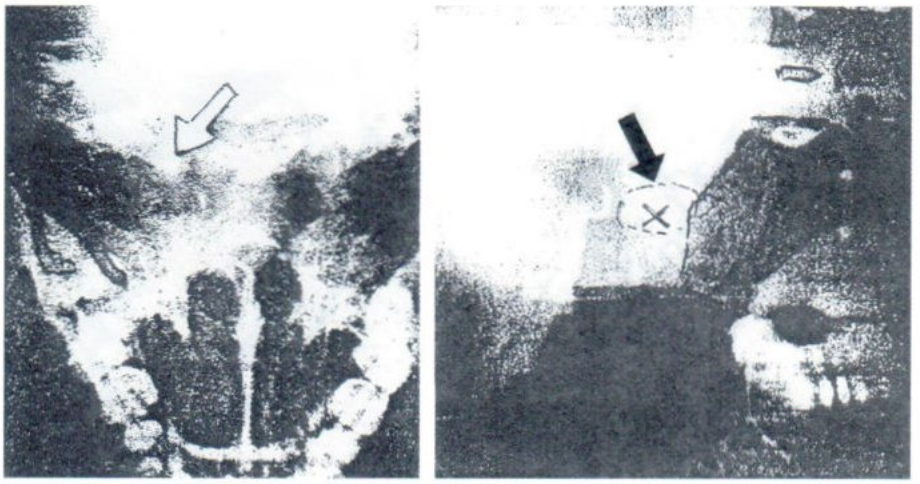

Fig.7A Fig.7B

Fig.7 X-ray picture of the base of Skull showing the erosion as pointed by an arrow at the Petrosphenoidal Region.

Fig.8A

Fig.8B

Fig.8A Widening of Posterior Wall showing the tumour mass in the Nasopharynx.

Fig.8B Tumour mass in the Nasopharynx.

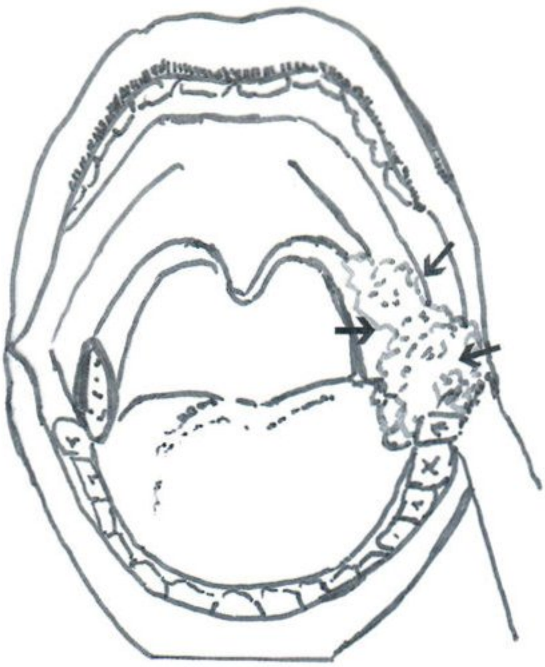

Fig.9 Papillary squamous cell ca. anterior pillar of soft palate spreading to base of tongue and buccal mucosa.

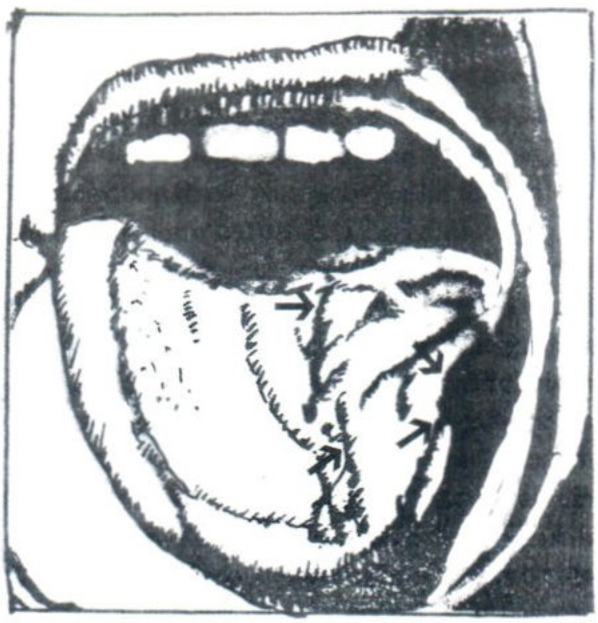

Fig.10 Hemiparalysis and atrophy of left side of tongue due to carcinoma of the nasopharynx involvement of the lateral wall of nasopharynx press on nerves and blood supply of that side.

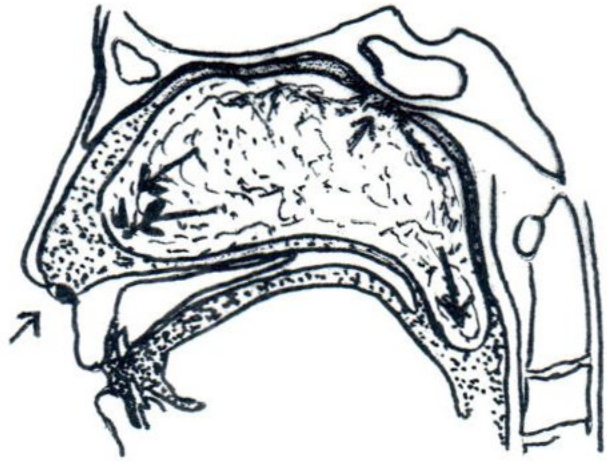

Fig.11 Nasophrayngeal fibroma showing the attachment at the base of skull in the form of pedunculated attachment and well-encapsulated extension toward the nasal cavity and oropharynx.

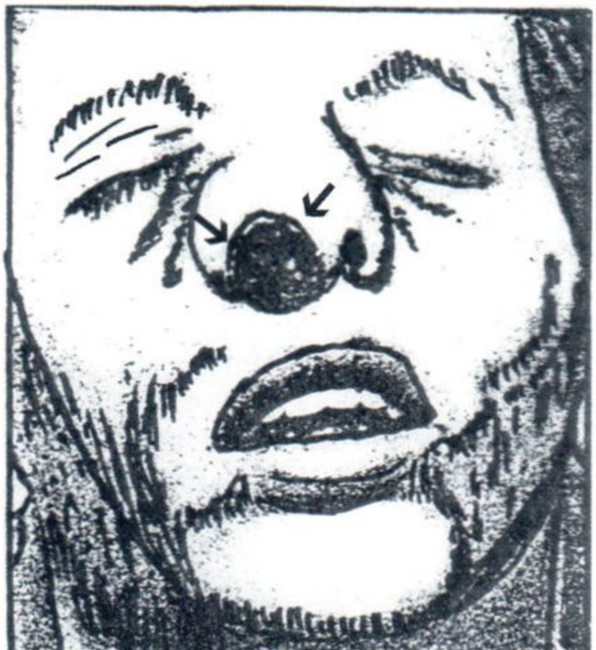

Fig.12 Nasopharyngeal fibroma protruding through Rt. Nostril in a child 12 years of age with bleeding on and off.

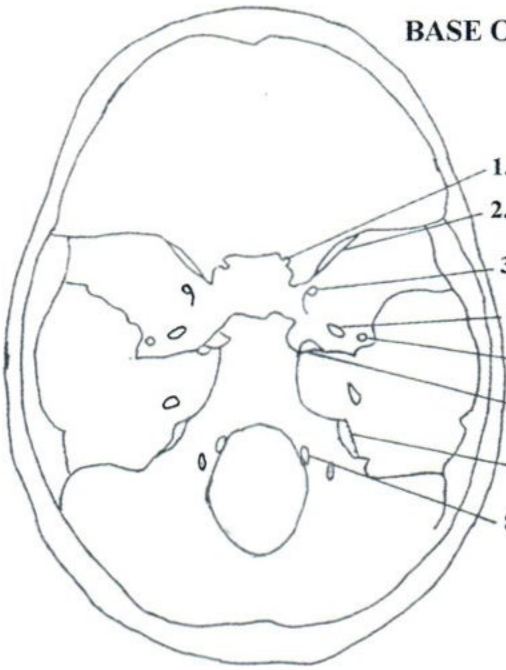

Fig.13

1. Optic canal for cranial nerve II (Optic nerve)
2. Supraorbital fissure for cranial nerve III, IV, VI, V_1 Occulomotor, trochlea, abducen, trigeminal first branch (Mandibular nerve)
3. Foramen rotundum for cranial nerve V_2 (Maxillary nerve)
4. Foramen ovale for cranial nerve V_3 (Ophthalmic nerve)
5. Foramen spinosum: Exit for Middle meningeal artery.
6. Foramen lacerum: Entrance foramen for Internal carotid artery
7. Jugular foramen: for CN X, IX, XI
8. Hypoglossal canal: nerve XII. Paralysis of any side will cause tongue atrophy of that half

Nerve V Trigeminal nerve: Sensory+motor nerve, sensory 3 branches
1. Handibular N.
2. Maxillary N.
3. Ophthalmic N.

Motor nerve supply Mastication muscles:

1. Optic Canal is the pathway of optic nerve to supply the Levator Palpebrae Muscle causing Ptosis of that side.
2. Supra orbital fissure is the pathway outlet of Cranial Nerve, Oculomotor N III, Pineal or Trochlea N IV., Abducen N VI., Trigeminal Nerve, branch I., Mandibular N.,
   Nerve IV, Trochlea supplying Superior Oblique N.
   Nerve VI Abducen supplying Lateral Rectus
   Nerve V Mandibular branch supplying Lateral Rectus, and supplying Muscles of Mastication; Median, Lateral Pterygoid and Masseter Muscle.
3. Foramen Rotundum, Nerve 5., branch II., paralysis cause numbness at the maxillary prominence.
4. Feramen Ovale, Nerve 5 branch III., Irritation of this branch cause pain at the floor of orbit, pain and numbness of the tongue of the affected half including the floor of mouth and buccal mucosa.
5. Foramen Spinosum, exit foramen for middle meningeal artery.
6. Foramen Lacerum, the entrance foramen for internal carotid artery.
7. Jugular Foramen N.9, 10, 11. Ask the patient to say "Ah" the Uvula will be deviated to the non-paralytic side.
8. Hypoglossal Canal, damages to N. XII., there will be atrophy of the tongue of that half which is affected.

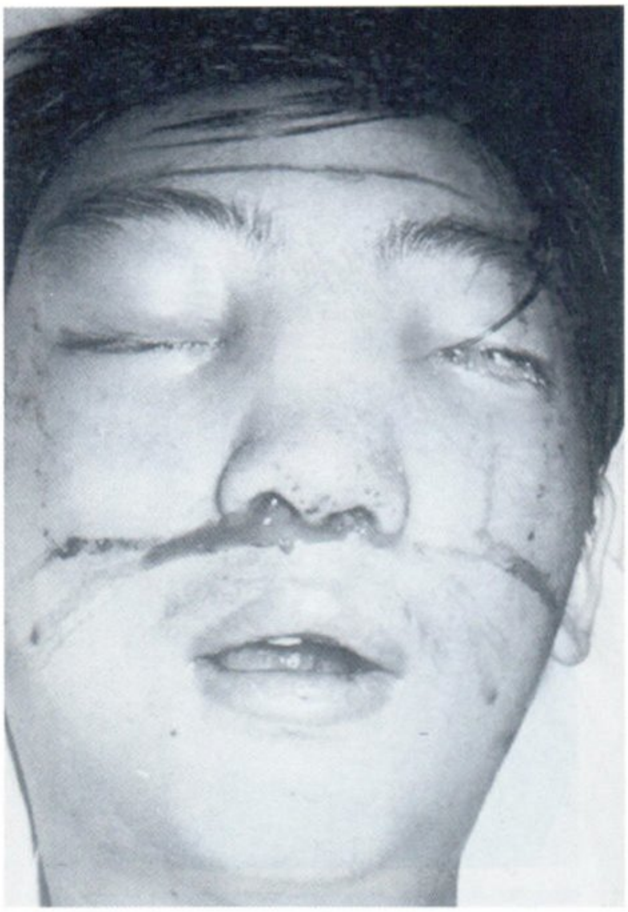

Before treatment

After treatment

Case I.

A Chinese patient was admitted to the Siriraj Hospital in Thailand for I day with the chief complaint of unconscious for 2 days with foul smell discharges running through both nostrils. The left eye was not fully closed with exposure keratitis. He could not close his mouth tightly and both lips were not fully closed. We can see the pus in the mouth, mucopurulent with blood stained discharge through his half-opened lips. He was treated by antibiotics and supportive therapy with I.V. fluid and Vitamins.

At the same time we have given him radiation therapy by external radiation to the Head & Neck by two lateral opposing fields with a daily dose of 200 rads/day, 1000 rads/week at midline to the Head & Neck Region. The upper border of the field cover the base of skull. The lower border of the field cover the upper 2/3 of neck node region. The radiation field cover the primary lesion in the Nasopharynx which was diagnosed by physical and X-ray examination. Lateral and Mento-Vertex Views of Head & Neck and skull were taken and the diagnosis of Ca. Nasopharynx with metastasis to cervical nodes and base of skull was diagnosed. He gain his conscious after he received roentgen treatment for a dose of 2000 rads in two weeks. He recover fully after a dose 6500 rads in 6.5 weeks. The histological diagnosis taken from a cervical node was squamous cell Ca. moderately differentiated. He was alive & well for about 7 months. He died about 8.5 months with liver metastasis and liver failure.

Case II

A Chinese labourer was admitted to Siriraj Hospital with the chief complaint of cannot open his eyes and toothache in the left lower mandibular area for 2 days. Roentgen investigation revealed that he had bone destruction at the middle part of left mandible and big mass in the nasopharynx. Physical examination revealed a mass in the nasopharynx with neck node enlargement in both sides of neck region. Histological biopsy of the primary lesion in the nasopharynx revealed moderately differentiated lymphosarcoma. Local radiation treatment were given for palliation to the base of skull, mandibular region Lt. side and neck node by bilateral opposing fields. The patient recovered well after a dose of 4500 rads in 4 weeks. He could open his eyes. No pain in the jaw, left side, and can help himself for about I year and died with liver metastasis.

Before treatment

After treatment

Case III

A case of lady, 35 years of age having a car accident about 6 months previously. She drove a motorcar and had a collision accident with the other car, having been treated in Siriraj Hospital. She recovered well with a scar of the injury and a scar of the previous suture in the forehead which healing up well. She came back to the hospital with a complaint of not be able to open her right eye with ptosis. Investigation was done and found that she was having Ca. Nasopharynx with a mass in the Rt. side of Nasopharynx. Mento-vertex view of the skull showed a big mass at the base of skull Rt. side. Nasopharyngeal biopsy was taken by direct Nasopharyngoscopy and found to have a lympho-epithelioma. Roengent treatment was given by 6 MeV. Linear accelerator for a dose of 6500 rads. After 4 weeks with a dose of 4000 rads, She can open up her right upper eye lid, She had completed her radiation treatment with a dose of 6500 rads with the complication of having the falling off her hair from her head. She survive and well after 4.5 years and had lost the followed up. The skin reaction had a complete healing and her hair had grown up as normal in 6 weeks after the radiation treatment had been completed and finished.

Before treatment

After treatment

Case III 4 week After treatment she have fallen hair from her head, with skin reaction. The skin reaction had healed up 6 weeks after treatment, and the hair had grown up as normal again.

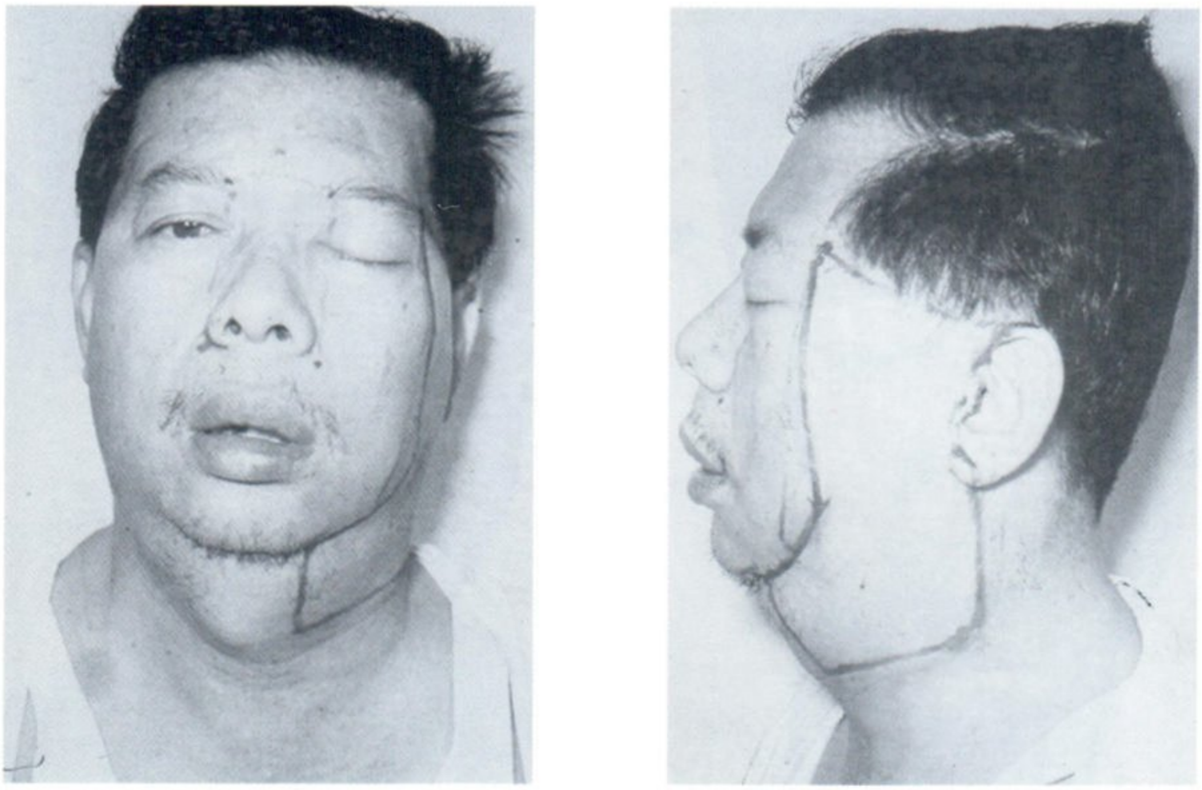

Case IV A Chinese male patient 42 years of age **before treatment**, having ptosis of his left eye.

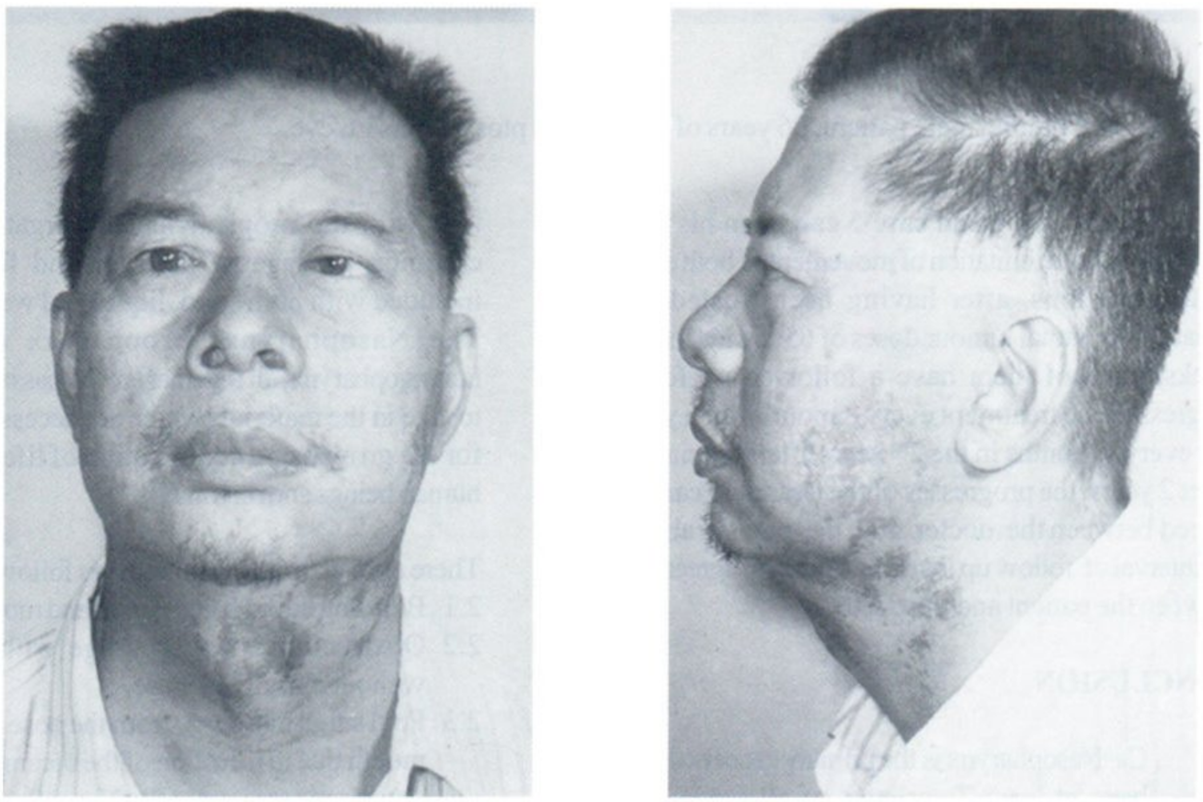

Case IV **After treatment**, he can open both eyes after a dose of 6500 rads.

Before treatment **After treatment**

Case V A Chinese, male patient, 26 years of age, he had ptosis of his Lt. eye.

Both, case 4 and case 5 can open his eye fully and without limitation of movement of both eyes in all directions, after having been treated by radiation for a total tumour doses of 6500 rads in 6.5 weeks. Both of them have a followed up for a progress of the treatment every 3 months for a year and every 4 months in the 2nd years after treatment. After 2 years. the progresses of the treatment can be agreed between the doctor and the patient about the interval of follow up that is convenient, agreeable between the patient and the doctor.

CONCLUSION

1. Ca. Nasopharynx is the primary cancer which have at least 7 varieties of all types and involving the organ of air passage in continuation with the orophanynx, the organ of common passage of both air and food included with both solid, liquid and water. The Nasopharynx, Oropharynx and Laryngopharynx, all together are the passages to take in the materials which are necessary for the growth and continuation of life for human beings and mammals.

2. There are 5 alarming symptoms as followed:
   - 2.1 Bleeding through the nose or/and mouth.
   - 2.2 Obstruction of air passage with or without mass in the nose.
   - 2.3 Foul smell discharge from the nose and mouth due to infection of the ulcerative or necrotic tumour in the Nasopharynx and its extension.

2.4 Headache due to cranial nerves involvement and especially the motor branch of Trigeminal nerve. The involvement of the motor branch of Trigeminal nerve making paralysis or weakness of the intrinsic muscles for the movement of eyeball of the involved side. This paralysis or paresis causes the patient have to accommodate the two eyes all the time to see any object or to talk with other people and this is the cause of headache.

2.5 Ptosis of the upper eye lid of the affected side due to the tumour involvement of the optic nerve and especially the branch which supply the muscle Levator Palpebrae. Mento-Vertex View of the skull will show involvement or bone destruction, especially the optic canal which is the path way of optic nerve from the skull.

3. Carcinoma of the Nasopharynx can be treated radically only by super voltage radiotherapy at least 6 MeV machine, because it is the cancer mostly needed high doses of radiation of at least 6500 rads or centigrays.

4. Curative treatment can be treated radically only by super voltage X-ray machine by an experient radiotherapist. It need a high dose of at least 6500-7000 rads in 6.5-7 weeks. The tumour dose lower than this or the treatment duration is longer than 7 weeks will end up with recurent or distant metastasis.

5. The chance of being cured in this cancer of the Nasopharynx could be attained only in stage I, II, stages later than this can be treated only palliatively to decrease the undesirable symptoms and extend a longer life.

6. Surgical or chemotherapy can not be used for currative purposes.

7. Carcinoma of the Nasopharynx, the primary site is under the base of skull and the posterior border is infront the cervical spinal cord, radical treatment can not be done by either surgery or chemotherapy, the only radical or curative treatment can be done only by radiotherapy with an experient team of Radiotherapists, Radiation Physicist and Radiographers. Otherwises, only palliative treatment can be done.

REFERENCES

1. Brachytherapy in Head+Neck Cancer: Rotterdam Low Dose Rate Experience. Peter C.Levandag., Wim L.J. van Pertten, 325-344.
2. The BriFish Practice in Radiotherapy, Head and Neck Cancer. Sir Ernest Rock Carling, B.W. Windeyer and D.W.Smithers. BulFer-woths Medical Publisher, 1955.
3. Treatment of Cancer in Clinical Practice. Kunkler and Rains, 1959. Tonsil and Naso-pharynx. Darid G.Bratherton and Kenneth F. Wilsdon, 345-354.
4. The treatment of Malignant Disease by Radiotherapy. Ralston Paterson, Second Edition, 1963. Tumours of Head and Neck 323-326.
5. Cancer Managerment: Part 12: Head and Neck Cancer; The Role of Radiotherapy for Head and Neck Cancer 323-326. Lippincott 1968: The American Cancer Society, Inc, New York 10017.
6. The Selectron HDR : plubsophy and design, in: Braclry therapy 1984, Procudings of the 3rd International Selectron user meeting, Mould RF:(Ed): Leersum, 1985.
7. Mould R.F., Radiotherapy Treatment Planning, Second Edition, Adam Hilger Ltd. ISBN 0-85274-788-8
8. Brachytherapy in the People's Republic of China. Procudings Brachytherapy Working Conference, Shanghai, P.R.China. Selection Users Meeting. April 1992 edited by RF. Mould.

Section IV Head+Neck, Chapter 14-20 (all in Chinese Language)

Chapter 14 Nasopharyngeal Cercinoma: An Analysis of 790 cases.

Chapter 15 Preliminary Experience with HDR Brachytherapy for 72 Nasopharyngeal.

Chapter 16 Preliminary Experience with HDR Brachytherapy for Residual or Recursent Head+ Neck Tumours.

Chapter 17 Teletherapy Combined eith Cobalt.60 Selectron HDR Brachytherapy for carcinoma of the Nasopharynx: Preliminary Results of 66 cases.

Chapter 18 Intracavitary Brachytherapy Combined with External Beam Therapy for Naropharyngeal Carcinoma.

Chapter 19 Selectron-LDR After loading Combined with External Radiation for Naropharyngeal Carcinoma.

Chapter 20 Preliminary Experience with External Beam Ivabiation Combined with micro-Selectron. HDR Braclrytherapy for Naropharyngeal Carcinoma: Reperton 28 Patients.